2017

Study of Thermodynamic and Dynamic Properties of Heterogeneous LiLSX Zeolite for Use in a Medical Oxygen Concentrator

Chin-Wen Wu
Lehigh University

Study of Thermodynamic and Dynamic Properties of Heterogeneous LiLSX Zeolite for Use in a Medical Oxygen Concentrator

by

Chin-Wen Wu

Presented to the Graduate and Research Committee

of Lehigh University

in Candidacy for the Degree of

Doctor of Philosophy

in

Chemical Engineering

Lehigh University

Jan, 2017

Copyright

Certificate of Approval

Approved and recommended for acceptance as a dissertation in partial fulfillment of the requirements for the degree of Doctor of Philosophy.

Date

Dissertation Director

Accepted Date

Committee Members:

Prof. Mayuresh V. Kothare

Prof. Shivaji Sircar

Prof. James F. Gilchrist

Prof. James T. Hsu

Dr. Timothy C. Golden (External Member)

Acknowledgements

I would like to extend my sincere gratitude to my advisor, Prof. Mayuresh V. Kothare and Prof. Shivaji Sircar. Without their patient guidance, discussion, encouragement, and support, my research work would not have been possible. I would like to thank my Prof. James F. Gilchrist, Prof. James T. Hsu, and Dr. Timothy C. Golden, for serving as my committee members and for their insightful discussion in my research work.

I'd like to thank Dr. Rama Rao Vemula for sharing the theoretical and experimental knowledge with me and Matt Urich for his creative ideas and supportive discussion. I also want to thank Shih-Chieh Kung and Fan Ni for helping me out whenever needed.

The steady progress of my work would not have been possible without the continuous support from the staff in Department of Chemical Engineering. I'd like to thank John Caffrey for helping set up the hardware of my experiment, and Paul N. Bader for electronics support and trouble-shooting. I would also like to thank Barbara Kessler, Tracey Lopez, and Janine Jekels for their kindly support throughout the course of my research work.

Finally, I wish to thank my family for their constantly support in my life and everything that cannot put into words.

Table of Contents

List of Tables

List of Figures

Abstract

An isothermal-isobaric column dynamic test apparatus was built to measure equilibrium adsorption isotherms of pure N_2, O_2, Ar and N_2-O_2 mixtures at 0, 30 and 65 ^oC in the pressure range of 0 – 6 atm on LiLSX zeolite. New experimental data successfully passed an integral and a differential thermodynamic consistency test between pure and binary gas isotherms. Three analytical adsorption isotherm models were tested. Pure gas isosteric heats of adsorption and model analysis of the data indicate that the zeolite behaved like a nearly homogeneous adsorbent for Ar adsorption while it exhibited substantial heterogeneity for adsorption of N_2 and milder heterogeneity for adsorption of O_2. Effective mass transfer coefficients (k^e, s^{-1}) for adsorption of pure N_2, O_2 and Ar into LiLSX zeolite were estimated. The over-all mass transfer coefficient for N_2, O_2 and Ar adsorption were comparable in magnitude and a large skin resistance at the adsorbent particle surface was observed.

The measured binary selectivities of N_2 over O_2 were functions of gas phase mole fraction and pressure and the performance of a MOC- RPSA process using a LiLSX zeolite was improved when the adsorbent exhibited higher selectivity of adsorption of N_2 over O_2. The results of a literature search (1995 – 2015) for experimental data on binary and ternary gas adsorption selectivity and their estimation from the corresponding pure gas adsorption isotherms by Ideal Adsorbed Solution Theory (IAST) are summarized which indicate the selectivity of adsorption of a component of a binary or a ternary gas mixture can be a complex function and it must be experimentally measured for reliable design of adsorptive gas separation processes.

Chapter 1

Introduction

Chronic Obstructive Pulmonary Disorder (COPD) is a group of lung diseases including emphysema, chronic bronchitis, pulmonary fibrosis and in some cases asthma. It primarily makes it difficult to breathe due to blockage of bronchial airways and is the third leading cause of death in United State in 2015.[1] The World Health Organization (WHO) estimates that more than 3 million people died because of COPD per year and by 2030 COPD will be the third leading cause of death in the world. The main cause of COPD is tobacco smoking and other risk factors include air pollution, smoke from biomass fuel or wood, dust, chemicals and frequent lower respiratory infections during childhood.[2] COPD cannot be cured but the effective treatments are available that include smoking cessation, medications, pulmonary rehabilitation and oxygen therapy.[3] Though the symptoms and the complications of COPD can be treated by medications, the appropriate use of supplemental oxygen can improve the quality of life, prolongs the lives of these pateients and improve cardiovascular health.[3]

Separation of gas mixtures by selective adsorption has found numerous commercial applications in the chemical, petrochemical, environmental, medical, and electronic gas industries.[4] The separation of air for direct production of 90% O_2 for use by COPD patients by employing a PSA process has been a very successful application in recent years. RPSA process using total cycle times of less than 10 seconds are generally used for this application. A stationary medical oxygen concentrator (MOC) for oxygen therapy typically produces about 1 to 8 standard liters per minute (SLPM) of 90%

oxygen by RPSA. A portable MOC deliver smaller flow rates (< 1 SLPM). Figure 1-1 reproduces the data from reference 5 which shows the market for MOCs producing 1 to 8 litres/min of ~ 90 % O_2 from compressed ambient air is rapidly growing and the global market in 2017 is valued at ~ $2 billion.[5] Figure 1-2 shows the result of a technical article search for gas separation, air separation and MOC by PSA in last twenty years (1996-2015). The figure also demonstrates that the work of PSA-based MOC is few in the literature. Figure 1-3 shows a summary of the languages used on MOC by PSA.

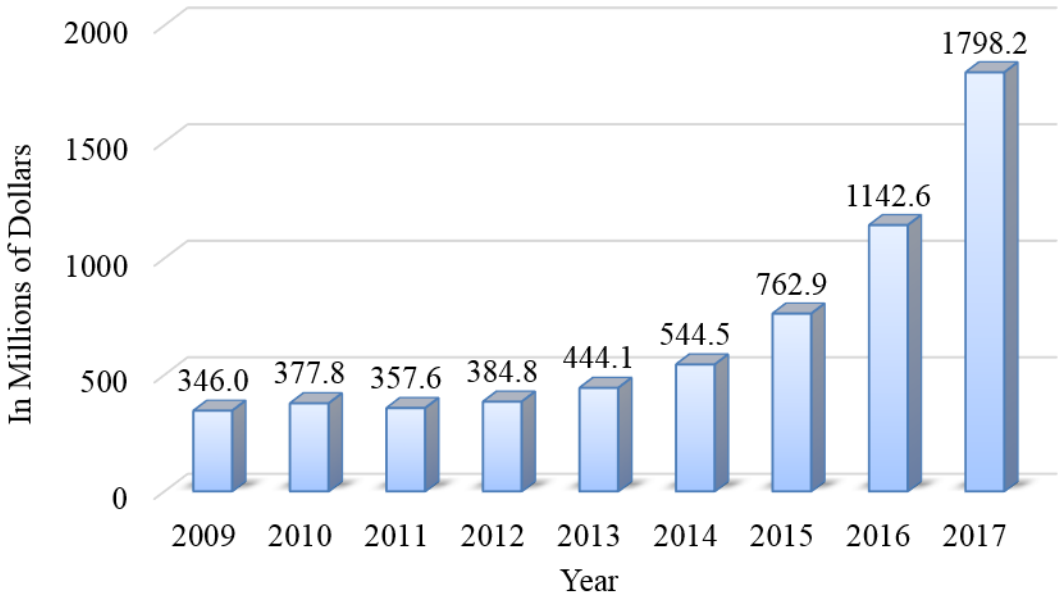

Figure 1-1. Oxygen concentrator market shipments forecasts, dollars, worldwide, 2011-2017.[5]

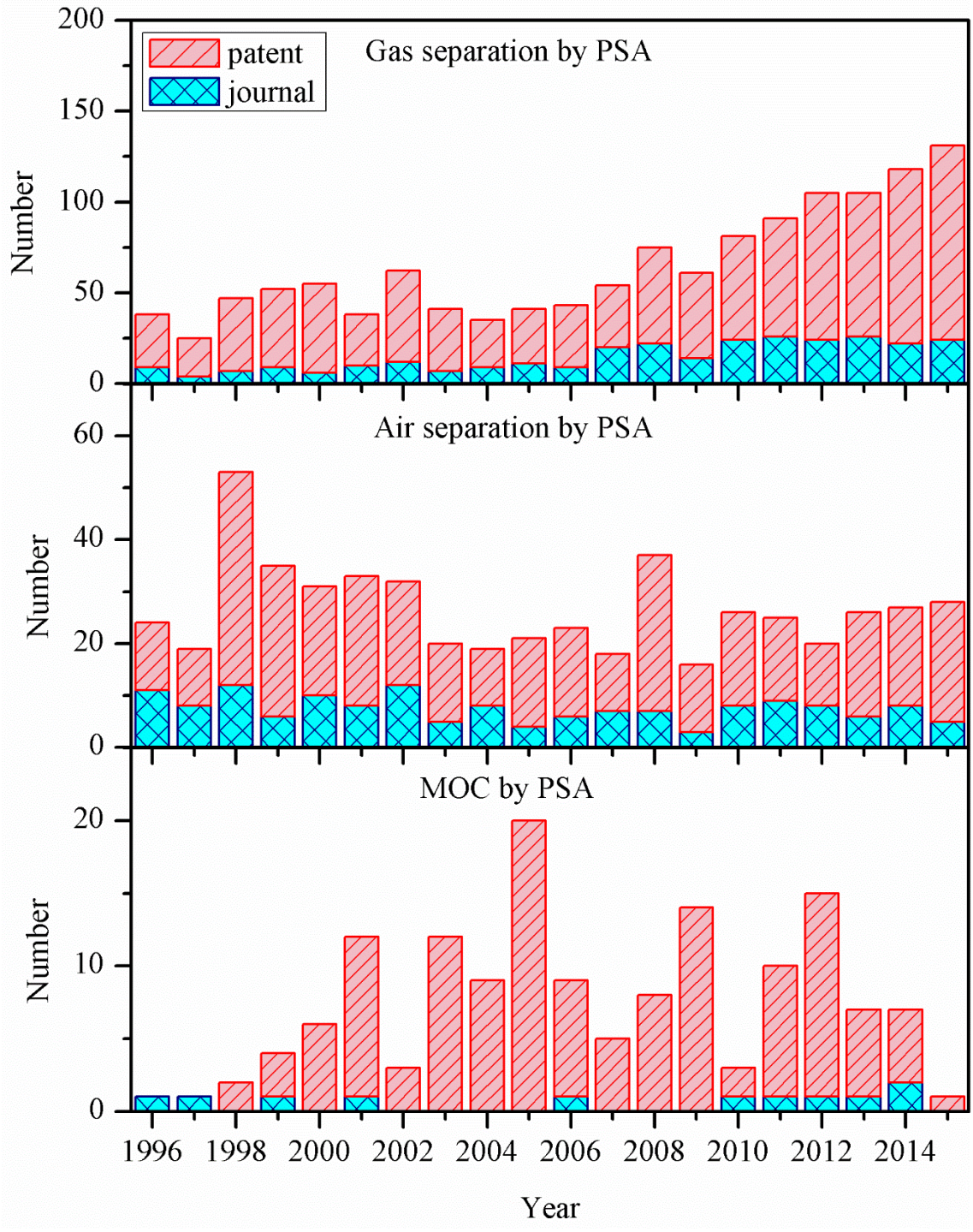

Figure 1-2. The result of literature search in the last twenty years using key word “gas separation by PSA”, “air separation by PSA” and “MOC by PSA”. (Database: SciFinder, published in any language)

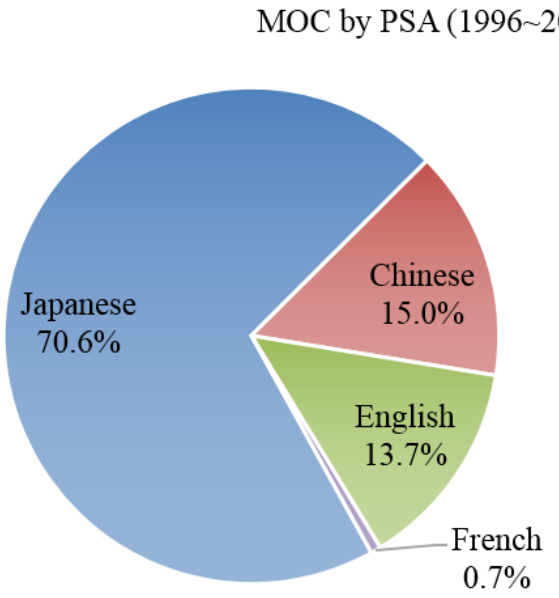

Language	Number of publication
Japanese	108
Chinese	23
English	21
French	1

Figure 1-3. Technical articles of MOC by PSA process in different languages.

1.1 Rapid pressure swing adsorption technology

A RPSA process uses a packed column of the zeolite which selectively adsorbs N_2 from air producing the O_2 enriched product gas. A fast cycle time of 3 – 10 seconds is used. Many zeolites (type A, type X and mordenite) have been used for air separation commercially. All of these zeolites are highly polar and the exhibit the adsorption selectivity for the component of air in the order N_2>O_2>Ar. [6]

Variations of the classical four-step Skarstron PSA cycle[7] are usually adapted for use in these RPSA schemes which are carried out cyclically, and the adsorbent is regenerated during blowdown and purge for reuse, consisting of four steps as follows:

(a) Adsorption: Selective adsorption of N_2 from compressed air by flowing air at a super-ambient adsorption pressure (P_A) over a packed column of the zeolite to produce an O_2 enriched effluent gas which is partly withdrawn as the product gas.

(b) Blowdown: Counter-current depressurization of column to a near ambient final desorption pressure level (P_D).

(c) Purge: Counter-current back purge of the column at P_D with a part of the O_2 enriched product gas.

(d) Pressurization: Re-pressurization of column from P_D to P_A using either fresh compressed air (co-current) or a part of the O_2 enriched product gas (counter-current) or both.

The key performance variables for RPSA process are product recovery (R) and bed size factor (BSF). R is a measure of efficiency of separation process, while BSF is an indicator of adsorbent requirement for a specific RPSA process under given operating conditions. The key design goals are to lower the adsorbent inventory in the MOC unit in order to produce a compact, light-weight device and raise the O_2 recovery of the process in order to lower the air compressor power, thereby extending battery run-time.

1.2 A novel RPSA unit for medical use at Lehigh University

A RPSA unit was built based on a novel ‘single column enclosed inside a product gas storage tank’ design concept recently. Figure 1-4 shows a photograph of the completely assembled RPSA unit.[8] This unit consists of a single adsorbent column surrounded by

a coaxial gas storage space that is used to store the O_2 enriched effluent gas from step (a). A part of storage gas is withdrawn continuously as the product gas through a separate port.

Major advantages of this novel RPSA process design include compact size, lesser number of switch valves, and easier process control due to the absence of synchronized operation of two or multi-column systems. This introduces more flexibility in selection of individual step times of the RPSA process so that each step can be operated more efficiently.[9] Moreover, this design provides a continuous product withdrawal that is preferred over pulsed product flow offered by many commercial portable units.

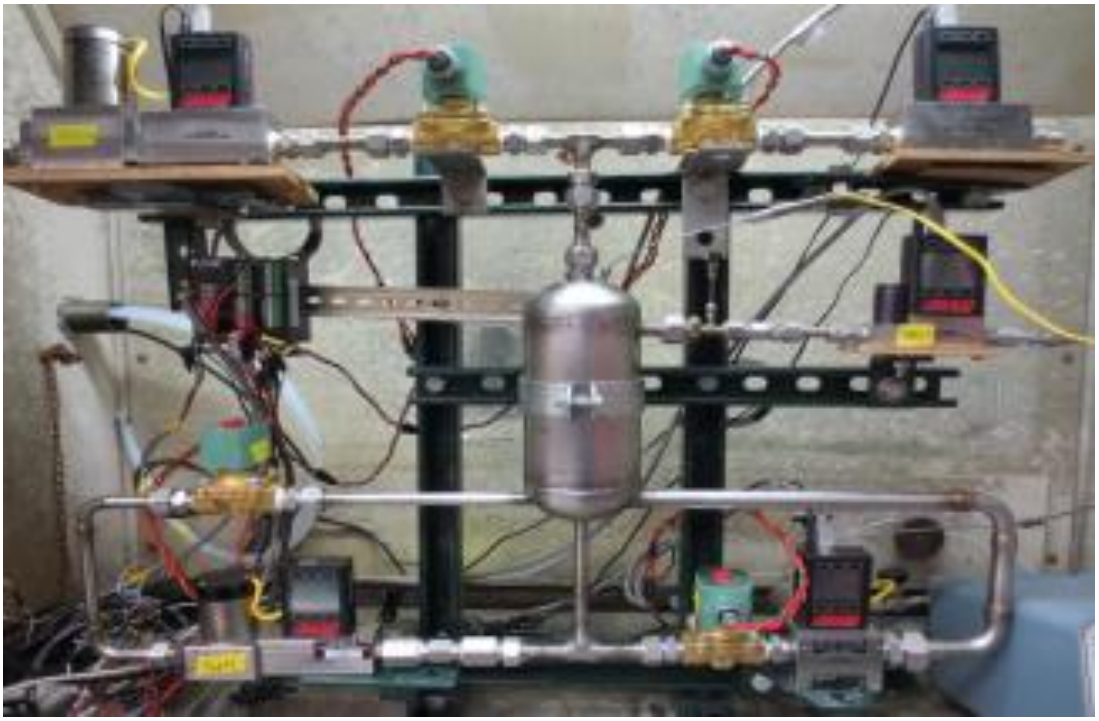

Figure 1-4. Photograph of assembled RPSA unit.[8]

1.3 Key factors for PSA process model

A design of PSA separation scheme is an optimum marriage between a process and a material. A PSA process is usually complex and a rigorous mathematical framework can be formulated to describe such process. The mathematical models of PSA processes require a set of partial differential equations (PDEs) which describe component mass balance, and gas and adsorbed phase energy balance, and the momentum balance within the adsrober. The fundamental understanding of adsorptive properties which govern the PSA performance must be known before the mathematical model can be solved. The PDEs are simultaneous solved using appropriate initial and boundary conditions for the steps.

The quality of a PSA process simulation using a process model highly depends on mathematical model framework, the integration technique used, and the precision of the input data. The simulated result can be very sensitive to small errors in input data for many process. The core input variables for the solutions for the system of practical interest are listed below.[10]

(a) Multicomponent adsorption equilibria:

Adsorption equilibrium is the most fundamental adsorptive property which provides the surface excess under a given conditions (composition, temperature and pressure) and the adsorption selectivity. These data must be experimentally measured or calculated from pure gas equilibrium data correlative multicomponent adsorption models. Even for the data from models, the

experimental measured data are required in order to verify the quality of model prediction.

The measurement of multicomponent adsorption equilibria by various method can be complex, time-consuming, and not accurate. For reliable multicomponent data using in process design, the pure and multicomponent gas adsorption data must obey the thermodynamics consistency.[11-13] Moreover, only the models which pass the thermodynamics consistency test can be used in a process design.

(b) Multicomponent isosteric heats of adsorption:

The heat used in PSA process design is isosteric heat of adsorption that is defined from isotherm at different temperatures. The heat is independent of adsorbate loading for an energetically homogeneous adsorbent. It decreases with increasing adsorbate loading for an energetically heterogeneous adsorbent. The heat determines the temperature inside the column during ad(de)sorption steps which will influence the local equilibrium and kinetics and overall process performance.

The isosteric heat of pure gas can be estimated as a function of adsorbate loadings with thermodynamics correlation using its isotherm data. The same method can be applied on the calculation of multicomponent heat, but it is usually practically impossible due to the difficulty and time-consuming. The isosteric heat of pure and multicomponent can be measured by adsorption calorimetry but an analytical correlation is usually needed for process design.

(c) Multicomponent adsorption kinetics:

The rate of physical adsorption is extremely rapid, of the order of microseconds. However, the transport of adsorbate from the gas phase outside the particle to the adsorption sites inside a crystal is slowed by series and parallel of mass transfer resistances. They are (1) external gas film resistance, (2) diffusional resistance through the meso- and macropores to the surface of the zeolite crystals, (3) diffusional resistance through the micropores of the zeolite crystals to the adsorption sites, and (4) possibly skin resistance at the surfaces of the adsorbent pellet and/or zeolite crystal.[4] A proper understanding of these mass transfer resistances is required to understand the kinetics effects in PSA process.

These adsorptive properties must be available in the entire range of gas pressure, composition, and temperature encountered during the separation processes for better understanding of the adsorption phenomenon, for design or optimization of models. In addition, analytical isotherm models are necessary for practical use and estimation of multi-component heats, and this model must account for adsorbent heterogeneity if needed. However, experimental and theoretical studies of these adsorptive properties are very challenging because of the complication of the adsorption of multicomponent gas mixtures, which have different sizes, polarizabilities and polarities on energetically heterogeneous adsorbents.[10]

1.4 Dissertation research goals

Currently, the commercially preferred adsorbent for air separation by pressure swing, vacuum swing, or pressure-vacuum swing adsorption processes are N_2 selective Li

exchanged X zeolites (standard LiX or low silica LiLSX with or without doping with other cations) because they offer relatively high N_2 working capacity, moderate to high N_2 selectivity over O_2 and Ar, moderate isosteric heats of adsorption for N_2 and O_2, and favorable isotherm shapes for ease of desorption by these processes.[4, 14-16] They are frequently used for both tonnage-scale plants [17, 18] and compact medical oxygen concentrators [19-21] for production of ~ 90+% O_2 from air.

An adsorber engaged in these processes may experience large cyclic swings in gas phase pressures (e.g. 0.2 – 4 atm), adsorbent temperatures (e.g. 10 - 50 ^oC), and gas phase N_2 mole fractions (e.g. 0.05 - 1) during a cycle. Consequently, design and optimization of these processes require reliable experimental data and explicit correlations (model describing pure and mixed gas adsorption isotherm and isosteric heats of adsorption) for data interpolation / extrapolation for all conditions prevailing inside an adsorber.

Surprisingly, only a few articles reporting equilibrium adsorption isotherms of pure N_2 and O_2 on LiLSX zeolite and only two articles reporting a very limited amount of the corresponding binary adsorption isotherms have been published until 2014. There was no published data on adsorptive mass transfer coefficients of N_2 and O_2 for this adsorbent which are required for design of a RPSA -MOC process. It will be a challenge to develop a reliable analytical model and test an available model in process design and optimization without wide range multicomponent gas adsorption data.

Thus, the major goal of this research is to experimentally measure the basic adsorptive properties (thermodynamic equilibrium, kinetics, isosteric heats of adsorption, and

degree of heterogeneity of adsorbent) for adsorption of N_2 and O_2 and their binary mixtures on the zeolite and carry out a rigorous evaluation of analytical models for correlating and predicting the properties.

This dissertation is organized as follows.

In Chapter 2, an isothermal-isobaric column dynamic test apparatus is built to measure equilibrium adsorption isotherms of pure N_2, O_2, Ar and N_2-O_2 binary mixtures at 0, 30 and 65 ℃ in the pressure range of 0 – 6 atm on LiLSX zeolite. The equilibrium adsorption isotherms of pure and multicomponent mixtures are verified by an integral and a differential thermodynamic consistency test. The isosteric heats of pure gas adsorption are calculated using measured isotherm and the degree of heterogeneity for pure N_2, O_2 and Ar is discussed in this chapter as well.

Chapter 3 tests three analytical adsorption isotherm models for energetically homogeneous (Langmuir) and heterogeneous (Toth, Sircar) adsorbents for describing pure gas isotherm data measured in Chapter 2. Estimated binary gas isotherms for this system by these models and the Ideal Adsorbed Solution Theory (IAST) are compared with the corresponding experimental data.

Chapter 4 estimates effective mass transfer coefficients (k^e, s^{-1}) for adsorption of pure gases into small particles of a pelletized sample of lithium exchanged low silica X (LiLSX) zeolite as functions of gas pressure (P) and temperature (T). The experimental column dynamic data is analyzed using a specific protocol based on assumptions of a constant pattern mass transfer zone (MTZ) formation, and a linear driving force model for mass transport. A resistance in series model is used for data interpretation for

isothermal-isobaric mass transport of an adsorbate having a linear adsorption isotherm into a pelletized zeolite particle.

Chapter 5 demonstrates the influence of selectivity on the performance of a MOC-RPSA process experimentally using two LiLSX zeolites which have different selectivity of adsorption of N_2 over O_2. In addition, the results of a literature search (1995 – 2015) for experimental data on binary and ternary gas adsorption selectivity and their estimation from the corresponding pure gas adsorption isotherms by Ideal Adsorbed Solution Theory (IAST) are also summarized in this chapter.

This research will be summarized and concluded in Chapter 6 as well as the recommendation of future work based on the finding of this research.

1.5 Reference

1. National Center for Health Statistics, Health, United States 2015 with Special Feature on Racial and Ethnic Health Disparities. http://www.cdc.gov/nchs/hus/ (June 2016)
2. World Health Organization, Causes of COPD. http://www.who.int/respiratory/copd/causes/en/
3. Mayo Clinic, COPD. http://www.mayoclinic.org/diseases-conditions/copd/home/ovc-20204882
4. Sircar, S.; Myers, A. L., Gas Separation by Zeolite. In *Handbook of zeolite science and technology*, Aurbach, S. M.; Carrado, K. A.; Dutta, P. K., Eds. M. Dekker: New York, N. Y, 2003; pp 1063-1104.
5. WinterGreen Market Research Inc., Oxygen Concentrator Market Opportunities, Market Forecasts, and Market Strategies: 2011-2017. www.wintergreenresearch.com (March 2011)
6. Sircar, S. Air Fractionation by Adsorption. *Sep. Sci. Technol.* **1988,** *23*, 2379-2396.
7. Skarstrom, C. W. Method and apparatus for fractionating gaseous mixtures by adsorption. U.S. Patent 2,944,627, 1960.
8. Rao, V. R.; Kothare, M. V.; Sircar, S. Novel design and performance of a medical oxygen concentrator using a rapid pressure swing adsorption concept. *AlChE J.* **2014,** *60*, 3330-3335.
9. http://www.medicalexpo.com/medical-manufacturer/oxygen-concentrator-2097.html
10. Hartzog, D. G.; Sircar, S. Sensitivity of PSA process performance to input variables. *Adsorption* **1995,** *1*, 133-151.
11. Sircar, S. Excess Properties and Thermodynamics of Multicomponent Gas-Adsorption. *J. Chem. Soc., Faraday Trans. I* **1985,** *81*, 1527-1540.
12. Rao, M. B.; Sircar, S. Thermodynamic consistency for binary gas adsorption equilibria. *Langmuir* **1999,** *15*, 7258-7267.
13. Sircar, S. Gibbsian surface excess for gas adsorption - Revisited. *Ind. Eng. Chem. Res.* **1999,** *38*, 3670-3682.
14. Chao, C. C. Process for Separating Nitrogen from Mixtures Thereof with Less Polar Substances. U.S. Patent 4,859,217, 1989.
15. Leavitt, F. W. Air separation pressure swing adsorption process. U.S. Patent 5,074,892, 1991.
16. Yang, R. T., Sorbents for Application – Air Separation. In *Adsorbents Fundamentals and Applications*, Wiley- Inter-science: Hoboken, N.J, 2003; pp 280-303.

17. Leavitt, F. W. Vacuum Pressure Swing Adsorption Process. U.S. Patent 5,415,683, 1995.

18. Sircar, S.; Naheiri, T.; Fisher, J. R. Oxygen Generation Process and System with Single Adsorber and Single Blower. U.S. Patent 6,146,447, 2000.

19. Kulish, S.; Swank, R. P. Rapid Cycle Pressure Swing Adsorption Oxygen Concentration Method and Apparatus. U.S. Patent 5,827,358, 1998.

20. Ackley, M. W.; Zhong, G. M. Medical Oxygen Concentrator. U.S. Patent 6,551,384, 2003.

21. Jagger, T. W.; Van Brunt, N. P.; Kivisto, J. A.; Lonnes, P. B. Personal Oxygen Concentrator. U.S. Patent 7,121,276, 2006.

Chapter 2

Equilibrium Adsorption Isotherms of Pure N_2, O_2, Ar and N_2-O_2 Binary Mixtures on LiLSX Zeolite - Experimental Data and Thermodynamic Analysis

Small particles of pelletized Lithium - exchanged low silica X (LiLSX) zeolite is frequently used as the preferred adsorbent for production of 90 % O_2 from air by a medical oxygen concentrator (MOC) employing a rapid pressure swing adsorption (RPSA) process concept.[1-3] Interestingly, the published data for equilibrium adsorption of N_2, O_2, Ar, and N_2-O_2 mixtures on LiX or LiLSX zeolites are sporadic in the literature. Thus, the goals of this chapter are to (a) construct an isothermal-isobaric column dynamic test apparatus for measuring equilibrium adsorption isotherms of pure and binary gases, (b) systematically measure pure gas isotherms for N_2, O_2 and Ar and N_2-O_2 binary mixtures on a commercial sample of LiLSX zeolite over an extensive range of conditions of pressure, temperature and mixture compositions, (c) check the thermodynamic consistency of the measured data using integral and differential tests, (d) estimate pure gas isosteric heats of adsorption as functions of adsorbate loadings to evaluate whether the adsorbent is energetically homogeneous or heterogeneous in nature. Thus, this chapter provides a detailed characterization of the equilibrium adsorptive properties for this system which cannot be found elsewhere.

2.1 Literature summary

Table 2-1 and Table 2-2 are the lists of key publications of pure N_2, O_2 and N_2-O_2 mixture adsorption isotherm data, respectively. It also reports the source, the types and the forms of the adsorbent used in these measurements. Most of the reported data were measured on homemade samples of LiX zeolite.It may be seen that nearly all publications report only pure gas N_2 and O_2 adsorption isotherms except two that additionally report a few binary gas adsorption isotherm data for this system. Furthermore, the published data range is very limited, particularly for the binary data, which covers only one pressure and one temperature. Thus, the scarcity of data for this system is evident.

Besides N_2 and O_2, air contains about 1 % of argon which dilutes the gas phase oxygen purity inside a RPSA adsorber as well as the purity of the O_2 - enriched product gas since the O_2 - Ar selectivity on most commercial zeolites is near unity (non-selective vis a vis O_2). The effects of the presence of ~ 1.0 % argon on the over-all performance of a rapid pressure swing adsorption (RPSA) process for production of ~ 90 % oxygen enriched air was recently measured in a continuous RPSA process system.[2] Figure 2-1 shows the steady state process performance of the RPSA system. It plots the bed size factor (BSF; Kg of adsorbent in the unit/ton per day of O_2 product/ day), and percent oxygen recovery (R; moles of O_2 in product gas per mole of O_2 in the feed air per cycle) as functions of total cycle time of the process. BSF and R are the key performance variables for the process. Lower BSF (translates to smaller adsorbent inventory) and higher R (translates to lower air compressor power) are the desired process design goals.

It may be seen from Figure 2-1 that the BSF was increased and the R was decreased by the presence of 1% argon in the feed air of the RPSA process at all total cycle times of the process in the range of the data compared to those for the argon - free feed air.

However, the detrimental effects of the presence of argon in the feed air on the over-all RPSA air separation process performances can be complex and not insignificant. According to the data of Figure 2-1, the presence of 1 % Ar in feed air increases the adsorber size and the air compressor power by ~ 11% and 5%, respectively, when the RPSA process is operated at the conditions of minimum BSF (total cycle time of 5.7 s). This suggests that measurement of basic adsorption characteristics of Ar on the adsorbent used in a RPSA air separation process is needed. Table 2-3 reports the equilibrium adsorption isotherms of argon on various homemade and commercial samples of LiX, LiLSX and Ag-LiX zeolite at different conditions of temperature and pressure.

Figure 2-2 is a comparative plot of the published Ar adsorption isotherms at ~ 300 K in the pressure range of 0 to 0.7 atm on various commercial samples of LiLSX listed in Table 2-3. It shows that there are appreciable differences in the Ar isotherms. Figure 2-3 reproduces the data from reference 27 which shows how the degree of Li+ exchange influence the surface excess of pure nitrogen and the selectivity of N_2 over O_2. These figures suggest that each adsorbent needs to be evaluated separately because of different degrees of Li ion exchange, and variations in nature and amount of binder used as well as method, conditions of reactivation and so on.

Table 2-1. Publications reporting pure N_2 and O_2 adsorption isotherms on LiX or LiLSX zeolites

Authors	Gas		Data range	Zeolite Source
	N_2	O_2		
Baksh et al.[4]	✓	✓	P: 0 – 1; 5 -25 atm T: 298 K	Homemade Beads 8×12 mesh
Chao et al.[5]	✓	✓	P: 0 – 5 atm	homemade
Yang et al.[6]	✓	✓	P: 0 – 1 atm T: 298 K	Homemade powder*
Bajusz et al.[7]	✓	×	P: 0 - 1.1 atm T: 303,318,328, 338 K	homemade
Rege et al.[8]	✓	✓	P: 0 – 1 atm T: 298 K	homemade
Hutson et al.[9]	✓	✓	P: 0 – 1 atm T: 298 K	Homemade powder*
Labasque et al.[10]	✓	×	P: 0 - 1.4 atm T: 293 K	homemade
Jale et al.[11]	✓	✓	P: 0 – 4 atm T: 298 K	Homemade powder* d_P: 1.5-2.0 mm
Shen et al.[12]	✓	✓	P: 0 – 5 atm T: 298 K	Homemade Particle* ≈ 1.5 mm
Yoshida et al.[13]	✓	×	P: 0 - 0.2; 0 – 1.2 atm T: 186,194,200, 216,245,273,398,313 K	Homemade Pellet* d_P: 0.5-2.0 mm
Sircar et al.[14]	✓	✓	P: 0-1.5 atm T: 298 K	commercial (Zeochem)
Kim [15]	✓	✓	P: 0 – 1.3 atm T: 293 K	Homemade Crystalline powder

Authors	Gas		Data range	Zeolite Source
	N_2	O_2		
Bulow et al.[16]	✓	✓	P: 0 – 2 atm T: 298 K	Homemade Li, RELSX (bead) LiLSX(crystal)
Jobic et al.[17]	✓	✓	P: 0 – 1 atm T: 260 K	N/A
Todd et al.[18]	✓	✓	P: 0 – 5 atm T: 273.65, 297.45, 321.85 K	Pellet d_P:1.7 $\pm$0.2mm
Park et al.[19]	✓	✓	P: 0 – 0.8 atm T: 293, 303,313 K	commercial (UOP) sphere 1.7 mm
Pillai et al.[20]	✓	×	P: 0.001 – 1.2 atm T: 303 K	homemade
Zanota et al.[21]	✓	✓	P: 0 – 30 atm T: 288, 303, 318 K	homemade & commercial (Tricat Zeolites GmbH)
Zanota et al.[22]	✓	✓	P: 0 – 30 atm T: 288, 303, 318 K	Homemade Pellet d_P:1.9mm L:3-10mm d_P:3mm L:5-15mm d_P5.6mm L:4mm
*:binderless				

Table 2-2. Publications reporting N_2-O_2 binary mixture adsorption isotherms on LiX or LiLSX zeolites

Authors	Data range	Zeolite	
		Source & Form	Size
Zanota et al.[21]	P: 4 atm T: 303K (5 and 8 compositions for homemade and commercial LiLSX, respectively)	homemade & commercial (Tricat Zeolites GmbH)	N/A
Zanota et al.[22]	P: 4 atm T: 303K (5 compositions)	Homemade pellet	d_P:1.9mm L:3-10mm d_P:3mm L:5-15mm d_P:5.6mm L:4mm

Table 2-3. Summary of published articles on adsorption characteristics of Ar on various types of LiX, LiLSX and Ag-LiX zeolites.

Authors (Adsorbent & test method)	Data range		Adsorptive Properties		Zeolite Source & Form
	P (atm)	T (K)	Isotherm	Isosteric heat**	
Hutson et al.[9] (Ag-LiX, volumetric)	0 – 1.0	298	yes	no	Homemade Powder
Maurin et al.[23] (LiX, calorimetric)	0 – 0.5	300	yes	3.23	Commercial Air Liquid Powder
Park et al.[19] (LiX, gravimetric)	0 – 0.8	293, 303, 313	yes	4.19[a]	Commercial UOP 1.70 mm Bead
Ferreira et al.[24] (Ag-LiLSX, volumetric)	0 – 7.0	288, 298, 308	yes	3.59	Commercial Air Products 1.60 mm Bead
Park et al.[25] (LiX, volumetric)	0 – 9.8	298, 308, 323	yes	3.11[a]	Commercial Zeochem 1.5-1.7 mm Bead

** Henry's Law region (Kcal/mole), [a] extracted from figure in reference

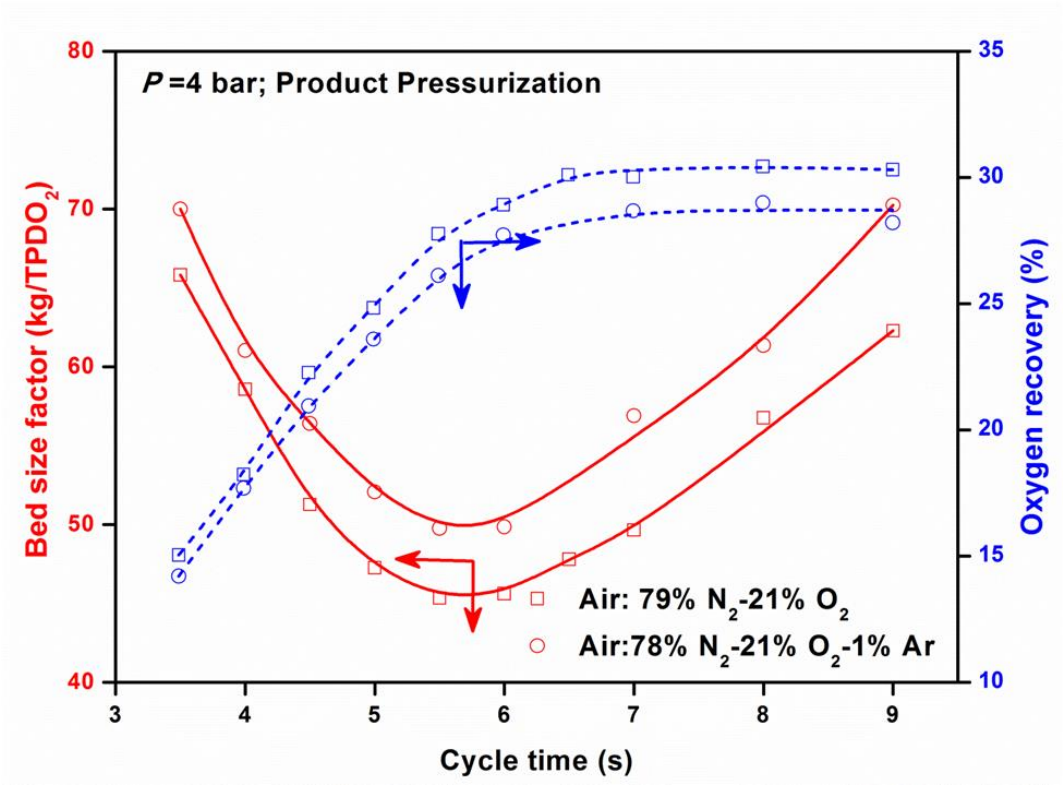

Figure 2-1. Effects of 1% argon in feed air on performance of a RPSA process.[26]

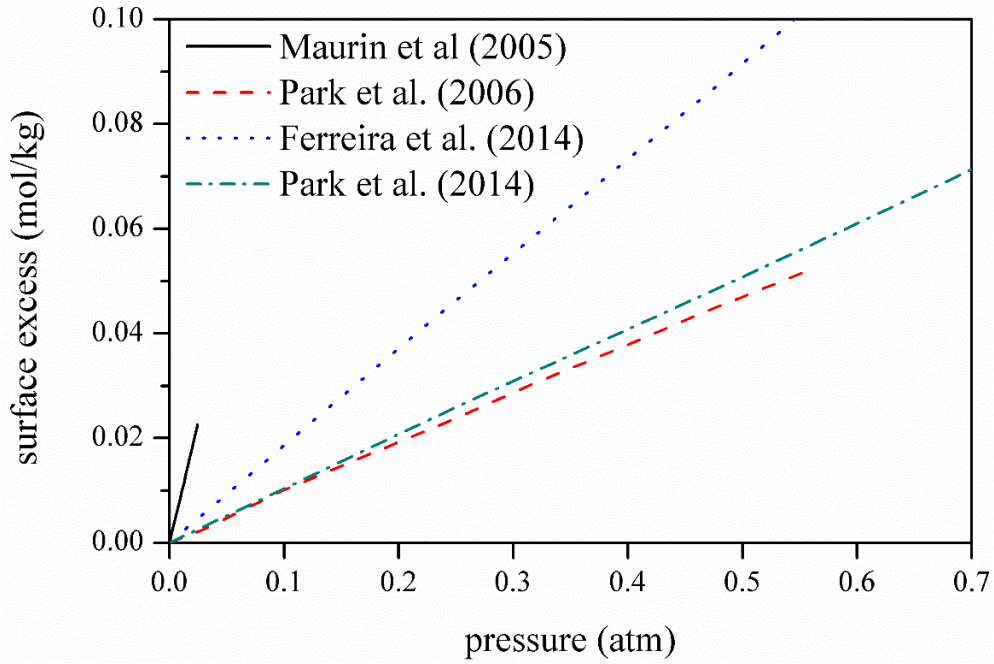

Figure 2-2. Argon adsorption isotherms on various commercial samples of pelletized LiLSX zeolite at ~ 300K.[19, 23-25]

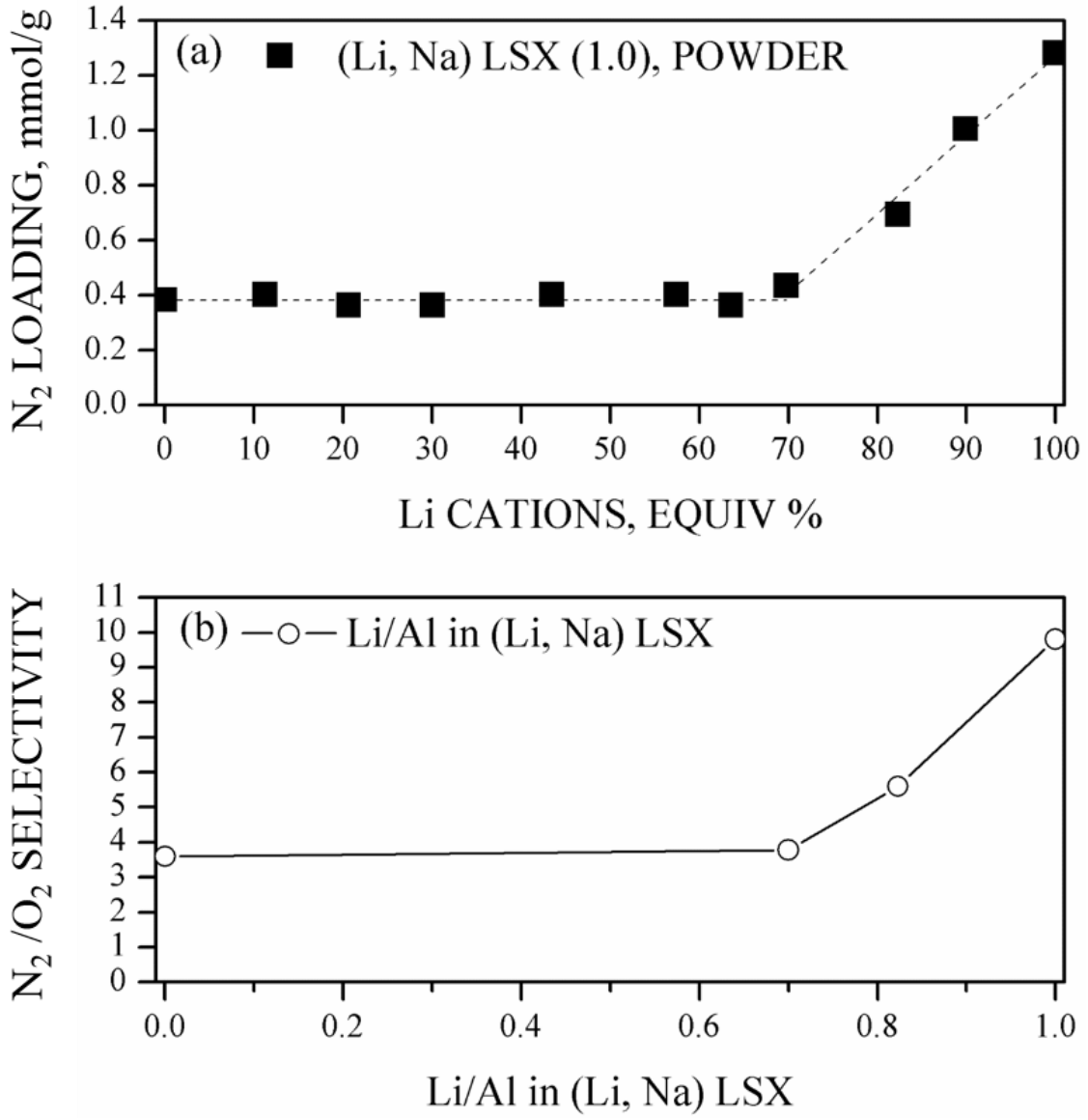

Figure 2-3. Effects of the degree of lithium ion exchange in Na-LSX zeolite: (a) nitrogen capacity; (b) nitrogen-oxygen selectivity.[27]

2.2 Experimental apparatus, measurement protocol and data processing

The LiLSX zeolite (Figure 2-4) was regenerated by heating at 633 K under a flow of dry, CO_2 free flow of N_2 for 8 hours in a separate apparatus shown in Figure 2-5. It was then cooled under N_2 flow and very quickly poured into the adsorption column of Figure 2-6(b). Dry helium was then passed through the column for one hour before the helium void fraction of the column was measured.

Figure 2-4. Commercial LiLSX zeolite used in this work.

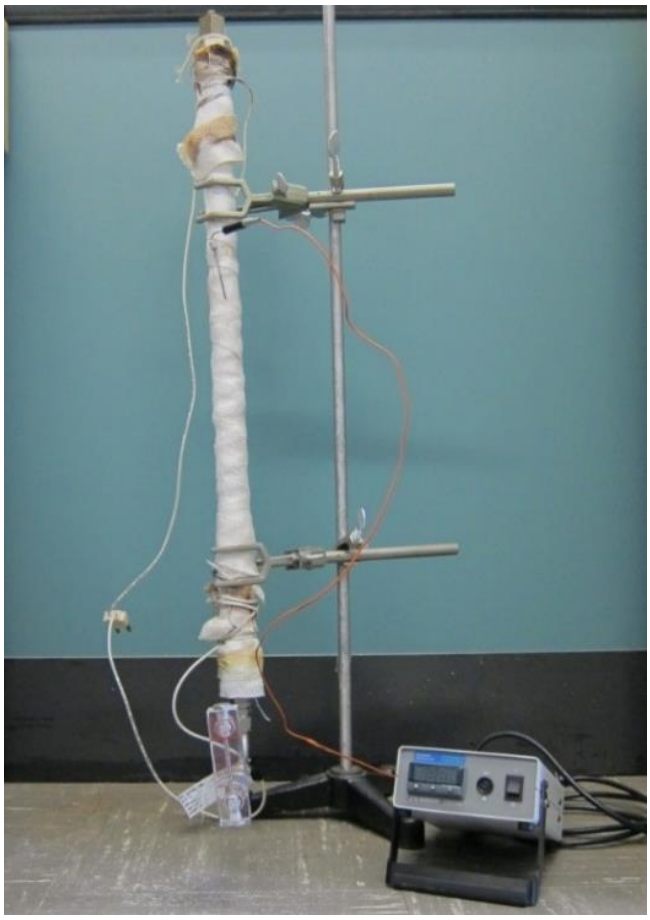

Figure 2-5. Regeneration apparatus

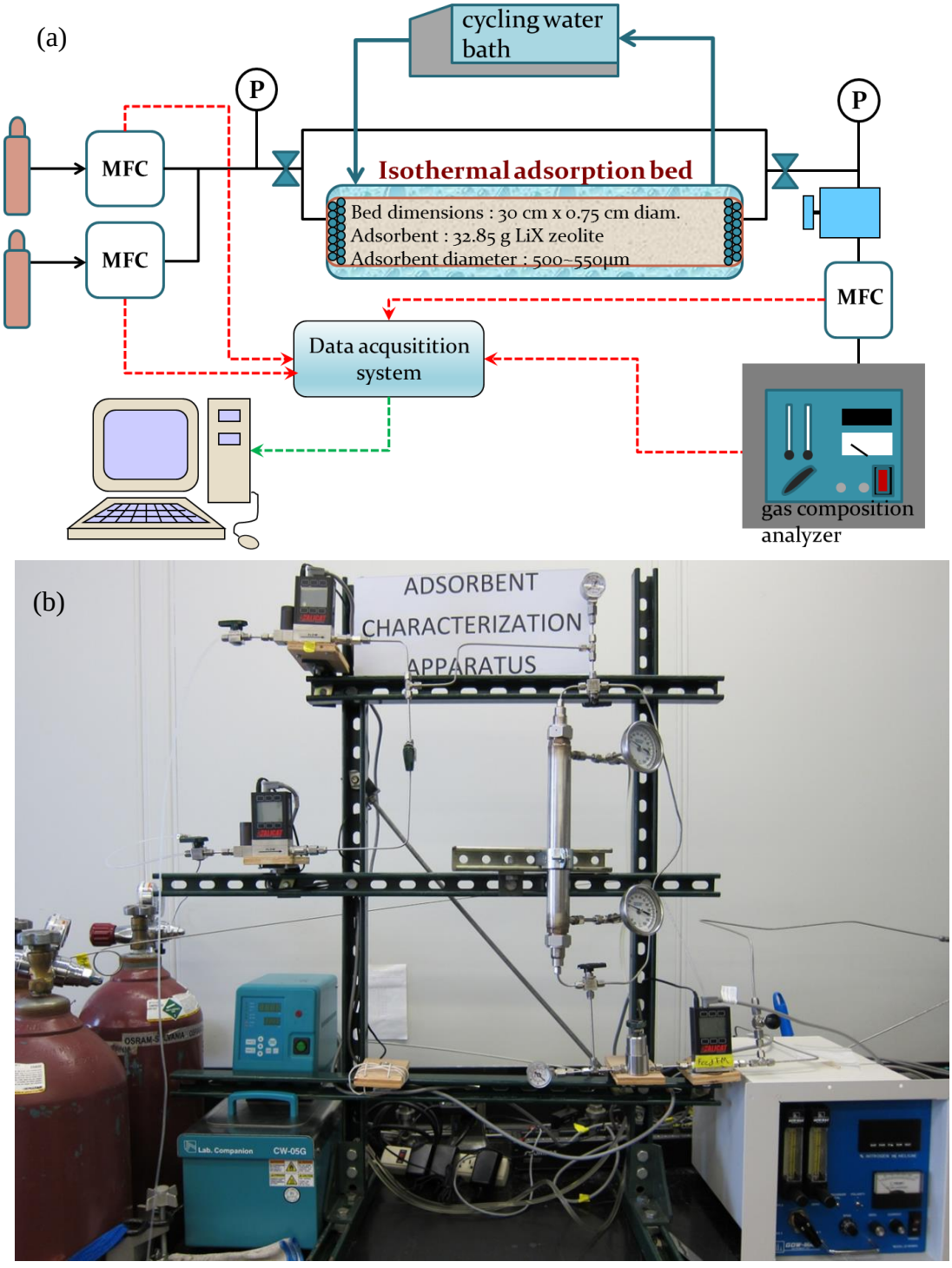

Figure 2-6. (a) Schematic diagram of the column dynamic test apparatus; (b) Photograph of the fully assembled apparatus.

Figure 2-6(a) is a schematic drawing of the isothermal column dynamic test apparatus constructed in our laboratory and used in measuring every adsorptive properties including pure and binary gas isotherm, isosteric heat from pure gas equilibrium data and column dynamic. Figure 2-6 (b) is a photograph of the assembled unit. It consists of a water-jacketed adsorption column (I.D = 1.5 cm, Length = 30 cm) packed with a screened sample of commercial, pelletized LiLSX zeolite (particle diameter = 500 – 550 μm, bulk density = 0.62 g/cm^3, weight =32.8g) obtained from Zeochem Corporation. The helium void fraction in the column was 0.7 cm^3/ cm^3. The column was thermostated at a chosen experimental temperature by circulating water through the jacket at that temperature from a constant temperature bath.

Two mass flow controllers at the feed end of the apparatus controlled the flow rates of the components of the feed gas before mixing and entering the column, and a mass flow meter measured the effluent gas flow rate. A back pressure control valve maintained a constant pressure in the column during a test. The effluent gas composition was continuously monitored using a thermal conductivity analyzer (manufactured by Gowmac Corporation) for N_2 + He and Ar + He mixtures, and a membrane based ZrO_{2000} O_2 analyzer (manufactured by ALPHAOMEGA Instruments) for O_2 + He and O_2 + N_2 mixtures. A data acquisition system (OMB-DAQ-3000 Series, manufactured by OMAGA) was used for continuously gathering and recording all data.

The isobaric and isothermal experiments for measurement of adsorption isotherms of pure gas consisted of equilibrating the column with pure helium (inert gas) at pressure (P, atm) and temperature (T, K), followed by flowing a binary gas mixture of N_2 (or O_2, Ar)

+ He of different compositions at P and T until the column was equilibrated with the feed gas. The same method was used for measurement of adsorption of N_2-O_2 mixtures. The column was equilibrated with pure O_2 at P and T followed by flowing a binary mixture of N_2 + O_2 of different compositions at P and T until the column was equilibrated with the feed gas. The column effluent gas flow rate and composition were measured as a function of time during the process (breakthrough curves).

The pure and binary gas equilibrium adsorption isotherms were estimated in terms of Gibbsian surface excess (GSE) which can be directly estimated unambiguously from the above- described experimental data as follows:[28]

The total specific amount of component *i* (N_i , $\mathrm{moles/g}$) in a packed adsorbent column with a total specific helium void volume of *v* cm^3/ cm^3, when it is equilibrated with an ideal gas mixture (mole fraction of component *i* = y_i) at pressure (P, atm) and temperature (T, K) is given by[28]

$$N_i = n_i^m(P, T, y_i) + v\rho_g y_i \qquad i = 1,2 \tag{2-1}$$

where $n_i^m\ (P, T, y_i)$ is the specific equilibrium GSE (moles/g) of component *i* at P, T and y_i , and $\rho_g = (\mathrm{P/RT})$ is the molar density ($moles/cm^3$) of the ideal gas at P and T.

The component *i* mass balance for an isothermal - isobaric dynamic test, where the column is initially equilibrated with a gas mixture characterized by P, T and y_i^S followed by passage of a feed gas mixture characterized by P, T, and y_i^F, where y_i^S and $y_i^F \left(> y_i^S \right)$ are, respectively, the mole fractions of component *i* in the initial equilibrating and feed gases, can be written as:

$$Q^F y_i^F t - \int_0^t Q^E(t) \cdot y_i^E(t) dt = \left[n_i^{mF}(P,T,y_i^F) - n_i^{mS}(P,T,y_i^S)\right] + \left[v\rho_g\left(y_i^F - y_i^S\right)\right] \quad (2\text{-}2)$$

Where Q^F and $Q^E(t)$ are, respectively, the specific feed gas and column effluent gas flow rates at time t (mole/g/s), $y_i^E(t)$ is the mole fraction of component *i* in the effluent gas at time t (s). Eq. (2-1) is used to derive Eq. (2-2).

It may be seen from Eq. (2-2) that the equilibrium GSE for component *i* at the feed gas conditions (n_i^{mF}) can be estimated by the dynamic test if the GSE for that component at the conditions of initial equilibration (n_i^{mS}) is known. For the case of pure N_2, O_2 or Ar GSE measurement, $n_{N_2}^{mS} = n_{O_2}^{mS} = n_{Ar}^{mS} = n_{He}^{mS} = 0$, when the initial equilibrating gas is pure non-adsorbing helium, and for the case of binary N_2 + O_2 GSE measurement, $n_{O_2}^{mS} =$ GSE for pure O_2 at P and T, and $n_{N_2}^{mS} = 0$.

It should be emphasized here that the experimentally measured adsorption isotherms for pure and binary gases actually report Gibbsian surface excesses (GSE).[28] We estimated the upper bounds of differences between the GSE and actual amount adsorbed for the present system by assuming that the entire micro-pore volume within the zeolite crystal constitutes the adsorbed phase under all conditions of measurements.[28] This indicated that the maximum possible differences under the worst case scenario for the reported data (highest pressure and lowest temperature) were less than ~ 4 % and ~ 25 % for N_2 and O_2, respectively. The actual differences will be much smaller. Therefore, the traditional practice of referring to the GSE as amount adsorbed is justified in the present case.

2.3 Experimental pure and binary gas equilibrium adsorption isotherms for N_2, O_2 and Ar on LiLSX zeolite

The mass balance protocol was employed in terms of GSE as variables (Eq. (2-2)) to estimate pure gas (N_2, O_2 and Ar) GSE isotherms for component *i* [n_i^{mo} as functions of P at constant T] and N_2-O_2 binary gas GSE isotherms for component *i* [n_i^m as functions of y_i at constant P and T] for N_2, O_2 and Ar on LiLSX zeolite at three temperatures (273.1, 303.1, and 338.1 K) and in the pressure range of 0 – 6 atm. A large volume of data was gathered.

2.3.1 Pure gas isotherms

Figure 2-7 shows the adsorption isotherms (n^m vs P at constant T) of pure N_2, O_2 and Ar on the LiLSX zeolite sample at three temperatures (273.1, 303.1, and 338.1 K) in the pressure range of 0 – 6 atm, and Figure 2-8 shows the corresponding isotherms at low pressures. All gases exhibited a Henry's law region at low pressures where the GSE was a linear function of pressure [$n_i^{mo} = K_i(T) \cdot P$; when $P \to 0$, where $K_i(T)$ is the Henry's law constant for pure gas *i* at temperature T].[28] All isotherms are Type I according to the Bruauner classification.[29] The pure gas isotherm data points can be found in tabulated form in Appendix A for easy access.

It should be mentioned here that the isotherms reported in this work cannot be justifiably compared with others reported in Table 2-1 because the amounts of N_2 and O_2 adsorbed on the zeolite sample depend on various factors such as, degree of Li exchange in the zeolite, amount of binder in the final product, types and conditions of regeneration, etc.[14], which may be different for different samples of LiX described in Table 2-1.

The isosteric heat of adsorption (q_i^*) of pure gas i in the Henry's law region is thermodynamically given by[28]

$$\frac{d \ln K_i}{d\left(\frac{1}{T}\right)} = \frac{q_i^*}{R} \quad K_i = K_i^* exp\left(\frac{q_i^*}{RT}\right) \tag{2-3}$$

where Ki* is a constant and R is the gas constant.

Table 2-4 gives the values of K_i and q_i^* obtained from the data of Figure 2-8. The Henry's law isosteric heat of adsorption of N_2 is nearly double of that for O_2 and Ar demonstrating that N_2 is much more strongly adsorbed than O_2 and Ar on LiLSX. This is caused by a stronger quadrupole moment – ion interaction between N_2 and LiLSX zeolite than that for O_2 and Ar.

Table 2-4. Thermodynamic properties in the Henry's law region on LiLSX zeolite

Temp.	Ki (mol/kg/atm)			q_i^* (Kcal/mol)			S_{O_2-Ar}	$S_{N_2-O_2}$
(K)	N_2	O_2	Ar	N_2	O_2	Ar		
273.1		0.297	0.262				1.15	
303.1		0.175	0.156	5.87	3.22	2.75	1.01	
328.1	0.611	0.110						5.55
338.1	0.458	0.096	0.0984				0.98	4.77

2.3.1 Binary gas isotherms

Figure 2-9 plots the adsorption isotherms for N_2 and O_2 from binary mixtures of these gases at different temperatures at total gas pressures of 1.0 and 6.0 atm, respectively. The component GSEs are plotted as functions of equilibrium compositions at a constant P and T. The experimental binary gas isotherm data points are given in tabulated form in Appendix A for easy access.

The binary component isotherms shown by Figure 2-9 are typical for systems with Type I pure gas adsorption isotherms where component 1 (N_2) is more selectively adsorbed than component 2 (O_2).

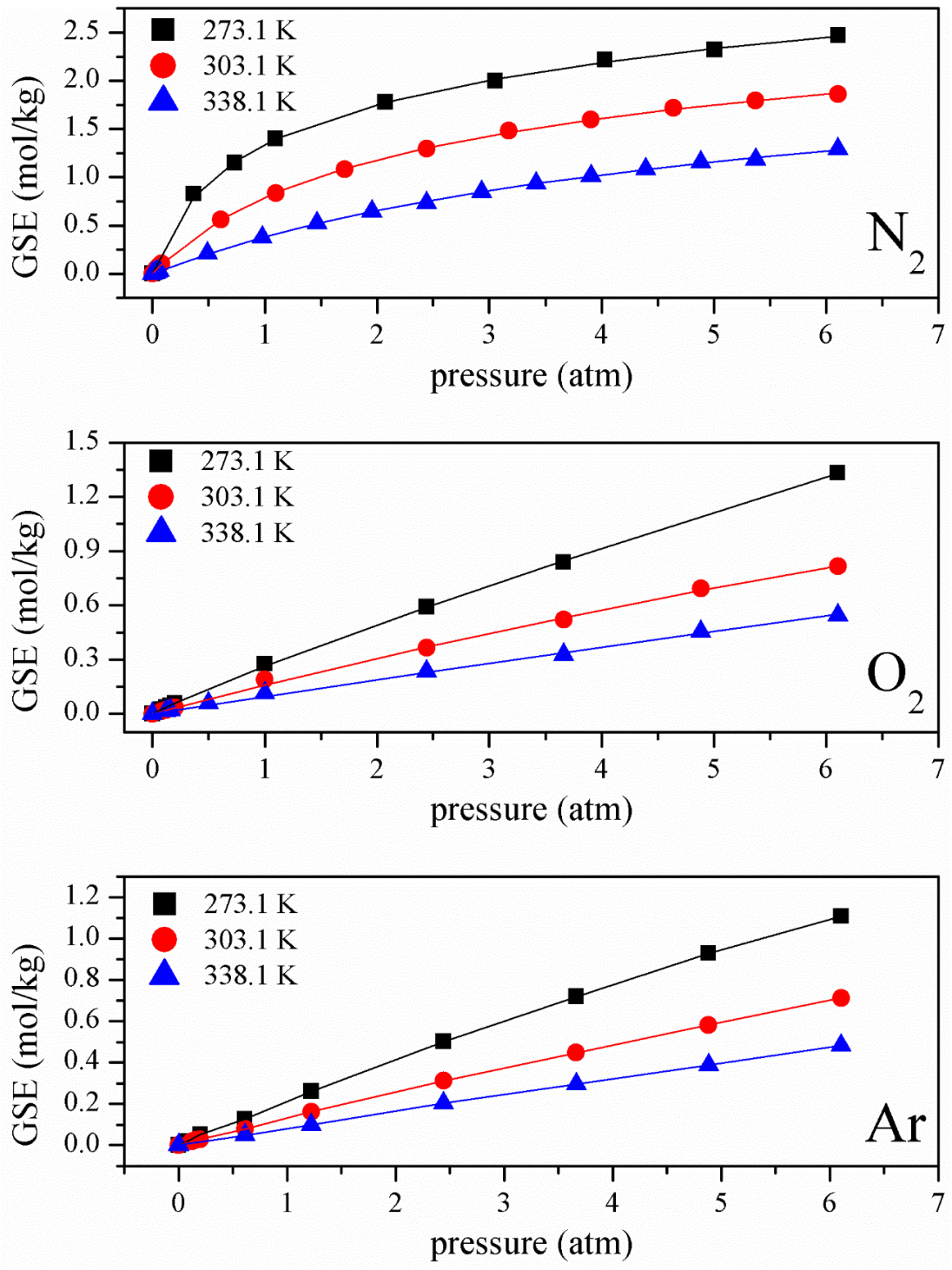

Figure 2-7. Pure gas adsorption isotherms on LiLSX zeolite at three temperatures in full pressure range

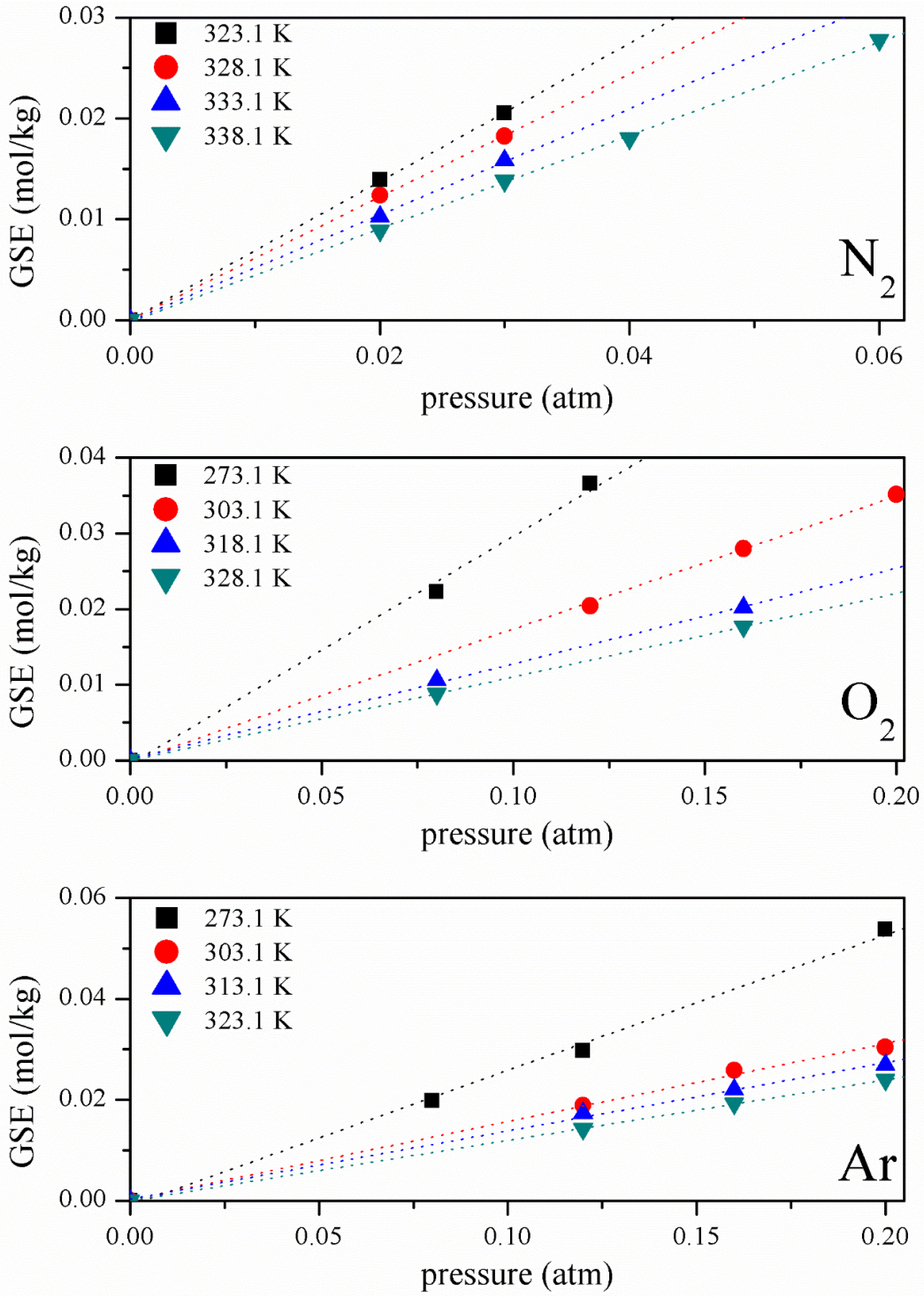

Figure 2-8. Pure gas adsorption isotherms on LiLSX zeolite at three temperatures in low pressure range.

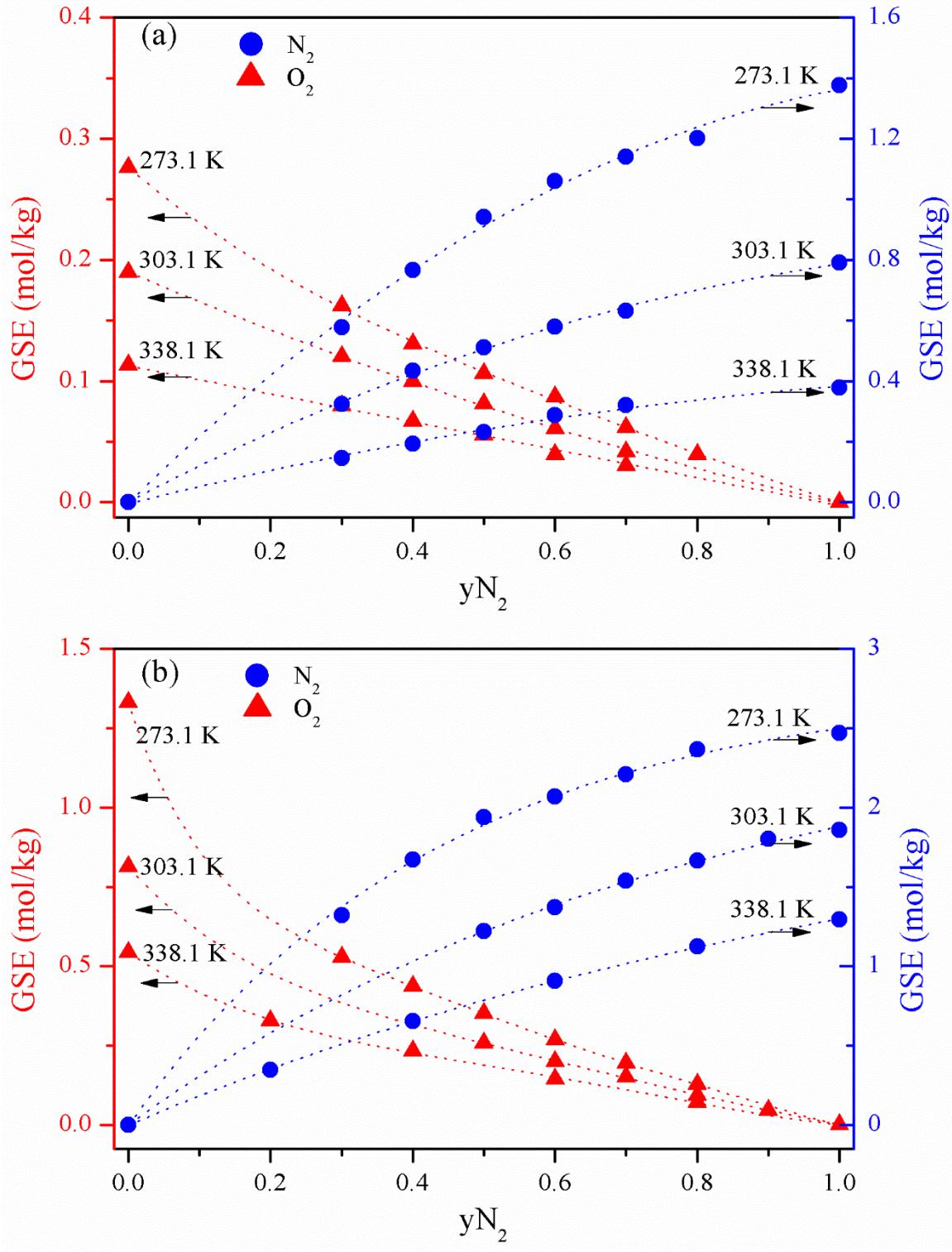

Figure 2-9. Binary gas adsorption isotherms for N_2 + O_2 mixtures at three different temperatures and two different total gas pressures: (a) 1 atm, (b) 6 atm.

2.4 Binary gas selectivity of adsorption

The selectivity of adsorption of component 1 over component 2 of a binary gas mixture (S_{12}) is defined in the GSE framework by[28]

$$S_{12} = \frac{n_1^m \cdot y_2}{n_2^m \cdot y_1} \tag{2-4}$$

The binary gas isotherms in the low pressure region (P→0) also follow Henry's law for the mixture[29] [$n_i^m(P,T,y_i) = K_i(T) \cdot P \cdot y_i$; when $P \to 0$]. Hence, the binary selectivity in the Henrys law region (S_{12}^*), according to Eq. (2-3) and (2-4), is given by

$$S_{12} = \frac{K_1^*}{K_2^*} exp\left[\frac{(q_1^* - q_2^*)}{RT}\right] \tag{2-5}$$

The last two columns of Table 2-4 show that the Henry's law region selectivity of adsorption of O_2 over Ar ($S_{O_2-Ar} = K_{O_2}/K_{Ar}$) is nearly unity in the data range indicating that these two gases cannot be practically separated by LiLSX zeolite, while the selectivity of adsorption of N2 over O2 ($S_{N_2-O_2} = K_{N_2}/K_{O_2}$) is large enough for separation of these gases.

Table 2-5 shows estimated values of S_{12} for each measured binary gas isotherm data point. The following observations can be made for the system of interest:

a) S_{12} for a given P and y_1 decreases with increasing T.

b) S_{12} at constant P and T remains approximately constant or decreases weakly as y_1 is increased. The effect is more pronounced at lower T.

c) S_{12} at constant T and y_1 decreases as P (or n_1) is increased.

Observation (a) is a general principle of binary gas adsorption which can be very easily demonstrated for binary gas adsorption in the Henry's law region. According to Eq.(2-5), $\left[\frac{dS_{12}^*}{dT}\right] < 0$, when $q_1^* > q_2^*$. Observations (b) and (c) are typically exhibited when the adsorbent is energetically heterogeneous for at least one of the components of a binary gas mixture.[30]

Table 2-5. Binary N_2 (1) + O_2 (2) gas adsorption selectivity on LiLSX zeolite at constant P and T.

273.1K				303.1K				338.1K			
P=1 atm		P=6 atm		P=1 atm		P=6 atm		P=1 atm		P=6 atm	
y_1	S_{12}	y_1	S_{12}	y_1	S_{12}	y_1	S_{12}	y_1	S_{12}	y_1	S_{12}
0.00		0.00		0.00		0.00		0.00		0.00	
0.30	8.31	0.30	5.83	0.30	6.30	0.50	4.75	0.30	4.26	0.20	4.21
0.40	8.77	0.40	5.74	0.40	6.51	0.60	4.57	0.40	4.32	0.40	4.22
0.50	8.80	0.50	5.52	0.50	6.32	0.70	4.37	0.50	4.14	0.60	4.17
0.60	8.12	0.60	5.13	0.60	6.33	0.80	4.48	0.60	4.89	0.80	3.91
0.70	7.89	0.70	4.85	0.70	6.46	0.90	4.26	0.70	4.58	1.00	
0.80	7.71	0.80	4.66	1.00		1.00		1.00			
1.00		1.00									

2.5 Thermodynamic consistency of equilibrium adsorption data

The pure gas and binary isotherm data presented in this work were subjected to an integral and a differential thermodynamic consistency test.[31] These tests provide relationships (identities) between thermodynamic quantities which can be independently estimated only from pure gas isotherms of the components of a binary mixture and only

from a binary gas isotherm. The relevant identities using the GSE framework are given as follows:

Integral Test:

$$\frac{\phi_2^0(P) - \phi_1^0(P)}{RT} = \int_0^1 \frac{[n_1^m y_2 - n_2^m y_1]}{y_1 y_2} dy_1 \; ; \qquad (2\text{-}6)$$

$$y_1 + y_2 = 1 \;\; constant\; P, T$$

$$\frac{\phi_i^0(P)}{RT} = -\int_0^P \frac{n_i^{m0}(P)}{P} dP \quad constant\; T \qquad (2\text{-}7)$$

Differential Test:

$$n_1^{m0}(P,T) = n^m(P,T,y_1) + P\frac{\delta}{\delta P}\left[\int_{y_1}^1 \left\{\frac{n_1^m y_2 - n_2^m y_1}{y_1 y_2}\right\}_{P,T} dy_1\right]_{T,y_1} ; \qquad (2\text{-}8)$$

$$n^m = n_1^m + n_2^m$$

$$n_2^{m0}(P,T) = n^m(P,T,y_1) - P\frac{\delta}{\delta P}\left[\int_0^{y_1} \left\{\frac{n_1^m y_2 - n_2^m y_1}{y_1 y_2}\right\}_{P,T} dy_1\right]_{T,y_1} ; \qquad (2\text{-}9)$$

$$n^m = n_1^m + n_2^m$$

Where $\phi_i^o(P)$ is the surface potential of pure gas i at P and T. It can be calculated from the pure gas isotherm of component i by the integral of Eq. (2-7). Thus, the quantity on the left hand side of Eq. (2-6) can be estimated from the pure gas isotherms of component 1 and 2 only. The quantity on the right hand side of Eq. (2-6) can be estimated using a binary isotherm of components 1 and 2 at constant T and P only. Hence Eq. (2-6) checks a thermodynamic consistency between pure gas and binary gas isotherms.

The quantities on the left hand sides of Eqs. (2-8) and (2-9) can be obtained from the pure gas isotherms only. The quantities on the right hand sides of these equations can be

estimated from binary gas isotherms at constant P and T, and at constant T and y_1 only. Hence these identities check thermodynamic consistency between pure gas and binary gas isotherms.

The data presented in Figure 2-8 and Figure 2-9 were used to apply the above-described consistency tests. Figure 2-10 shows plots of the integrand of Eq. (2-7) as a function of P for pure nitrogen and oxygen. The area under the curves between P=0 and a chosen pressure gives a corresponding value of $(\phi_i^0(P)/RT)$. Figure 2-11 is the plots of the integrands of right hand side of Eq. (2-6) as a function of y_1 at constant P and T. The area under the curves give the values of right hand side of Eq. (2-6).

The integrands of right hand side of Eq. (2-8) can be estimated from the areas under the curves of Figure 2-11 between a different chosen y_1 and y_1=0. The values of this integrals are functions of P at different y1 at constant T as illustrated in Figure 2-12.

Table 2-6 and Table 2-7, respectively, report the results of the integral and the differential consistency tests. It can be concluded that the data presented in this work pass both thermodynamic consistency tests. It should be mentioned that the binary isotherm data at 4 atm and 303 K, reported in Table 2-2, was also tested by the integral consistency test.

Table 2-6. Integral consistency test of pure and binary gas isotherm data for N_2 and O_2 on LiLSX.

Temperature (K)	P = 1 atm		P = 6 atm	
	Left hand side Eq. (2-6) (mol/kg)	Right hand side Eq. (2-6) (mol/kg)	Left hand side Eq. (2-6) (mol/kg)	Right hand side Eq. (2-6) (mol/kg)
273.1	1.72	1.68	3.96	3.94
303.1	0.77	0.85	2.37	1.98
338.1	0.31	0.36	1.23	1.21

Table 2-7. Differential consistency test of pure and binary gas isotherm data for N_2 and O_2 on LiLSX zeolite.

Temperature (K)	y_1	P=1 atm		P=6 atm	
		Right hand side Eq. (2-8) (mol/kg)	Left hand side Eq. (2-8) (mol/kg)	Right hand side Eq. (2-8) (mol/kg)	Left hand side Eq. (2-8) (mol/kg)
273.1	0	1.36	1.38	2.21	2.47
	0.2	1.28		2.01	
	0.4	1.32		2.31	
	0.6	1.40		2.45	
	0.8	1.32		2.52	
303.1	0	0.77	0.79	1.34	1.86
	0.2	0.79		1.40	
	0.4	0.83		1.56	
	0.6	0.82		1.70	
	0.8	0.81		1.81	
338.1	0	0.42	0.38	1.11	1.29
	0.2	0.43		1.09	
	0.4	0.43		1.18	
	0.6	0.43		1.24	
	0.8	0.41		1.29	

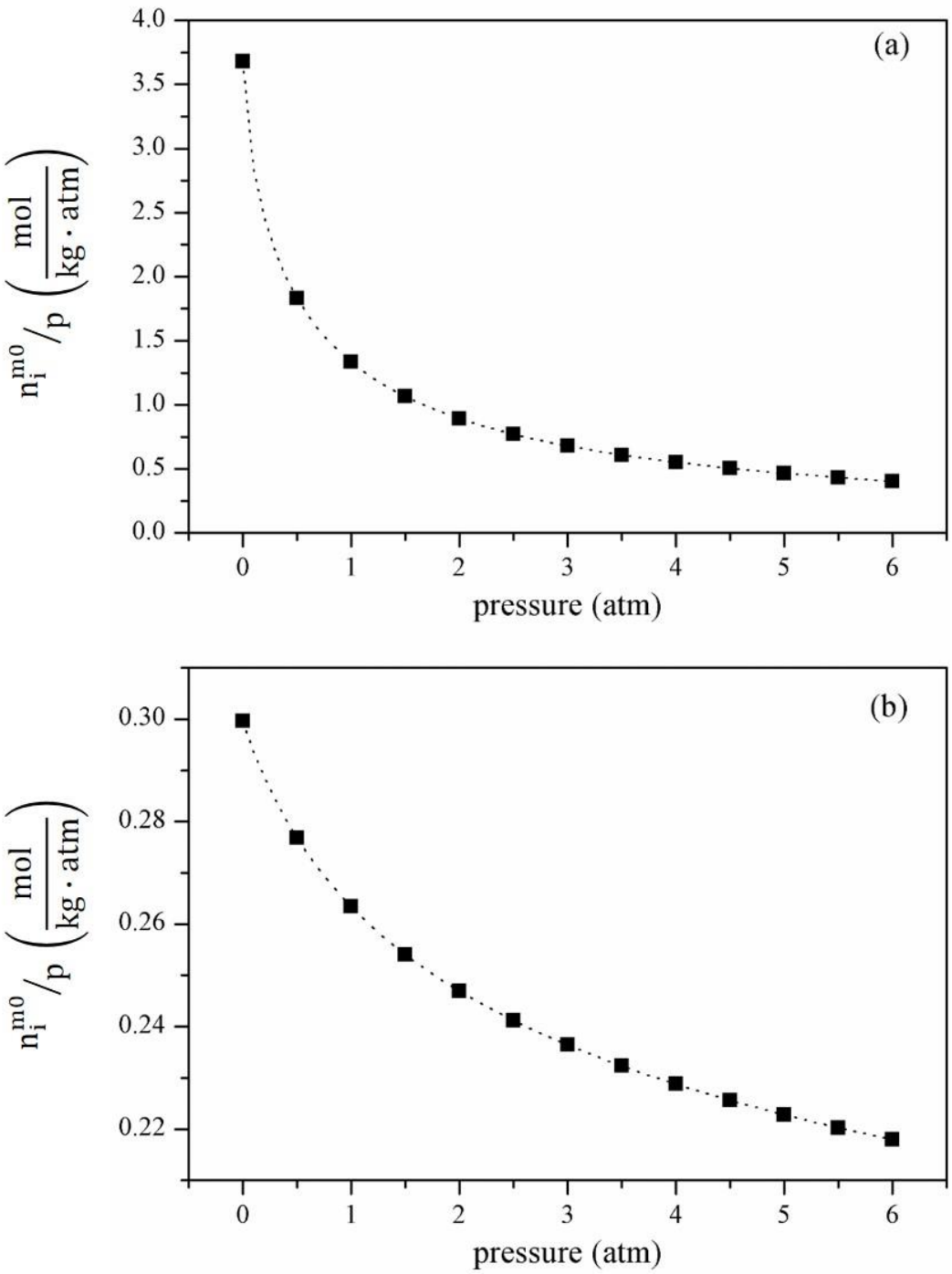

Figure 2-10. Plots of integrands of Eq. (2-7) at for calculation of pure gas surface potentials at 273.1K on LiLSX zeolite: (a) nitrogen; (b) oxygen.

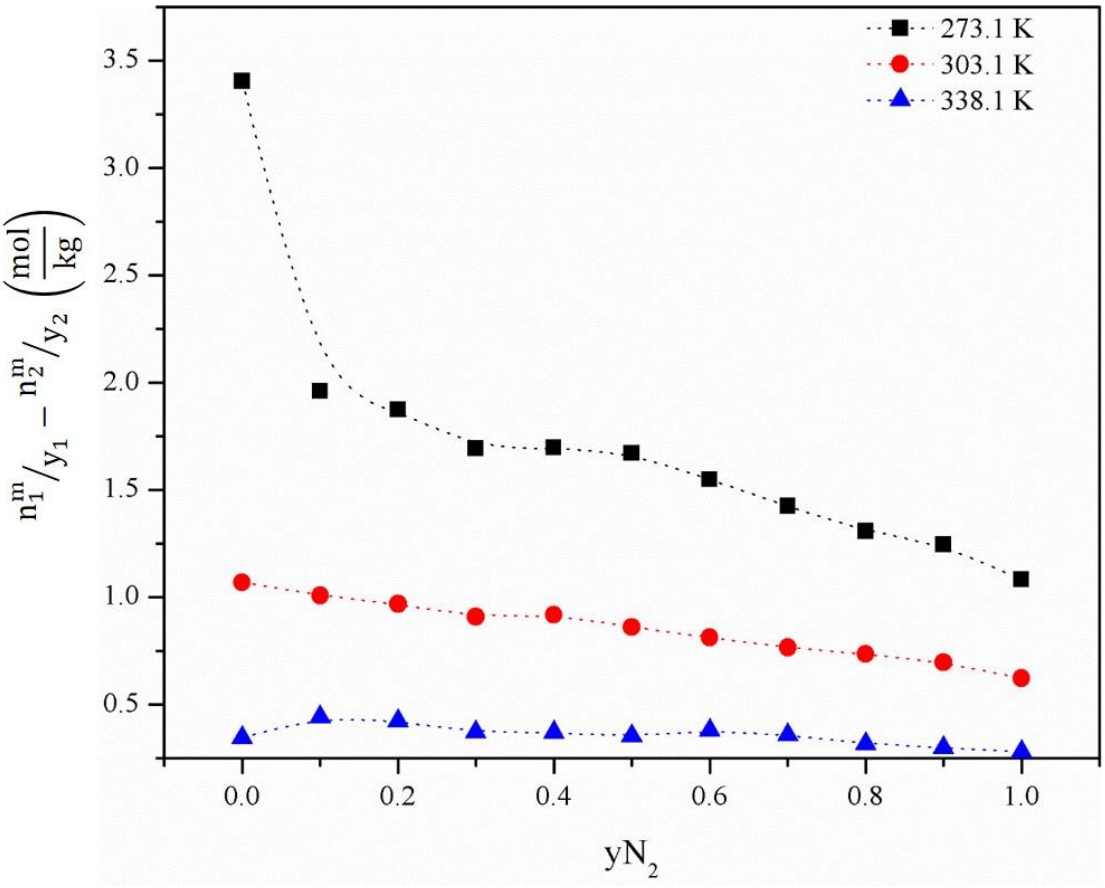

Figure 2-11. Plots of integrands of Eq. (2-6) at 1 atm for calculation of differences in pure gas surface potential from $N_2(1)$ + $O_2(2)$ binary adsorption equilibrium data on LiLSX zeolite.

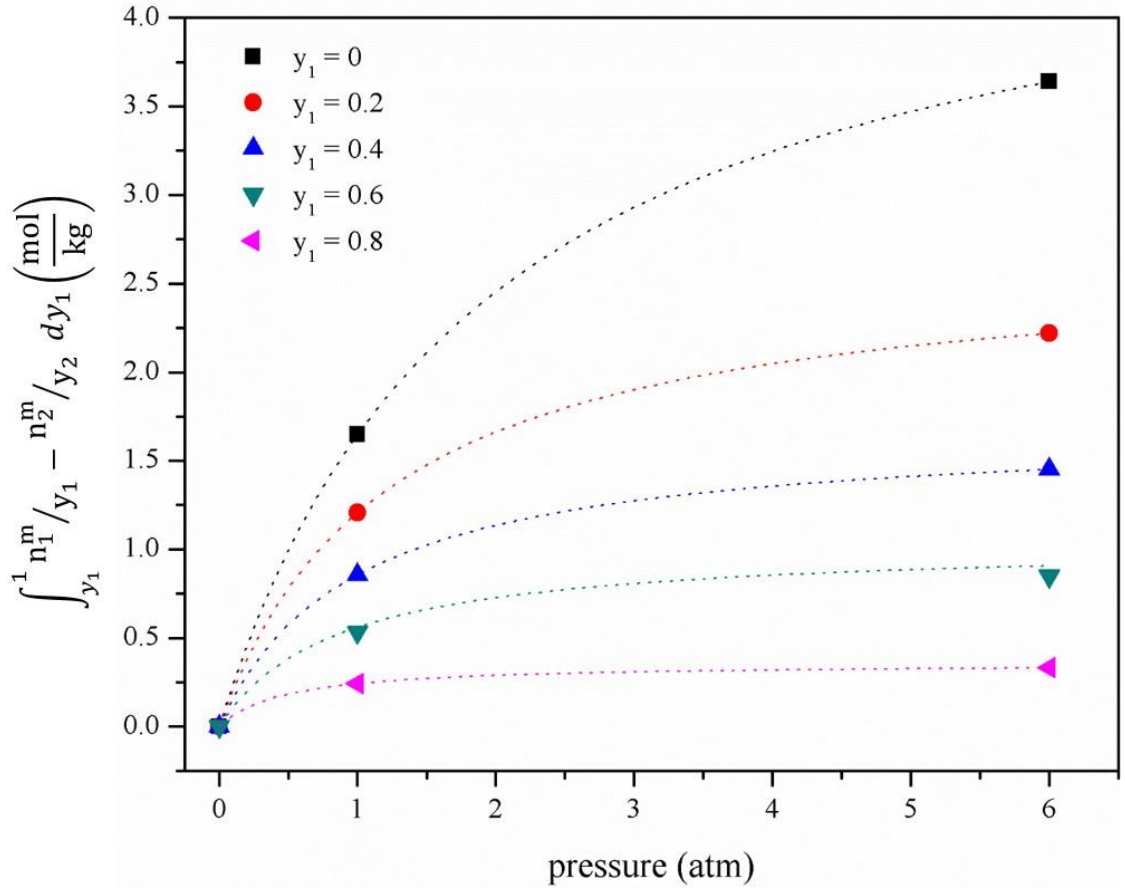

Figure 2-12. Plots of the integrands of Eq.(2-8) as a function of P at different y_1 at constant T at 273.1K for adsorption of N_2 (1) + O_2 (2) on LiLSX zeolite.

2.6 Isosteric heats of adsorption of pure gas on LiLSX zeolite

According to the GSE framework, the isosteric heat of adsorption of a pure gas i, $[q_i^o(n_i^{mo})]$, at an adsorbate loading of n_i^{mo} is given by[28]

$$\left[\frac{\partial \ln(P)}{\partial T}\right]_{n_i^{mo}} = -\frac{q_i^0}{RT^2} \tag{2-10}$$

Eq. (2-10) can be used to calculate q_i^o as a function of n_i^{mo} from a set of pure gas GSE isotherms at different temperatures as shown by the data in Figure 2-7. A plot of ln P vs 1/T at a constant n_i^{mo} should yield a straight line (if q_i^o is independent of T) with a slope equal to $\left[{q_i^o}/{R}\right]$, as illustrated in Figure 2-13. The isosteric heats which can be taken at different loading is a function of loading. The isosteric heat of adsorption of a pure gas should be the same as the Henry's law isosteric heat at all adsorbate loadings for an energetically homogeneous adsorbent, while the isosteric heat will decrease with increased loading for an energetically heterogeneous adsorbent.[30]

Figure 2-14 (a) shows the q vs n^m plot for pure N_2, O_2 and Ar on LiLSX zeolite. Figure 2-14 (b) plots the deviations of isosteric heat of those gases on the LiLSX sample, relative to their isosteric heats in the Henry's Law region [$q^0 - q$], with increase in GSE. It may be seen from Figure 2-14 (a) that the isosteric heats of adsorption of all three gases decrease with increasing GSE, which indicates that the adsorbent exhibits energetic heterogeneity for these gases. However, Figure 2-14 (b) shows that the degree of heterogeneity for the gases are different. The adsorption of Ar is nearly homogeneous [$q(n^m) \sim q^0$], while O_2 adsorption is moderately heterogeneous and N_2 adsorption is

substantially heterogeneous. The relative magnitudes of q^0 for these gases increase in the order of Ar < O_2< N_2 which indicates the the strength of adsorption of N_2 > O_2 > Ar on the zeolite. The difference vanishes for an energetically homogeneous adsorbent.

Figure 2-14 (c) is a plot which shows that the isosteric heat of adsorption of a gas on the LiLSX zeolite increases as the permanent quadrupole moment of the gas increases. The isosteric heat of adsorption of CO_2 on LiLSX zeolite shown in Figure 2-14 (c) was obtained from the literature.[25] An exponential relationship empirically correlates the isosteric heat of adsorption and the permanent quadrupole moment of the adsorbate gas very well. Consequently the electrostatic interactions between the quadrupole moment of the adsorbate gas and the – zeolite cation is dominating for adsorption of these gases.

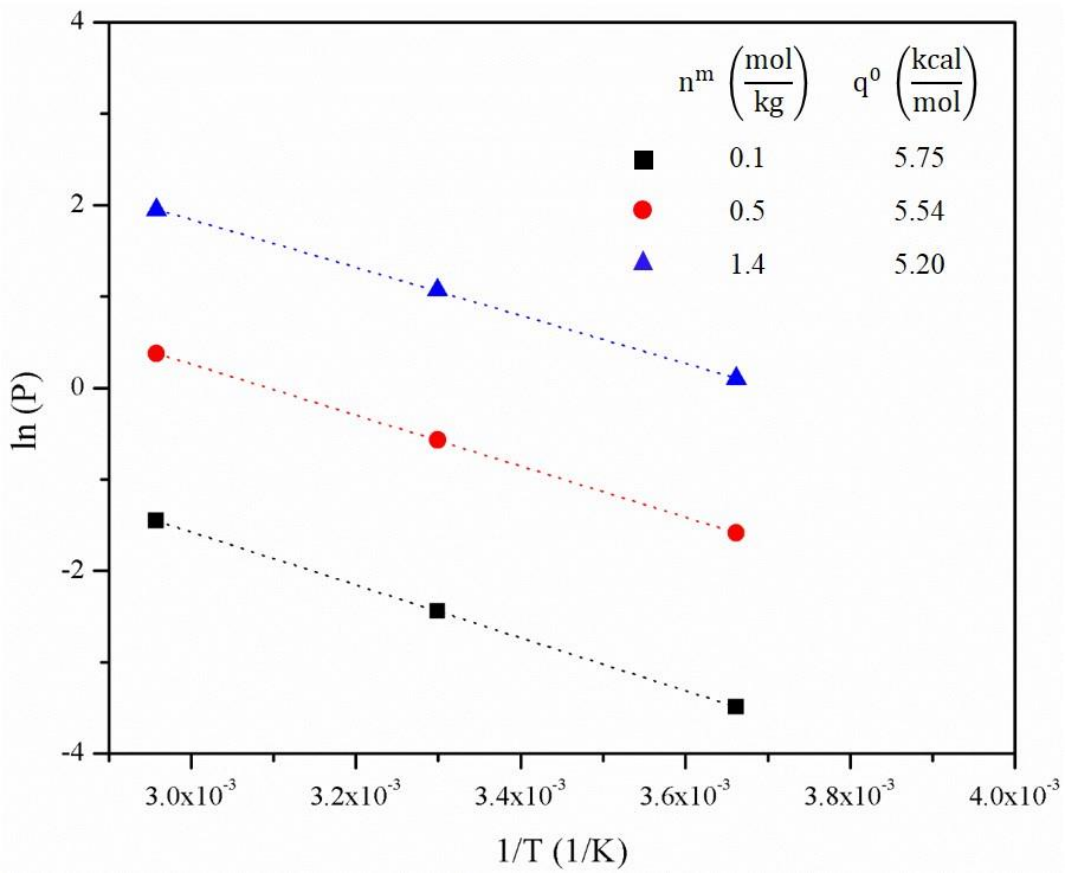

Figure 2-13. Plots of ln P vs. (1/T) for adsorption of nitrogen on LiLSX zeolite.

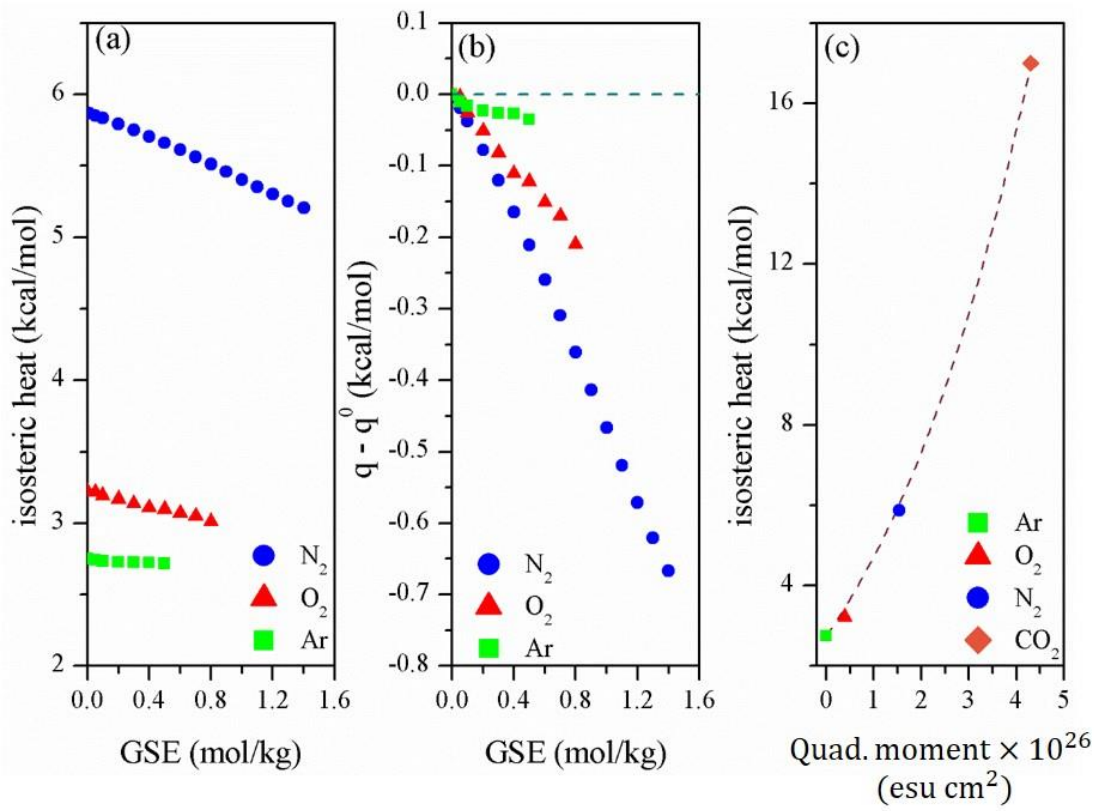

Figure 2-14. (a) Isosteric heats of adsorption of pure N_2, O_2 and Ar on LiLSX zeolite sample, (b) Deviations from Henry's Law region isosteric heats for the components, (c) Henry's Law region isosteric heat on LiLSX zeolite vs quadrupole moment of adsorbate gas.

2.7 Summary

An isothermal-isobaric column dynamic test apparatus was constructed and used for measurement of adsorption isotherms of pure N_2, O_2, Ar and N_2-O_2 mixtures on a commercial sample of LiLSX zeolite at 0, 30 and 65 ^oC and in the pressure range of 0 – 6 atm. The data passed both an integral and a differential thermodynamic consistency test between pure gas and binary gas isotherms.

The binary selectivity of adsorption of N_2 over O_2 at constant pressure and temperature was practically independent of gas phase N_2 mole fraction at higher temperatures but it decreased with increasing N_2 mole fraction at lower temperatures. The binary selectivity at constant temperature and N_2 mole fraction decreased with increasing. These characteristics implied adsorbent heterogeneity (energetic) for adsorption of these gases.

Estimation of pure gas isosteric heats of adsorption as functions of adsorbate loadings by using thermodynamic relationships to the isotherm data showed that the heats for both gases decreased with increasing loadings which proved that the sample of LiLSX zeolite was energetically heterogeneous. The heat data also indicated that the degree of heterogeneity exhibited by the adsorbent for O_2 and Ar adsorption was mild, while that for N_2 adsorption was moderately strong.

2.8 Reference

1. Chai, S. W.; Kothare, M. V.; Sircar, S. Rapid Pressure Swing Adsorption for Reduction of Bed Size Factor of a Medical Oxygen Concentrator. *Ind. Eng. Chem. Res.* **2011,** *50*, 8703-8710.
2. Rao, V. R.; Kothare, M. V.; Sircar, S. Novel design and performance of a medical oxygen concentrator using a rapid pressure swing adsorption concept. *AIChE J.* **2014,** *60*, 3330-3335.
3. Wu, C.-W.; Kothare, M. V.; Sircar, S. Equilibrium Adsorption Isotherms of Pure N2 and O2 and Their Binary Mixtures on LiLSX Zeolite: Experimental Data and Thermodynamic Analysis. *Ind. Eng. Chem. Res.* **2014,** *53*, 7195-7201.
4. Baksh, M. S. A.; Kikkinides, E. S.; Yang, R. T. Lithium Type-X Zeolite as a Superior Sorbent for Air Separation. *Sep. Sci. Technol.* **1992,** *27*, 277-294.
5. Chao, C. C.; Sherman, J. D.; Mullhaupt, J. T.; Bolinger, C. M. Mixed ion-exchanged zeolites and processes for the use thereof in gas separations. U.S. Patent 5,413,625, 1995.
6. Yang, R. T.; Chen, Y. D.; Peck, J. D.; Chen, N. Zeolites containing mixed cations for air separation by weak chemisorption-assisted adsorption. *Ind. Eng. Chem. Res.* **1996,** *35*, 3093-3099.
7. Bajusz, I. G.; Goodwin, J. G. N-2 adsorption in LiX zeolite: Isotopic transient analysis. *Langmuir* **1997,** *13*, 6550-6554.
8. Rege, S. U.; Yang, R. T. Limits for air separation by adsorption with LiX zeolite. *Ind. Eng. Chem. Res.* **1997,** *36*, 5358-5365.
9. Hutson, N. D.; Rege, S. U.; Yang, R. T. Mixed cation zeolites: LixAgy-X as a superior adsorbent for air separation. *Aiche J.* **1999,** *45*, 724-734.
10. Labasque, J.; Moreau, S.; Rouge, D. Process for the separation of gas mixtures containing oxygen and nitrogen. U.S. Patent 5,922,107, 1999.
11. Jale, S. R.; Bulow, M.; Fitch, F. R.; Perelman, N.; Shen, D. Monte Carlo simulation of sorption equilibria for nitrogen and oxygen on LiLSX zeolite. *J. Phys. Chem. B* **2000,** *104*, 5272-5280.
12. Shen, D. M.; Bulow, M.; Jale, S. R.; Fitch, F. R.; Ojo, A. F. Thermodynamics of nitrogen and oxygen sorption on zeolites LiLSX and CaA. *Microporous Mesoporous Mater.* **2001,** *48*, 211-217.
13. Yoshida, S.; Hirano, S.; Harada, A.; Nakano, M. Nitrogen adsorption properties of cubic and orthorhombic Li-exchanged low silica X. *Microporous Mesoporous Mater.* **2001,** *46*, 203-209.
14. Sircar, S.; Myers, A. L., Gas Separation by Zeolite. In *Handbook of zeolite science and technology*, Aurbach, S. M.; Carrado, K. A.; Dutta, P. K., Eds. M. Dekker: New York, N. Y, 2003; pp 1063-1104.

15. Kim, J. B. Li+- and H+-exchanged low-silica X zeolite as selective nitrogen adsorbent for air separation. *Bull. Korean Chem. Soc.* **2003,** *24*, 1814-1818.

16. Bulow, M.; Jale, S. R.; Ojo, A. F.; Fitch, F. R.; Shen, D. Sorption equilibria of nitrogen and oxygen on Li,Re-LSX zeolite for oxygen PVSA processes. *Rec. Adv. . Sci. .Technol. .Zeolites .Relat. Mater., Pts A - C* **2004,** *154*, 1961-1970.

17. Jobic, H.; Schober, H.; Pullumbi, P. Adsorption and diffusion of N-2 and O-2 in LiLSX studied by neutron scattering techniques. *Adsorption* **2005,** *11*, 449-454.

18. Todd, R. S.; Webley, P. A. Macropore diffusion dusty-gas coefficient for pelletised zeolites from breakthrough experiments in the O-2/N-2 system. *Chem. Eng. Sci.* **2005,** *60*, 4593-4608.

19. Park, Y. J.; Lee, S. J.; Moon, J. H.; Choi, D. K.; Lee, C. H. Adsorption equilibria of O-2, N-2, and Ar on carbon molecular sieve and zeolites 10X, 13X, and LiX. *J. Chem. Eng. Data* **2006,** *51*, 1001-1008.

20. Pillai, R. S.; Sethia, G.; Jasra, R. V. Sorption of CO, CH4, and N-2 in Alkali Metal Ion Exchanged Zeolite-X: Grand Canonical Monte Carlo Simulation and Volumetric Measurements. *Ind. Eng. Chem. Res.* **2010,** *49*, 5816-5825.

21. Zanota, M. L.; Heymans, N.; Gilles, F.; Su, B. L.; Frere, M.; De Weireld, G. Adsorption Isotherms of Pure Gas and Binary Mixtures of Air Compounds on Faujasite Zeolite Adsorbents: Effect of Compensation Cation. *J. Chem. Eng. Data* **2010,** *55*, 448-458.

22. Zanota, M. L.; Heymans, N.; Gilles, F.; Su, B. L.; De Weireld, G. Thermodynamic study of LiNaKLSX zeolites with different Li exchange rate for N-2/O-2 separation process. *Microporous Mesoporous Mater.* **2011,** *143*, 302-310.

23. Maurin, G.; Llewellyn, P. L.; Poyet, T.; Kuchta, B. Adsorption of argon and nitrogen in X-faujasites: relationships for understanding the interactions with monovalent and divalent cations. *Microporous Mesoporous Mater.* **2005,** *79*, 53-59.

24. Ferreira, D.; Magalhães, R.; Bessa, J.; Taveira, P.; Sousa, J.; Whitley, R. D.; Mendes, A. Study of AgLiLSX for Single-Stage High-Purity Oxygen Production. *Ind. Eng. Chem. Res.* **2014,** *53*, 15508-15516.

25. Park, Y.; Moon, D.-K.; Kim, Y.-H.; Ahn, H.; Lee, C.-H. Adsorption isotherms of CO2, CO, N-2, CH4, Ar and H-2 on activated carbon and zeolite LiX up to 1.0 MPa. *Adsorption* **2014,** *20*, 631-647.

26. Wu, C.-W.; Kothare, M. V.; Sircar, S. Equilibrium Isotherm and Mass Transfer Coefficient for Adsorption of Pure Argon on Small Particles of Pelletized Lithium-Exchanged Low Silica X Zeolite. *Ind. Eng. Chem. Res.* **2015,** *54*, 2385-2390.

27. Kirner, J. F. Nitrogen adsorption with highly Li exchanged X-zeolites with low Si/Al ratio. U.S. Patent U.S. Patent 5,268,023, 1993.

28. Sircar, S. Gibbsian surface excess for gas adsorption - Revisited. *Ind. Eng. Chem. Res.* **1999,** *38*, 3670-3682.

29. Young, D. M.; Crowell, A. D., *Physical adsorption of gases*. Butterworths: London, 1962; p xi, 426 p.

30. Sircar, S. Role of Adsorbent Heterogeneity on Mixed Gas-Adsorption. *Ind. Eng. Chem. Res.* **1991,** *30*, 1032-1039.

31. Rao, M. B.; Sircar, S. Thermodynamic consistency for binary gas adsorption equilibria. *Langmuir* **1999,** *15*, 7258-7267.

Chapter 3

Equilibrium Adsorption Isotherms of Pure N_2, O_2, Ar and N_2-O_2 Binary Mixtures on LiLSX Zeolite - Model Analysis

In chapter 2, we reported extensive adsorption isotherm data for pure N_2, O_2, Ar and N_2-O_2 binary mixtures on a commercial sample of pelletized LiLSX zeolite (obtained from Zeochem Corp.) at temperatures of 0, 30 and 65 ℃, and in the pressure range of 0 – 6 atm, which covers much of the operating conditions encountered in a typical air separation PSA/VSA process.[1] Analytical multi-component isotherm models are needed for process design and estimation of multi-component heats and model must account for adsorbent heterogeneity if needed.

Thus, the major work of this chapter is to analyze (a) how different analytical pure gas adsorption isotherm models for homogeneous and heterogeneous adsorbents describe the measured pure gas isotherms for the present system, (b) how well the analytical mixed gas isotherm models describe the experimental binary adsorption data using parameters obtained from the pure gas isotherm fits, and (c) how well the classic Ideal Adsorbed Solution Theory work for this system. This work was published in Industrial & Engineering Chemistry Research.[2]

3.1 Selection of model equilibrium adsorption isotherms

Analytical pure and mixed gas model adsorption isotherms are very useful for numerical simulation of adsorptive gas separation processes and many such models for homogeneous and heterogeneous adsorbents can be found the literature. However, only

a few have been tested for describing pure N_2 and O_2 and their binary mixture adsorption isotherms on LiX and LiLSX zeolites as summarized by Table 3-1.

Table 3-1. List of models used to correlate pure N_2 and O_2 and binary gas adsorption data on LiLSX zeolite

Authors	Adsorbent	Isotherm Model	
		Pure Gas	Binary Gas
Rege, Yang (1997)[3]	LiX	Empirical modified Langmuir[4]	
Santos, Cruz, Regala, Magalhaes, Mendes (2007)[5]	Li-Ag- LSX	Sips[6]	IAST[7]
Zhong, Rankin, Ackley (2010)[8]	LiX	Langmuir[4]	
Rama Rao, Farooq, Krantz (2010)[9]	Li-Ag-X	Langmuir[4]	

We chose to test the following models for this work:

a) Homogenous model of Langmuir[4]

b) Heterogeneous empirical model of Toth[10]

c) Heterogeneous - Langmuir model of Sircar[11]

d) Ideal Adsorbed Solution Theory (IAST) of Myers and Prausnitz[7]

All of these models are capable of describing Type I adsorption isotherms for pure gas and mixtures, and they satisfy thermodynamic consistency tests between pure and binary gas isotherms albeit under a few constraints on the model parameters.[12] Furthermore, models (a) – (c) provide analytical isotherm equations for pure and mixed gases, and the isotherms obey Henry's law in the low pressure region. They also yield analytical correlations describing isosteric heats of adsorption for pure gases and components of a mixture as functions of adsorbate loadings which are very important for numerical

simulation of adsorptive separation processes. The numbers of adjustable parameters are manageable, being three for model (a) and four for models (b) and (c). The parameters are, however, constrained by the physics and thermodynamics of adsorption.

Table 3-2 provides a summary of analytical, pure and multi-component gas adsorption isotherms for models (a) – (c). It also lists the thermodynamic and physical constraints for the models. Table 3-3 shows the analytical correlations for isosteric heats of adsorption of pure gases and components of a mixture as functions of adsorbate loadings for these models. The pure and mixed gas isosteric heat correlations for model (c) were previously unpublished.

The Langmuir model is mathematically simple and most widely used for describing gas adsorption on an energetically homogeneous adsorbent. It may be seen from Table 3-1 that it has been frequently used for the present system.

The empirical Toth model describes Type I adsorption isotherms on an energetically heterogeneous adsorbent using an explicit but empirical parameter representing the degree of adsorbent heterogeneity for a gas. The model reduces to the Langmuir model for a homogeneous adsorbent. It has been extensively tested for fitting pure gas adsorption isotherms on heterogeneous adsorbents.[13] However, the degree of heterogeneity for each gas of a mixture must be the same in order to satisfy the integral thermodynamic consistency test.[12] This constraint limits the flexibility of the model. Another physical inconsistency of the Toth model is that the isosteric heat of adsorption of a pure gas at the limit of saturation loading ($\theta_i^0 \rightarrow 1$) approaches negative infinity which is physically

meaningless. This can be easily shown from the model equation for isosteric heat given in Table 3-3.

The heterogeneous Sircar model is based on a 'patch-wise homogeneous' concept of adsorbent heterogeneity. It assumes that the Langmuir model describes the pure and mixed gas isotherms on a homogeneous patch, a uniform distribution of Langmuir Henry's law constants with superimposition of cumulative distribution functions for different gases account for adsorbent heterogeneity and site matching relationship, respectively.[11] The model describes type I isotherms on heterogeneous adsorbents using an explicit parameter for degree of heterogeneity which can be different for each component of a gas mixture. The isosteric heat of adsorption of a pure gas is finite at the limit of saturation loading which is physically consistent. A detailed study of the characteristics of this model can be found elsewhere.[11] The Sircar model also reduces to the Langmuir model for a homogeneous adsorbent. Further discussion of the distribution of Langmuir Henry's law constants can be found in Appendix B.

The IAST concept, which is based on an elegant thermodynamic mixing rule (at constant surface potential and temperature) in an ideal adsorbed phase (no lateral interactions between adsorbed species), allows calculation of mixed gas adsorption isotherms from the corresponding pure gas isotherm data. No model fit of the pure gas data is necessary. However, a model pure gas isotherm is often necessary to facilitate data inter- and extrapolation. We used the Sircar model for this purpose in this work since it describes the nature of adsorbent energetic heterogeneity of the present system and provides the best fit (smallest deviations between experiment and model) of the pure gas

isotherms over the entire range of the data as shown by Figure 3-1. IAST is thermodynamically consistent and has often been used in the literature as a benchmark for computing mixed gas isotherms. It works very well when the adsorbent is energetically homogeneous or when the degrees of heterogeneity of the components of a gas mixture are similar, and when the adsorbate molecules of the gas mixture have similar sizes.[14] On the other hand, IAST is not analytical and may require tedious and time-consuming numerical computations for a process design. It should be mentioned here that the multicomponent isotherm predictions by IAST is identical to those by the analytical heterogeneous Sircar model when the component gases have the same degrees of heterogeneity.[11]

Table 3-2. Analytical model isotherms for pure and multi-component gas adsorption (P: Pure gas; M: Mixed gas)

Models		Isotherm model	Thermodynamic and physical constrains
Langmuir (1914)[4] (Homogeneous)	P:	$\theta_i^o = \frac{b_i P}{[1 + b_i P]}$	$m_i = m \neq m(T)$
	M:	$\theta_i = \frac{b_i P y_i}{[1 + \sum_i b_i P y_i]}$	
Toth (1962)[10] (Heterogeneous)	P:	$\theta_i^o = \frac{b_i P}{[1 + (b_i P)^{k_i}]^{\frac{1}{k_i}}}$	$m_i = m \neq m(T)$ $k_i(T) = k(T)$ $0 < k \leq 1$ $\frac{dk}{dT} > 0$
	M:	$\theta_i = \frac{b_i P y_i}{[1 + (\sum_i b_i P y_i)^{k_i}]^{\frac{1}{k_i}}}$	
Sircar (1991)[11] (Heterogeneous)	P:	$\theta_i^o = \theta_{iH}^o \left[1 - \frac{(1 - \theta_{iH}^o)}{\theta_{iH}^o} f(z_i^o)\right]$ $\theta_{iH}^o = \frac{\mu_i P}{[1 + \mu_i P]};\ \mu_i = \mu_i^* \exp\left(\frac{q_i^*}{RT}\right)$ $z_i^o = \psi_i \theta_{iH}^o;\ \psi_i = \sqrt{3}\left[\frac{\sigma_i}{\mu_i}\right]$ $\sigma_i = \sigma_i^* \exp\left(\frac{\lambda_i^*}{RT}\right)$ $f(z_i^o) = \frac{1}{2z_i^o} \ln\left[\frac{1 + z_i^o}{1 - z_i^o}\right] - 1$	$m_i = m \neq m(T)$ $0 \leq \psi_i(T) < 1$ $\frac{d\psi_i}{dT} < 0$
	M:	$\theta_i = \theta_{iH}\left[1 - \frac{(\psi_i - z)}{z} f(z)\right]$ $\theta_{iH} = \frac{\mu_i P y_i}{[1 + \sum_i \mu_i P y_i]};\ z = \sum_i \psi_i \theta_{iH}$ $f(z) = \frac{1}{2z} \ln\left[\frac{1 + z}{1 - z}\right] - 1$	
$\theta_i^o = \frac{n_i^o}{m_i};\ \theta_i = \frac{n_i}{m_i};\ b_i(T) = b_i^0 \exp\left(\frac{q_i^*}{RT}\right)$			

Table 3-3. Analytical model correlations for isosteric heats of adsorption of pure and multi-component gas (P: Pure gas; M: Mixed gas)

Langmuir ($m_i = m$)	P:	$q_i^o(\theta_i^o) = q_i^*$
	M:	$q_i(\theta_i) = q_i^*$
Toth ($k_i = k$), ($m_i = m$)	P:	$q_i^o(\theta_i^o) = q_i^* + \left(\frac{RT^2}{k}\right)\left(\frac{dlnk}{dT}\right)F_i(\theta_i^o)$ $F_i(\theta_i^o) = \frac{[1-(\theta_i^o)^k]\ln[1-(\theta_i^o)^k] + (\theta_i^o)^k \ln(\theta_i^o)^k}{[1-(\theta_i^o)^k]}$
	M:	$q_i(\theta_i) = q_i^* + \left(\frac{RT^2}{k}\right)\left(\frac{dlnk}{dT}\right)F(\theta)$ $F(\theta) = \frac{[1-(\theta)^k]\ln[1-(\theta)^k] + (\theta)^k \ln(\theta)^k}{[1-(\theta)^k]}$; $\theta = \sum_i \theta_i$
Sircar ($m_i = m$)	P:	$\left[\frac{q_i^o(\theta_i^o) - q_i^*}{q_i^{**} - q_i^*}\right] = \frac{z_i^o \frac{df(z_i^o)}{dz_i^o} \cdot G(\psi_i)}{\theta_{iH}^o[1+f(z_i^o)] - (1-\theta_{iH}^o)\left\{z_i^o \frac{df(z_i^o)}{dz_i^o}\right\}}$ $z_i^o \frac{df(z_i^o)}{dz_i^o} = -\{1+f(z_i^o)\} + \frac{1}{\{1-(z_i^o)^2\}}$ $G(\psi_i) = \frac{\left[\frac{(1-\psi_i^2)}{2\psi_i}\right]\ln\frac{(1+\psi_i)}{(1-\psi_i)}}{1-\left[\frac{(1-\psi_i^2)}{2\psi_i}\right]\ln\frac{(1+\psi_i)}{(1-\psi_i)}}$
	M:	$\left[\frac{q_i^{**} - q_i^*}{RT^2}\right] = \frac{\left[1-\frac{(1-\psi_i^2)}{2\psi_i}\ln\frac{(1+\psi_i)}{(1-\psi_i)}\right]}{\left[\frac{(1-\psi_i^2)}{2\psi_i}\ln\frac{(1+\psi_i)}{(1-\psi_i)}\right]}\frac{dln\,\psi_i}{dT}$ $\left[\beta_i\left(\frac{\partial z}{\partial T}\right)_{\theta_i} - \left(\frac{f\psi_i}{z}\right)\left(\frac{dln\psi_i}{dT}\right)\right] = -A_i[\alpha_i - \sum_1^N \alpha_k\theta_{kH}]$ $A_i = \left[1-\frac{(\psi_i - z)}{z}f(z)\right]$; $\alpha_i = \frac{(q_i - q_i^o)}{RT^2}$; $\beta_i = \frac{\psi_i}{z}\left[\frac{f}{z} - f'\right] + f'$ $f' = -\frac{1}{2z^2}\ln\left[\frac{1+z}{1-z}\right] + \frac{1}{z(1-z^2)}$ $\left(\frac{\partial z}{\partial T}\right)_{\theta_i} = \sum_1^N(\psi_i\theta_{iH})\frac{dln\psi_i}{dT} + \sum_i(\psi_i\theta_{iH})\left[\alpha_i - \sum_1^N \alpha_k\theta_{kH}\right]$

n_i^o (P, T) is the specific equilibrium amount adsorbed of pure gas i at pressure (P) and temperature (T); n_i (P, T, y_i) is the specific equilibrium amount of component *i* adsorbed from a gas mixture (mole fraction of component $i = y_i$) at P and T. m_i is the specific saturation adsorption capacity of component *i* on the adsorbent. θ_i and θ_i^o are, respectively, fractional amounts adsorbed of component *i* from a pure gas and a mixture. $q_i^0(\theta_i^o)$ and q_i (θ_i) are, respectively, the isosteric heats of adsorption of pure gas *i* and from a mixture as functions of adsorbate loadings. The parameter b_i (T) is the Langmuir gas-solid interaction parameter for component *i* at temperature T and b_i^* is a constant. q_i^* and q_i^{**} are the isosteric heats of adsorption of pure gas *i* , respectively in the Henry's law region ($\theta_{iH}^o \rightarrow 0$) and at the saturation level ($\theta_{iH}^o \rightarrow 1$). The variable $k_i(T)$ is an empirical parameter for Toth model representing the degree of heterogeneity for adsorption of pure gas *i* at temperature T. An adsorbent is homogeneous for gas *i* when $k_i = 1$. The variable $\mu_i(T)$ is the mean of the Henry's constant distribution function for pure gas *i* at temperature T and $\sigma_i(T)$ is the corresponding dispersion used in the derivation of the heterogeneous Langmuir model of Sircar.[11] λ_i^* is an energy parameter governing the temperature coefficient of σ_i . The parameters μ_i^* and σ_i^* are constants. The variable $\psi_i(T)$ is the degree of heterogeneity ($= \sqrt{3}\left[\frac{\sigma_i}{\mu_i}\right]$) for adsorption for pure gas *i* at temperature T. An adsorbent is homogeneous for gas *i* when $\psi_i = 0$. Other functionalities of the Heterogeneous Langmuir model [θ_{iH}^o, θ_{iH}, z_i^o, z, $f(z_i^o)$ and f (z)] are defined in the Table 3-3.

3.2 Model analysis of pure gas adsorption isotherms

Figure 3-1 shows the best fit of the experimental pure N_2, O_2 and Ar isotherm data on LiLSX zeolite at different temperatures and pressures by models (a) –(c). The best fit model parameters for N_2, O_2 and Ar are given in Table 3-4. The saturation capacities of both gases were chosen to be identical and temperature independent in order to satisfy the constraints imposed by adsorption physics and thermodynamics for all models. The heterogeneity parameter for each component of the gas mixture in the Toth model was chosen to be same for satisfying thermodynamic consistency requirement.

The average absolute percentage deviations between experimental and model estimated values of amounts adsorbed [((Expt – Model)/Expt) x 100] for each isotherm are given in Table 3-5. It shows that each model fits the isotherm data fairly well. However, the Sircar heterogeneous model provides a better fit over the entire range of pressure and temperature of the reported data. This is because (a) the Langmuir model does not account for the energetic heterogeneity of adsorption for this system, (b) the Sircar heterogeneity model captures the energetic behavior (different degrees of heterogeneity for N_2 and O_2) for this system while, (c) the Toth heterogeneity model ignores that characteristic.

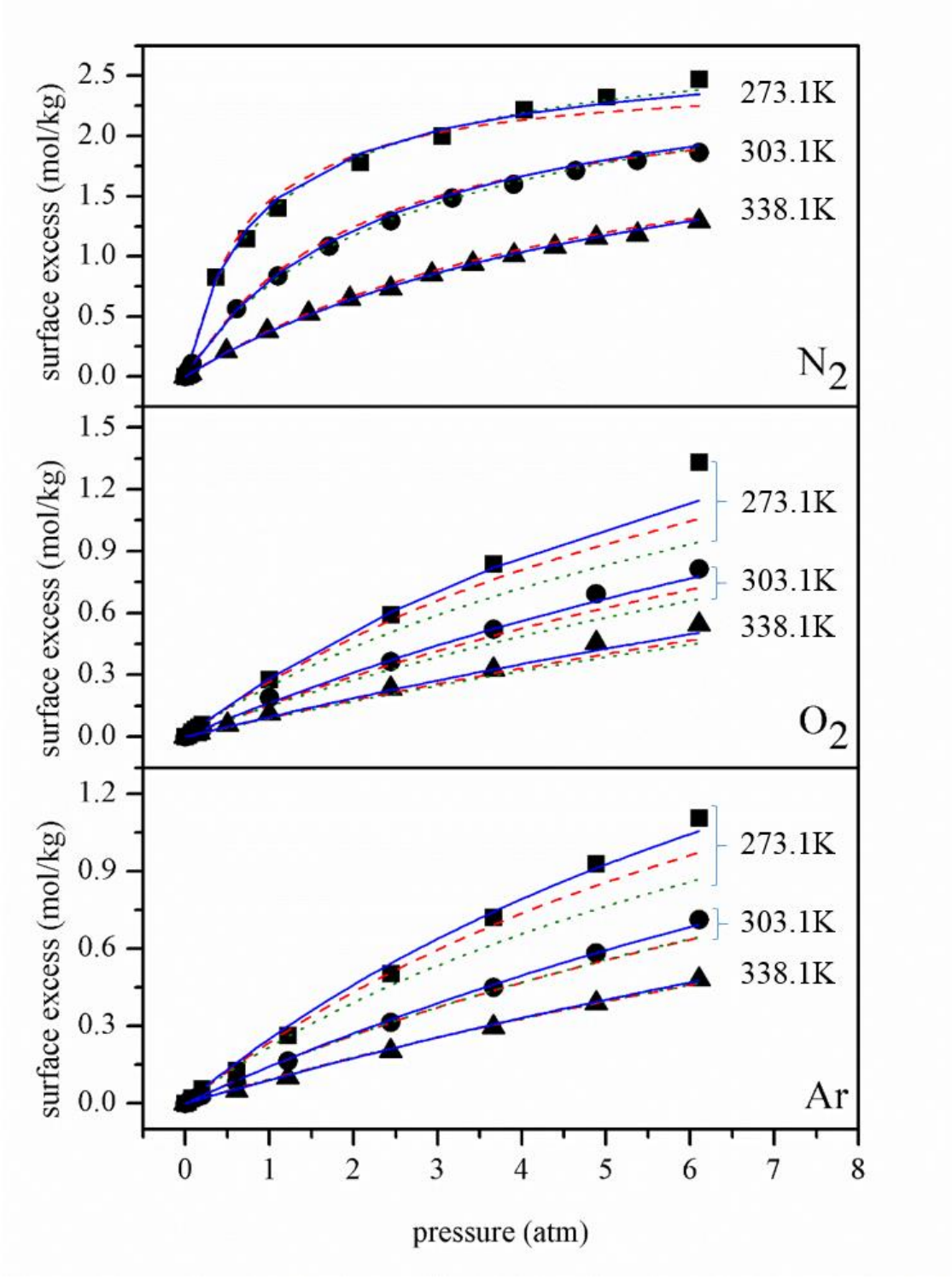

Figure 3-1. Model fit of pure N_2 ,O_2 and Ar adsorption isotherms of LiLSX zeolite at three temperatures, Symbols: experimental; --- Langmuir; ··· Toth; — Sircar

Table 3-4. Isotherm model parameters for adsorption of pure N_2, O_2 and Ar on LiLSX zeolite (Units: T = K; m = mol/kg; b_0 , μ_0 = atm^{-1}; q_o = kcal/mol)

Gas	T	q_o	Homogeneous (Langmuir)		Heterogeneous (Toth)			Heterogeneous (Sircar)		
			m	b_0	m	b_0	k	m	μ_o	ψ
N_2	273.1	5.87	2.50	2.95×10^{-5}	3.05	2.42×10^{-5}	0.78	2.87	2.56×10^{-5}	0.995
	303.1						0.81			0.884
	338.1						0.86			0.834
O_2	273.1	3.22	2.50	3.18×10^{-4}	3.05	2.60×10^{-4}	0.78	2.87	2.89×10^{-4}	0.24
	303.1						0.81			0.06
	338.1						0.86			0.0003
Ar	273.1	2.75	2.50	6.57×10^{-4}	3.05	5.39×10^{-4}	0.78	2.87	3.50×10^{-4}	0.0014
	303.1						0.81			1.63×10^{-6}
	338.1						0.86			6.95×10^{-7}

Table 3-5. Average deviations (absolute %) between experimental and model isotherm data

Temperature (K)	gas	Average absolute deviations (%)		
		Homogeneous (Langmuir)	Heterogeneous (Toth)	Heterogeneous (Sircar)
273.1	N_2	6.9	2.7	3.7
	O_2	5.9	10.3	5.8
	Ar	7.7	10.8	7.8
303.1	N_2	4.6	3.2	4.8
	O_2	8.9	12.8	4.1
	Ar	5.2	4.8	4.7
338.1	N_2	2.7	1.9	2.1
	O_2	15.6	17.8	10.9
	Ar	8.8	6.7	4.8

3.3 Model analysis of binary gas adsorption isotherms

The binary $N_2 + O_2$ adsorption isotherms at the conditions of experimental data[1] were estimated using the analytical isotherm equations for models (a) – (c) given by Table 3-2 and the pure gas model parameters reported in Table 3-4. They were also estimated using the IAST model and the pure gas isotherm data. The comparative results are reported here in Figure 3-2 as binary selectivities of N_2 (1) over O_2 (2) defined by $\left[S_{12} = \frac{\theta_1 y_2}{\theta_2 y_1}\right]$ as functions of total gas pressure (P), temperature (T), and gas phase mole fraction of component *i* (y_i) because S_{12} can be a very sensitive function of these variables.

The binary gas adsorption selectivity (S_{12}) by both the homogeneous Langmuir model and the thermodynamically consistent form of the heterogeneous Toth model [$k_1 = k_2$] is given by the ratios of the henry's Law constants [$= \frac{b_1}{b_2}$]. Thus S_{12} is a function of T only, and these two models cannot describe the functional dependence of S_{12} on P and y_i as shown by Figure 3-2. On the other hand, the IAST and the heterogeneous model of Sircar capture the variation of S_{12} with y_1 at constant P and T. However, it was found that the Sircar model traced the experimental selectivity data more closely than IAST. The models generally over-predicted the selectivity value compared to the experiment when there was a substantial difference between the two. The over prediction was more pronounced at lower temperatures where the effect of heterogeneity was more severe. The experimental and model estimated selectivity for each binary data point as well as the average deviation (%) between them are given in Table 3-6 and Table 3-7.

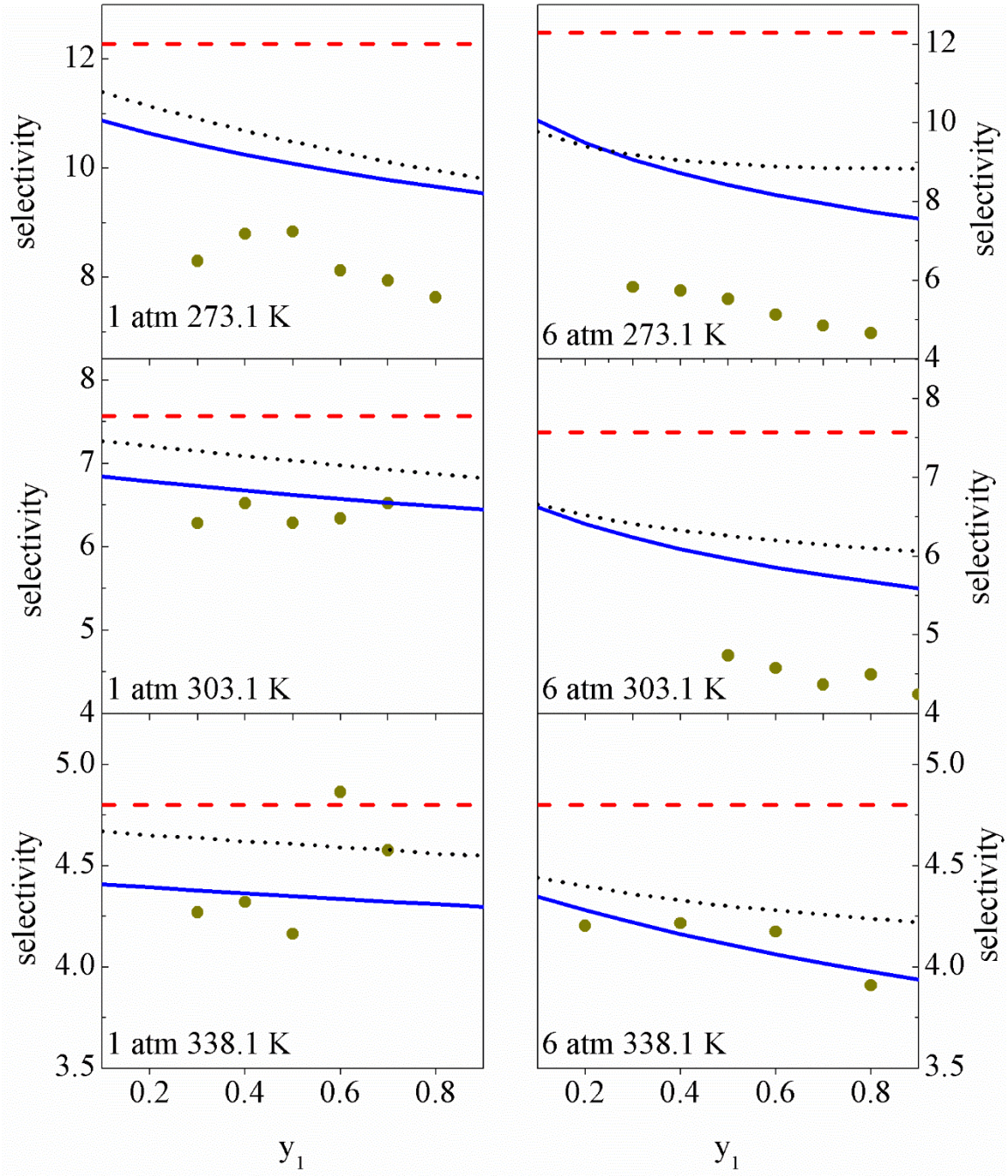

Figure 3-2. Plots of S_{12} vs y_1 at different temperatures (T) for total gas pressures (P). Circles: Experimental; …… IAST; ---- Homogeneous Langmuir or Heterogeneous Toth; ——— Heterogeneous Sircar

Table 3-6. Average percentage deviations [((Expt – Model)/Expt) x 100] between experimental and 3different model adsorption selectivity data at 1 atm

y_1	Exp	Model								
		Langmuir/Toth			IAST			Heterogeneous Langmuir		
	S_{12}	S_{12}	Error (%)	Avg. (%)	S_{12}	Error (%)	Avg. (%)	S_{12}	Error (%)	Avg. (%)
					273.1 K					
0.3	8.30	12.28	47.99		10.91	31.45		10.43	25.69	
0.4	8.80	12.28	39.59		10.69	21.48		10.25	16.47	
0.5	8.84	12.28	38.95	48.90	10.49	18.67	26.07	10.08	14.06	24.41
0.6	8.12	12.28	51.21		10.30	26.85		9.93	22.27	
0.7	7.94	12.28	54.74		10.12	27.46		9.79	23.37	
0.8	7.63	12.28	60.89		9.96	30.54		9.66	26.59	
					303.1 K					
0.3	6.29	7.57	20.46		7.15	13.67		6.73	7.05	
0.4	6.52	7.57	16.10		7.09	8.74		6.68	2.36	
0.5	6.29	7.57	20.45	18.51	7.04	11.92	10.14	6.63	5.39	3.73
0.6	6.34	7.57	19.42		6.98	10.09		6.58	3.73	
0.7	6.52	7.57	16.11		6.93	6.29		6.53	0.15	
					338.1 K					
0.3	4.27	4.80	12.46		7.15	13.67		4.38	2.55	
0.4	4.32	4.80	11.14		7.09	8.74		4.36	1.01	
0.5	4.16	4.80	15.34	9.03	7.04	11.92	6.40	4.35	4.50	4.89
0.6	4.86	4.80	1.29		6.98	10.09		4.34	10.85	
0.7	4.58	4.80	4.91		6.93	6.29		4.32	5.54	

Table 3-7. Average percentage deviations [((Expt – Model)/Expt) x 100] between experimental and 3different model adsorption selectivity data at 6 atm

y_1	Exp	Model								
		Langmuir/Toth			IAST			Heterogeneous Langmuir		
	S_{12}	S_{12}	Error (%)	Avg. (%)	S_{12}	Error (%)	Avg. (%)	S_{12}	Error (%)	Avg. (%)
					273.1 K					
0.3	5.83	12.28	110.66		9.19	57.63		9.06	55.44	
0.4	5.74	12.28	114.06		9.05	57.67		8.72	51.92	
0.5	5.52	12.28	122.45	48.90	8.96	62.32	26.07	8.43	52.62	24.41
0.6	5.13	12.28	139.55		8.90	73.49		8.18	59.44	
0.7	4.85	12.28	153.38		8.86	82.68		7.95	64.04	
0.8	4.66	12.28	163.38		8.85	89.91		7.75	66.19	
					303.1 K					
0.5	4.74	7.57	59.86		6.26	32.07		5.97	25.98	
0.6	4.58	7.57	65.42		6.20	35.37		5.86	27.96	
0.7	4.37	7.57	73.26	69.08	6.15	40.73	37.33	5.76	31.78	28.72
0.8	4.50	7.57	68.37		6.10	35.56		5.67	26.10	
0.9	4.24	7.57	78.48		6.06	42.92		5.59	31.79	
					338.1 K					
0.2	4.20	4.80	14.23		4.4	4.76		4.28	1.81	
0.4	4.22	4.80	13.92	16.50	4.33	2.61	4.61	4.16	1.24	1.86
0.6	4.17	4.80	15.04		4.28	2.64		4.06	2.65	
0.8	3.91	4.80	22.81		4.24	8.44		3.98	1.72	

It may be seen from Table 3-6 and Table 3-7 that the deviation between model estimated selectivity and experiment is largest for the Langmuir/Toth model, followed by IAST followed by the Sircar model under most of the conditions of P, T, and y_1. This indicates that the critical issues in estimating binary isotherms from pure gas isotherm data for this system are to account for adsorbent heterogeneity and the difference in the degree of heterogeneity of different components of a gas mixture on the same adsorbent. The analytical heterogeneous isotherm model of Sircar provides a simple framework (with different ψ_i values) to cover those issues.

It should be mentioned here that an earlier work by Zanota et al reported binary N_2 + O_2 adsorption isotherm on a home-made pelletized sample of LiLSX zeolite at a single temperature (303 K) and a single total gas pressure (3.95 atm), and compared them with binary IAST estimation using their pure gas isotherms at that temperature.[15] The deviation between experimental and estimated selectivity was ~ 19.7%, which is comparable with the deviation noticed in this work.

3.4 Model analysis of pure gas isosteric heats of adsorption

Figure 3-3 compares the pure gas isosteric heats of adsorption [q_i^0] of N_2, O_2 and Ar estimated from experimental adsorption isotherms at different temperatures (Figure 3-1) using the thermodynamic relationship $\left[q_i^0 = RT^2 \left(\frac{\partial lnP}{\partial T}\right)_{\theta_i^0}\right]$with those estimated by the model correlations and appropriate parameters (Table 3-3, Table 3-6 and Table 3-7). It may be seen that the variations of $[q_i^0]$ as functions of θ_i^0 are fairly well traced by the models. The average percentage deviations between the thermodynamic heats obtained

from pure gas isotherms and the analytical models were less than 2 and 5 % for N_2 and O_2, respectively. The relatively steeper decrease of $[q_i^0]$ with increasing loading for N_2 than O_2 is indicative of larger degree of heterogeneity for N_2 (larger ψ_i) than O_2, and it is explicitly accounted for by the Sircar model.

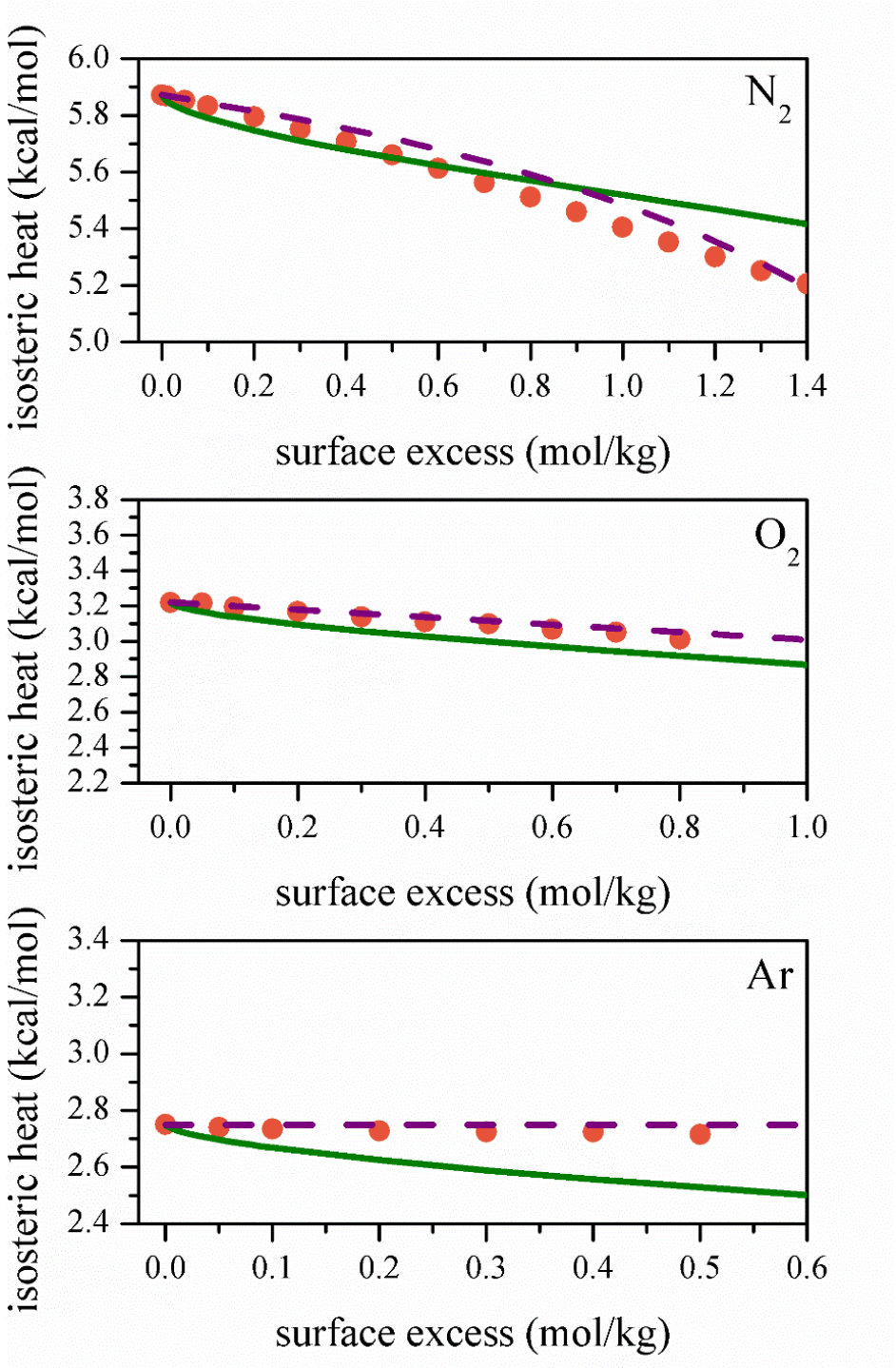

Figure 3-3. Pure gas isosteric heats of adsorption of pure N_2, O_2 and Ar as functions of adsorbate loading (surface excess). Circles: Estimated from isotherms using thermodynamic relationship; ─ ─ ─ Sircar model; ─── Toth model

3.5 Summary

LiLSX zeolite exhibits different degrees of adsorbent heterogeneity for adsorption of pure N_2, O_2 and Ar. Nevertheless, the pure gas adsorption isotherms of these gases over a large range of temperature (T) and pressure (P) can apparently be described reasonable well (Figure 3-1) by several analytic and thermodynamically consistent but diverse models like (a) homogeneous Langmuir, (b) heterogeneous Toth (same degree of heterogeneity for components), and (c) heterogeneous Sircar (different degrees of heterogeneity for components). However, model (c) provided the closest correlation between the estimated and the experimental binary selectivity values for this system as compared to the other models as well as IAST under various conditions of P, T and gas composition. The model also provides analytical expressions for pure and multicomponent iso-steric heats of adsorption. This demonstrates the importance of accounting for the degree of adsorbent heterogeneity of different components of a gas mixture in predicting mixed gas adsorption equilibria from the corresponding pure gas isotherms. Furthermore, the study shows that the ability of a model to describe pure gas adsorption isotherms does not guarantee its validity for predicting the mixed gas isotherms. They must be extensively tested using experimental mixed gas isotherm data.

3.6 Reference

1. Wu, C. W.; Kothare, M. V.; Sircar, S. Equilibrium Adsorption Isotherms of Pure N2, O2 and Their Binary Mixtures on LiLSX Zeolite- Experimental Data and Thermodynamic Analysis. *Ind. Eng. Chem. Res.* **2014**.
2. Wu, C. W.; Kothare, M. V.; Sircar, S. Model Analysis of Equilibrium Adsorption Isotherms of Pure N-2, O-2, and Their Binary Mixtures on LiLSX Zeolite. *Ind. Eng. Chem. Res.* **2014,** *53*, 12428-12434.
3. Rege, S. U.; Yang, R. T. Limits for air separation by adsorption with LiX zeolite. *Ind. Eng. Chem. Res.* **1997,** *36*, 5358-5365.
4. Young, D. M.; Crowell, A. D., *Physical adsorption of gases*. Butterworths: London, 1962; p xi, 426 p.
5. Santos, J. C.; Cruz, P.; Regala, T.; Magalhaes, F. D.; Mendes, A. High-purity oxygen production by pressure swing adsorption. *Ind. Eng. Chem. Res.* **2007,** *46*, 591-599.
6. Sips, R. On the Structure of a Catalyst Surface. *J. Chem. Phys.* **1948,** *16*, 490-495.
7. Myers, A. L.; Prausnitz, J. M. Thermodynamics of Mixed-Gas Adsorption. *Aiche J.* **1965,** *11*, 121-127.
8. Zhong, G. M.; Rankin, P. J.; Ackley, M. W. High Frequency PSA Process for Gas Separation. U.S. Patent 2010.
9. Rama Rao, V.; Farooq, S.; Krantz, W. B. Design of a Two-Step Pulsed Pressure-Swing Adsorption-Based Oxygen Concentrator. *Aiche J.* **2010,** *56*, 354-370.
10. Jaroniec, M.; Toth, J. Adsorption of Gas-Mixtures on Heterogeneous Solid-Surfaces .1. Extension of Toth Isotherm on Adsorption from Gas-Mixtures. *Colloid. Polym. Sci.* **1976,** *254*, 643-649.
11. Sircar, S. Role of Adsorbent Heterogeneity on Mixed Gas-Adsorption. *Ind. Eng. Chem. Res.* **1991,** *30*, 1032-1039.
12. Rao, M. B.; Sircar, S. Thermodynamic consistency for binary gas adsorption equilibria. *Langmuir* **1999,** *15*, 7258-7267.
13. Valenzuela, D. P.; Myers, A. L., *Adsorption Equilibrium data handbook*. Prentice Hall: Englewood Cliffs, New Jersey, 1989.
14. Sircar, S. Influence of Adsorbate Size and Adsorbent Heterogeneity on IAST. *Aiche J.* **1995,** *41*, 1135-1145.
15. Zanota, M. L.; Heymans, N.; Gilles, F.; Su, B. L.; De Weireld, G. Thermodynamic study of LiNaKLSX zeolites with different Li exchange rate for N-2/O-2 separation process. *Microporous Mesoporous Mater.* **2011,** *143*, 302-310.

Chapter 4

Column Dynamic Study of Mass Transfer of Pure N_2, O_2 and Ar into Small Particles of Pelletized LiLSX Zeolite

In Chapter 2, the pure gas adsorption isotherms were measured by employing an isothermal and isobaric column dynamic apparatus. The column packed with the adsorbent particles was initially saturated with pure Helium (inert) at pressure (P, atm) and temperature (T, K) and then a stream N_2 (or O_2, Ar) + He, having an adsorbate mole fraction of y^0, at P and T was passed through the column at a constant mass flow rate (Q^0, moles/cm^2/s based on empty cross sectional area of the column) until the column was saturated with the feed gas at P, T and y^0. The transient effluent gas mass flow rate [$Q(t)$, moles/cm^2/s] and mole fraction [$y(t)$] were monitored as functions of time. The component and over-all mass balances for the column breakthrough curves (BTC) measured during these displacement tests allowed estimation of the equilibrium surface excess of component i (n_i^m, moles/g) at a given P, T, and y^0.

A literature search revealed that there was no published data on adsorptive mass transfer coefficients of N_2 and O_2 for this adsorbent which are required for design of a RPSA - MOC process. Only one article reports experimental mass transfer data for argon adsorption.[1] Some N_2, O_2 and Ar transport data were available for a commercial sample of large pelletized beads (d_P = 2- 4 mm) of Li- RE (rare earth) –LSX zeolite measured by a frequency response technique at low pressures (5 – 50 torr) and different temperatures (258 – 333 K).[2, 3] Consequently, the goal of this work was to estimate the effective mass transfer coefficients for transport of pure N_2, O_2 and Ar into LiLSX zeolite

pellets under different conditions of P and T, and identify the mechanism of the transport process. Some of the same column BTC profiles, where the feed gas was pure N_2, O_2 or Ar ($y^0 = 1$), were used for this purpose.

4.1 Isothermal-isobaric constant pattern model for estimation of mass transfer coefficients

An analytical model describing isobaric and adiabatic column dynamics for adsorption of a binary gas mixture where a constant pattern MTZ is formed, and where the local rate of adsorbate mass transfer is given by the linear driving force (LDF) model can be found in the literature.[4] The present case deals with a specialized version of that model where a pure adsorbate gas (component 1) at P and T is passed through an isobaric and isothermal adsorber, which is initially filled with an inert gas (component 2) at P and T.

Figure 4-1 is a schematic drawing of profiles of gas phase adsorbate mole fraction [$y_1(z,t)$], Gibbs surface excess or adsorbate loading [$n_1(z,t)$, moles/g], and gas mass flow rate [$Q(z,t)$, moles/cm^2/s] through the column as functions of column distance (z) inside the column at a time (t) for the present case. There are three distinct sections: (I) an expanding equilibrium section at the feed gas end (z = 0) which is saturated with the pure feed gas at P, T, (II) a MTZ which moves through the column unchanged in shape and size with a constant velocity (β, cm/s), and (III) a shrinking equilibrium section at the effluent gas end (z = L) which is saturated with the pure inert gas (y = 0) at P and T. The gas mass flow rates in sections I and III, are respectively, Q^0 and Q^S, and the

equilibrium adsorption capacities (or Gibbs excess) of the adsorbate [n_1^* (P, T, y), moles/g] in these sections are, respectively, n_1^0 and n_1^s (= 0).

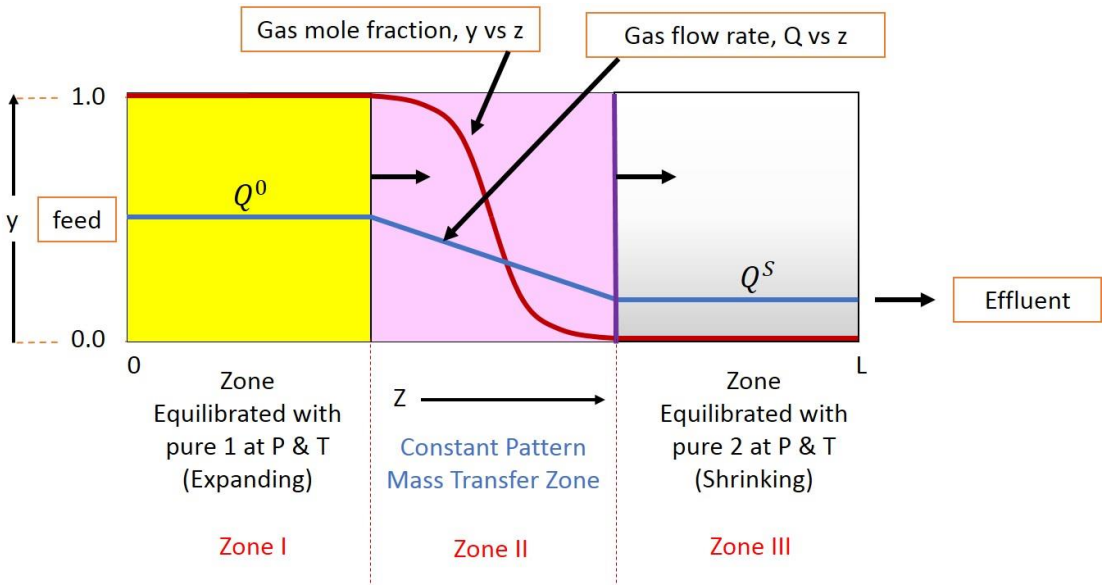

Figure 4-1. Schematic drawing of column profiles inside an Isothermal and Isobaric adsorber with a constant pattern MTZ (a pure adsorbate gas displacing a pure inert gas at constant P and T).

4.2 Model framework

A differential mass balance for the adsorbate at z and t yields:[4]

$$\left[\frac{\partial \bar{n}_i}{\partial t}\right]_z = -\left[\frac{\partial Q y_i}{\partial z}\right]_t ;\ \bar{n}_i = [\rho_b n_i + \alpha y_i];\ \alpha = \frac{\varepsilon P}{RT} \qquad (4\text{-}1)$$

where $\bar{n}_i$ (moles/cm^3) is the total amount (adsorbed + void) of component i per unit volume of the packed adsorbent column at z and t, and ε is the total void fraction (helium void) in the column [$\bar{n}_2 = \alpha y_2;\ n_2 = 0$].

The velocity β of the constant pattern MTZ is given by:[4]

$$\beta = \left[\frac{\partial z}{\partial t}\right]_M = -\left(\frac{\partial M}{\partial t}\right)_z \Big/ \left(\frac{\partial M}{\partial z}\right)_t \tag{4-2}$$

where M can be any of the characteristic properties (y, Q, n_1 or $\bar{n}_1$) of the MTZ.

Eqs. (4-1) and (4-2) can be combined for a constant pattern MTZ to get:

$$\left[\frac{\partial (Q y_1)}{\partial \bar{n}_1}\right]_z = \beta \tag{4-3}$$

Eq. (4-3) can be integrated to get the following relationships between y, $\bar{n}_1$, and Q in the constant pattern MTZ by using the boundary values of these variables in the leading [$y_1^S = n_1^S = n^S = 0$, $Q = Q^S$] and trailing [$y_1^0 = 1$, $\bar{n}_1^0 = (\rho_b n_1^0 + \alpha)$, $Q = Q^S$] edges of the MTZ:

$$[Q y_1 - \beta \bar{n}_1] = [Q^0 y_1^0 - \beta \bar{n}_1^0] = [Q^S y_1^S - \beta \bar{n}_1^S] = 0 \tag{4-4}$$

$$\beta = \frac{Q^0 y_1^0}{\bar{n}_1^0};\ \bar{n}_1 = \frac{Q y_1}{\beta} \tag{4-5}$$

The constant pattern MTZ propagates through the section III [$y_2^S = 1$, $\bar{n}_2^S = \alpha$] with a constant velocity β by displacing the pure inert gas from that section. Consequently, a mass balance of component 2 yields:

$$Q^S = \bar{n}_2^S \beta = \alpha \beta \tag{4-6}$$

The experimental column breakthrough data provide $Q(t)$ and $y_1(t)$ at the effluent end of the column (z = L). These profiles are mirror images of the corresponding profiles $Q(z)$ and $y_1(z)$ inside the constant pattern MTZ.

Linear Driving Force (LDF) Model of mass transfer:

According to the traditional LDF model, the rate of mass transfer of a single adsorbate (component 1) from the gas phase to the adsorbed phase inside a constant pattern MTZ at a distance z inside the column and time t is given by:[4, 5]

$$\left[\frac{\partial n_1}{\partial t}\right]_z = k(n_1^* - n_1) \tag{4-7}$$

where k (s^{-1}) is the LDF mass transfer coefficient at z and t. n_1 and n_1^* are, respectively, the amounts (mol/g) of component 1 adsorbed and that would be in equilibrium with the local gas phase (P, T, y_1) prevailing in the MTZ at z and t. The variable n_1 (z, t) can be estimated using Eqs. (4-1) and (4-5) in conjunction with the experimental column breakthrough data $Q(L, t)$ and y (L, t), while the equilibrium variable n_1^* can be estimated from the adsorption isotherm of the pure gas (component 1)at partial pressure $p1$ $(= Py_1)$ at T. The LDF model is chosen for its simplicity, practicality and popularity.[5]

Eq. (4-7) can be integrated to obtain an effective mass transfer coefficient, k^e (s^{-1}), over the entire length of the constant pattern MTZ for the pure adsorbate at P and T as:

$$\int_{\theta_\psi}^{\theta_{(1-\psi)}} \frac{d\theta}{(\theta^* - \theta)} = k^e\left[t_{(1-\psi)} - t_\psi\right];\ \theta = \left[\frac{n_1}{n_1^0}\right], \theta^* = \left[\frac{n_1^*}{n_1^0}\right] \tag{4-8}$$

where, θ_ψ and $\theta_{(1-\psi)}$ are, respectively, the values of variable θ defining the lower and the upper bounds of the MTZ. Variables t_ψ and $t_{(1-\psi)}$are the corresponding times in the θ vs t breakthrough curve. The length of the MTZ (LMTZ, cm) is then given by:

$$L_{MTZ} = \beta\left[t_{(1-\psi)} - t_{\psi}\right] \tag{4-9}$$

4.3 Experimental column dynamic tests and data analysis

We experimentally measured isothermal and isobaric column breakthrough data for pure N_2, pure O_2 and pure Ar displacing pure He at gas pressures of P = 2.0, 4.0 and 6.0 atm and temperatures of T = 273.1, 303.1 and 338.1 K. The feed gas mass flow rate was same (Q^0 = 0.193 mmoles/cm^2/s = 1.42 lbmoles/hr/ft^2) for all tests. Figure 4-2 shows typical examples of experimental column breakthrough data [$\lambda = y/y^0$, and $\phi = (Q - Q^S)/Q^0 - Q^S)$] vs dimensionless time ($\tau = t/t^*$) for (a) N_2 displacing He and (b) O_2 displacing He at P = 6.0 atm and T = 303.1 K. The variable $t^*(= L \cdot \bar{n}_1^0/Q^0)$ was the stoichiometric time for a hypothetical MTZ of zero length to reach the column end under local equilibrium condition, ($k^e \rightarrow \infty$) for the present cases.

The plots in Figure 4-2 were smoothed because raw data were somewhat discontinuous at times due to slow response of the analyzers. The later part of the ϕ vs τ plot was extrapolated for the same reason. However, it was estimated that the error in estimation of k^e due to uncertainty in that extrapolation was less than $+/-$ 5%. The column breakthrough data for all cases studied in this work were similar to those shown in Figure 4-2. They are not shown here for brevity. They can be found in Appendix C.

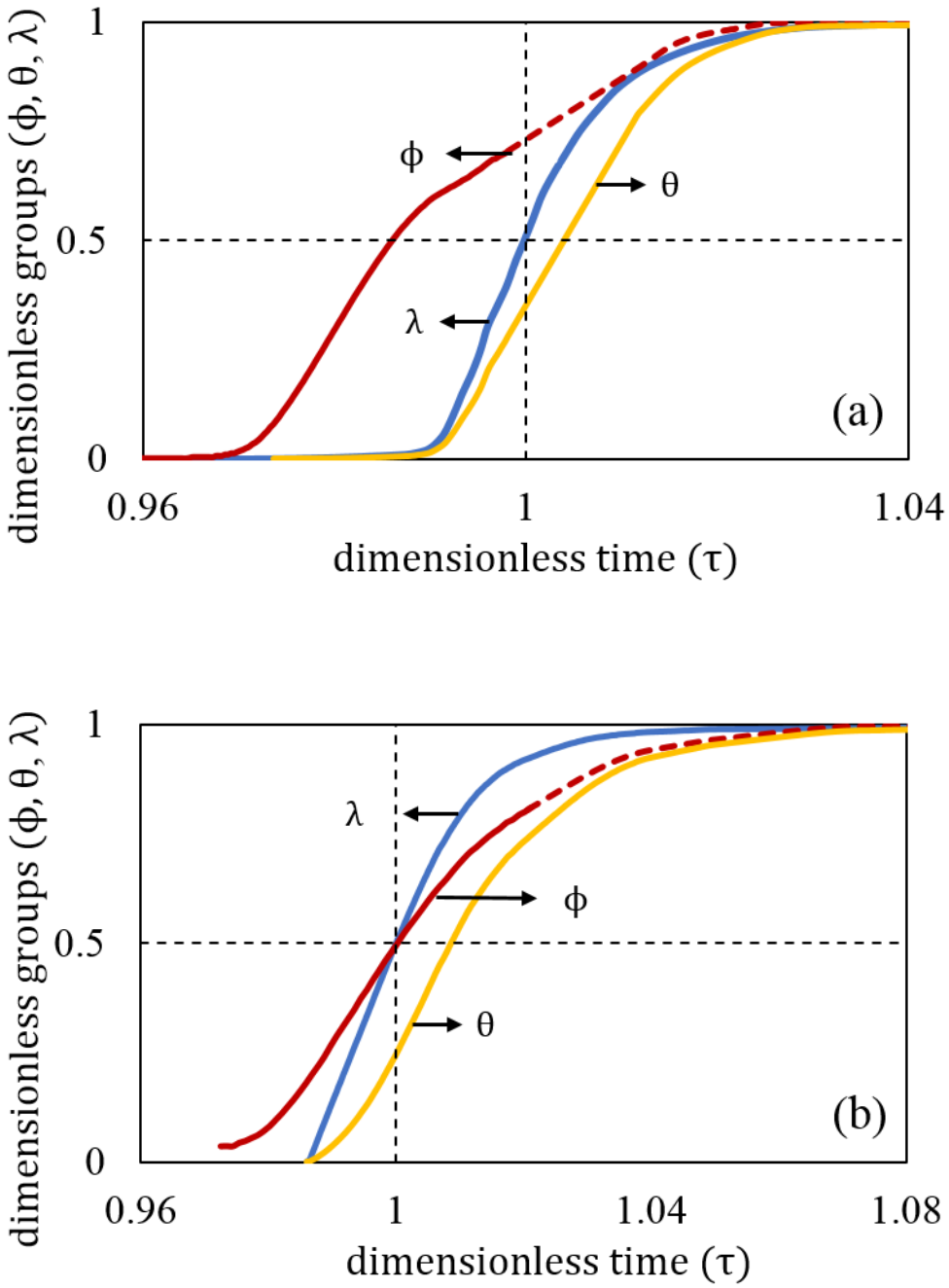

Figure 4-2. Experimental breakthrough curves for (a) N_2 displacing He, (b) O_2 displacing He: P = 6.0 atm; T = 303.1 K.

The experimental breakthrough data of Figure 4-2 were used to estimate n_1 and θ [$= (n_1/n_1^0)$] as functions of y_1 (or τ) using Eqs. (4-1) and (4-5). Representative plots of θ vs τ for N_2 and O_2 are shown in Figure 4-2. The corresponding equilibrium amounts adsorbed (n_1^* at p1 and T; n_1^0 at P and T) were obtained from an analytical heterogeneous –Langmuir adsorption isotherm model by Sircar which described the pure gas isotherms of N_2, O_2 and their binary mixtures on the adsorbent of interest very well.[6]

Finally, k^e for pure gases were estimated as functions of P and T by using Eq. (4-8). The bounds of the MTZ were defined by ψ = 0.01. Figure 4-3 shows exemplary plots of the integrand [$\frac{1}{(\theta^*-\theta)}$] of Eq. (4-8) as functions of θ for both N_2 and O_2 for the case where P = 6.0 atm, and T = 303.1 K.

Figure 4-4 summarizes the results of the breakthrough data analysis. It shows that (a) k^e decreases with increasing P approximately linearly for both gases in the range of the data presented in this work, (b) k^e increases with increasing T, which can be described by a weak exponential function of T for both gases, and (c) the mass transfer coefficients for N_2, O_2 and Ar for any value of P and T are comparable (within the limits of uncertainty in the experimental data). Observation (c) is not unexpected since the size and molecular weights of these gases are close.

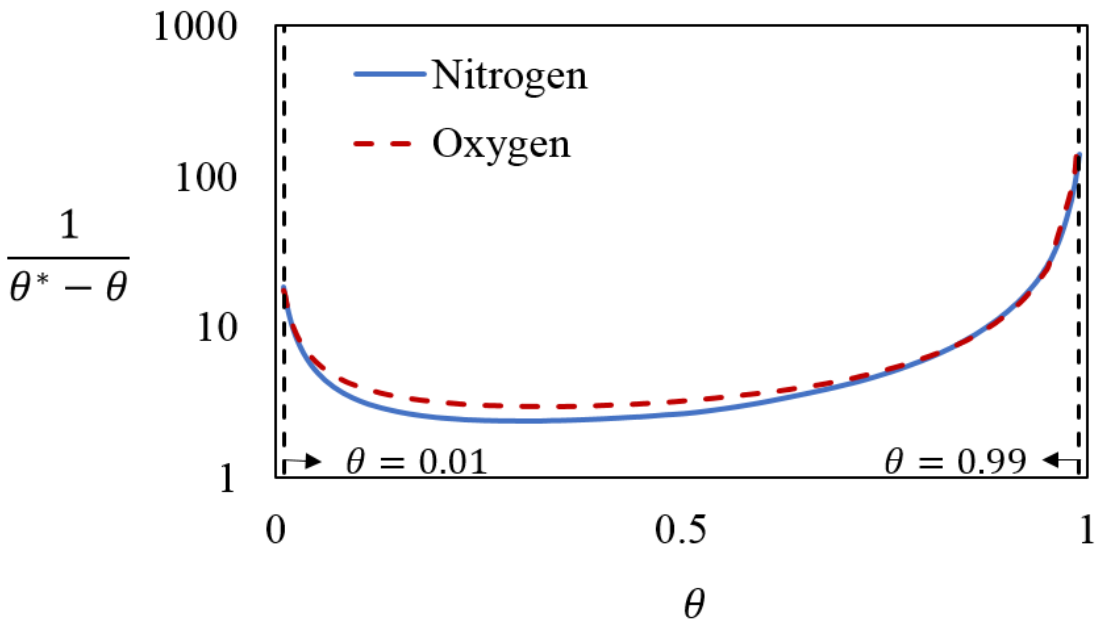

Figure 4-3. Plot of integrand of Eq. (4-8) as function of θ for pure N_2 and O_2 column dynamic data: P = 6.0 atm; T = 303.1 K.

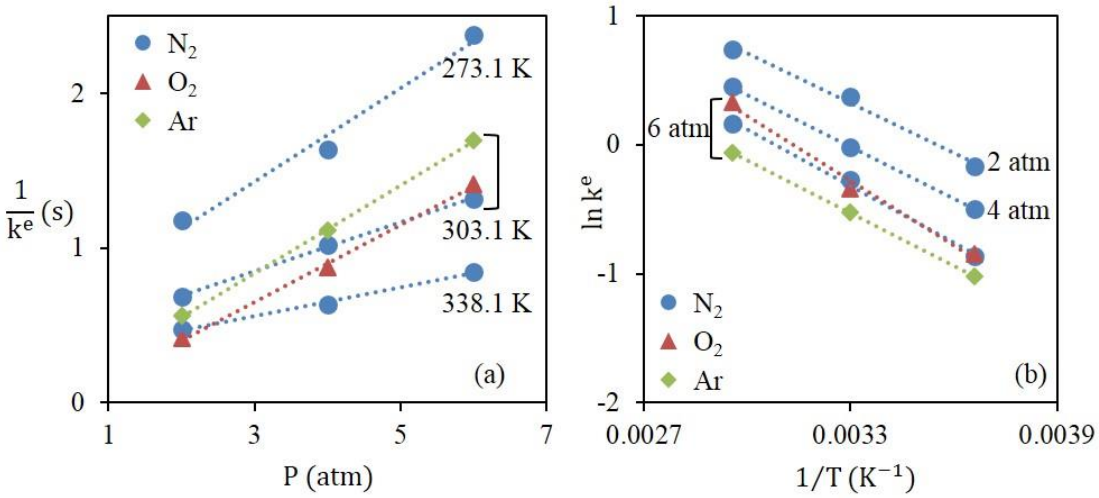

Figure 4-4. Temperature and Pressure dependence of k^e: (a) plots of $1/k^e$ as functions of P at different T for N_2, O_2 and Ar, (b) plots of $\ln k^e$ vs 1/T at different P for N_2, O_2 and Ar.

4.4 Model estimation of various transport resistances in the zeolite pellet

Transport of a pure adsorbate from an ideal gas phase inside a packed bed adsorber to an adsorption site inside the zeolite crystal may encounter a series of mass transfer resistances.[7] Eq. (4-10) provides a simplified and idealized correlation between the over-all effective mass transfer coefficient (k^e, s^{-1}) and the individual resistance in the path for isothermal and isobaric transport of a single adsorbate from an inert gas where (a) the pure adsorbate has a linear adsorption isotherm [$n_1^*\ (P, T, y_1 = 1)\ = K_H\ (T) \cdot P$], and (b) the mass transfer rate is given by a LDF model (Eq.(4-7)). The variable K_H [$= K_H^0 exp\ (q_H/RT)$] is the Henry's Law constant (moles/g/atm) for the adsorbate at T, q_H is the isosteric heat of adsorption for the adsorbate in the Henry's Law region, and K_H^0 is a constant.

$$\frac{1}{k^e} = \frac{1}{k_{ax}} + \frac{1}{k_{ex}} + \frac{1}{k_{sk}} + \frac{1}{k_M} + \frac{1}{k_m} \tag{4-10}$$

where $1/k_{ax}$, $1/k_{ex}$, $1/k_{sk}$, $1/k_M$, $1/k_m$ are, respectively, resistances (equivalent) introduced by axial dispersion in adsorber gas phase, external gas film resistance at pellet surface, skin resistance created by a denser pellet surface than the interior, binder macro-pore resistance, and zeolite micro-pore resistance for mass transport. The resistances occur in series in the order described by Eq.(4-10).

No correlation exists in the literature for estimation of the skin resistance. Hence, it should be treated as an empirical parameter.[8, 9] Magnitudes of other resistances can be approximately estimated by the following correlations:[7]

$$\frac{1}{k_{ax}} = \frac{D_{L.}K\,(1-\,\varepsilon_b)}{\varepsilon_b\,\cdot\,V^2};\ \frac{1}{k_{ex}} = \frac{R_P K}{3k_f};\ \frac{1}{k_M} = \frac{R_P^2 K}{15\varepsilon_P D_P};\ \frac{1}{k_m} = \frac{R_c^2}{15D_c} \qquad (4\text{-}11)$$

where D_L [$= (\,0.7D_m\, +\, 0.5d_P\, QRT/\varepsilon_b P)$] is the axial dispersion coefficient for the adsorbate in the gas phase of the adsorber; D_P[$= D_m D_K/\tau(D_m +\, D_K)$] is the effective binder- pore diffusivity of adsorbate; D_m is the molecular diffusivity of the adsorbate gas in helium at P and T, D_K is the Knudsen diffusivity of the adsorbate through the binder pores, (diameter = d), and τ is the tortuosity factor of the binder pores. D_c is the adsorbate diffusivity in the crystal micro-pores. Q is the mass flow rate of gas through the adsorber, ε_b is the inter- pellet void fraction in the adsorber, ε_P is the adsorbent porosity, V ($=$ $QRT/\varepsilon_b P$) is the linear velocity of the gas through the external void space in the column at P and T, R_P is the radius of the adsorbent particle, R_C is the zeolite crystal radius, and K ($=\ K_H RT\rho_P$) is the dimensionless Henry's Law constant for the adsorbate at T. ρ_P (g/cm^3) is the adsorbent particle density, and R is the gas constant. The mass transfer coefficient for external film (k_f) can be calculated at the average gas flow rate [$(Q^0\ +$ $Q^S)/2$] across the MTZ using an empirical correlation.[10] Standard literature correlations can be used for estimation of various diffusivities as functions of P and T.

The model was used in this work only to obtain approximate values of the various resistances, and to compare their relative contributions to the over-all mass transfer resistance. A realistic view of the adsorbent binder pore structure is obviously much more complex and cannot be experimentally characterized or mathematically modelled. The empirical fudge factor τ covers up for this deficiency.

The adsorption isotherms of pure O_2 and pure Ar on the pelletized LiLSX zeolite sample of this work were approximately linear in the pressure and temperature ranges of the data analyzed in this work.[6] Consequently, the above described model protocol was used to evaluate the contributions of different resistances for O_2 and Ar transport into the zeolite pellet under various conditions.

For example, the model estimated value of k^e for P = 2 atm, and T = 303.1 K, in absence of a skin resistance [$k_{sk} \rightarrow \infty$], was ~ 7.8 s^{-1}. On the other hand, Figure 4-4a shows that the experimental value of k^e under these conditions was ~2.4 s^{-1}. This difference clearly suggests that a substantial skin resistance [$1/k_{sk} \sim 0.29\ s$] was present at the pellet surface. The relative contributions of different resistances may be estimated to be as skin ~ 69.1 %, axial dispersion ~18.0 %, external film ~ 11.4 %, binder macro-pore ~ 1.4 %, and zeolite micro-pore ~ 0.2 %. Thus, intra-particle transport resistance was not significant. Extraneous resistances dominated the mass transfer process.

It can be easily shown by the model that the resistances created by axial dispersion $(k_{ax})^{-1}$, external film $(k_{ex})^{-1}$, and binder macro-pore $(k_M)^{-1}$ increase linearly with increasing P since D_m is inversely proportional to P. The net effect is that $(k^e)^{-1}$ increase with increasing P as shown by Figure 4-4a.

The temperature coefficient of k^e is complex since the temperature dependent variables in Eq.(11), ρ_g, D_m, D_K and μ, are proportional to, respectively,T^{-1}, $T^{1.5}$, $T^{0.5}$, and $T^{0.5}$, while K_H is an exponential function of T.[11] The net effect is that k^e can be empirically described by a weak exponential function of T in the range of the data as shown by Figure 4-4b.

The existence of a skin resistance was observed under all conditions of operation of this work. Table 4-1 lists values of model estimated $1/k_{sk}$ (s) for O_2 and Ar under various P and T. Transport data for O_2 and Ar only were considered because the O_2 and Ar isotherms were nearly linear at all P and T ranges of this study. The numbers in parenthesis indicate the % ratio of skin resistance $(1/k_{sk})$ to over-all mass transfer resistance $(1/k^e)$.

Table 4-1. Estimated effective skin resistance ($1/k_{sk}$, s) for O_2 and Ar mass transfer into LiLSX zeolite pellet at different P and T.

Gas	P (atm)	T (K)	k^e (s^{-1})	skin resistance as % of overall resistance
O_2	2.0	303.1	0.287	69.1
	4.0	303.1	0.623	71.1
	6.0	273.1	1.676	72.1
	6.0	303.1	1.023	72.6
	6.0	338.1	0.511	71.0
Ar	2.0	303.1	1.78	79.8
	4.0	303.1	0.90	79.6
	6.0	273.1	0.36	79.7
	6.0	303.1	0.59	79.9
	6.0	338.1	0.94	79.1

The data in Table 4-1 indicates several interesting features: (a) a substantial skin resistance (about 70~80% of total resistance) is present under all conditions of P and T evaluated in this work, (b) the percentage ratio of skin to total resistance $(1/k^e, s)$ is practically the same under all conditions.

It should be pointed out that the lengths of the mass transfer zones for adsorption of N_2, O_2 and Ar on LiLSX pellets (d_P = 0.05 cm) under all conditions reported in this work were very short. The percentage ratios of the length of the unused bed (LUB) to the column length [$LUB/L = (1 - {t^0}/{t^*})] \times 100$, where t^0 is the time of incipient breakthrough ($\lambda = 0$), were less than 2 – 3 % indicating fairly sharp MTZ (high column capacity utilization) for all cases.

4.5 Comparison with published data

A commonly used correlation [$k^e = 60D^e/d_p^2$] was used between an effective overall diffusivity (D_e, m^2/s) and an overall mass transfer coefficient (k^e, s^{-1}) for transport of a pure gas into an adsorbent particle of diameter d_p(cm) in order to calculate D^e for Ar at a pressure of 1 atm and ~300 K on the LiLSX zeolite sample (d_p = 0.052 cm) of the present work. The value of k^e (= 3.61 s^{-1}) under these conditions was obtained by extrapolation of $1/k^e$ vs P plot of Figure 4-4a. The estimated value of D^e was 1.63 x 10^{-8} m^2/s.

A value of k^e = 0.23 s^{-1} was reported in the literature for transport of pure Ar under similar conditions (P = 1, atm, T = 298 K) using an Ag exchanged LiX zeolite sample (d_p = 0.16 cm).[1] Thus, the estimated value of D^e for Ar on that material was 0.98 x 10^{-8} m^2/s. Consequently, the LiLSX zeolite sample of the present work exhibited ~ 66 % larger overall diffusivity than the Ag-LiX zeolite sample. This re-emphasizes the need for independent measurement of adsorption characteristics of each different sample before use in practice.

4.6 Summary

Effective mass transfer coefficients for pure N_2, O_2 and Ar into a sample of small diameter LiLSX zeolite pellet were estimated by analysis of isothermal and isobaric column dynamic breakthrough data of pure gases at different pressures and temperatures. A specific protocol based on assumption of a constant pattern mass transfer zone formation during the column dynamic test and a linear driving model for the transfer process was used for data analysis. The coefficients were found to decrease with increasing pressure and increase with increasing temperature.

The study suggested the presence of a pronounced skin resistance (about 70~80 % of total resistance) at the binder surface, which, in conjunction with the resistances created by the external gas film and axial dispersion in the column gas phase, accounted for most of the over-all mass transfer resistance. The intra- particle macro and micro-pore transport resistances were comparatively very small. Such extensive experimental data on adsorptive mass transfer coefficients and their characteristics for the system of interest have not been reported in the literature.

4.7 Reference

1. Ferreira, D.; Magalhães, R.; Bessa, J.; Taveira, P.; Sousa, J.; Whitley, R. D.; Mendes, A. Study of AgLiLSX for Single-Stage High-Purity Oxygen Production. *Ind. Eng. Chem. Res.* **2014,** *53*, 15508-15516.
2. Bulow, M.; Shen, D. Mobility of nitrogen in Li, Re-LSX zeolite beads. *Rec. Adv. . Sci. .Technol. .Zeolites .Relat. Mater., Pts A - C* **2004,** *154*, 2070-2077.
3. Bulow, M.; Shen, D. M. Sorption kinetics of atmospheric gases on Li,RE(rare earth)-LSX zeolite beads as sorbents for oxygen PVSA processes. *Microporous Mesoporous Mater.* **2007,** *105*, 163-169.
4. Sircar, S.; Kumar, R. Adiabatic Adsorption of Bulk Binary Gas-Mixtures - Analysis by Constant Pattern Model. *Ind. Eng. Chem. Proc. Des. Dev.* **1983,** *22*, 271-280.
5. Sircar, S.; Hufton, J. R. Why does the Linear Driving Force model for adsorption kinetics work ? *Adsorption* **2000,** *6*, 137-147.
6. Wu, C.-W.; Kothare, M. V.; Sircar, S. Model Analysis of Equilibrium Adsorption Isotherms of Pure N2, O2, and Their Binary Mixtures on LiLSX Zeolite. *Ind. Eng. Chem. Res.* **2014,** *53*, 12428-12434.
7. Ruthven, D. M., *Principles of Adsorption and Adsorption Processes*. Wiley: 1984.
8. Kumar, R.; Sircar, S. Skin Resistance for Adsorbate Mass-Transfer into Extruded Adsorbent Pellets. *Chem. Eng. Sci.* **1986,** *41*, 2215-2223.
9. Satterfield, C. N., *Mass transfer in heterogeneous catalysis*. M.I.T. Press: 1970.
10. Hsiung, T. H.; Thodos, G. Mass-transfer factors from actual driving forces for the flow of gases through packed beds (0.1 < Re < 100). *Int. J. Heat Mass Transfer* **1977,** *20*, 331-340.
11. Bird, R. B.; Stewart, W. E.; Lightfoot, E. N., *Transport Phenomena*. Wiley: 2007.

Chapter 5

Effect of Adsorbent Selectivity on MOC process

The selectivity of adsorption plays a crucial and complex role in determining the performance of an adsorptive gas separation process. For example, consider the separation of a binary gas mixture by a basic pressure swing adsorption (PSA) process, such as the four-step Skarstrom PSA cycle, where component 1 is selectively removed ($S_{12}>1$) from a binary feed gas mixture by an adsorbent in order to generate a component 2- enriched product gas, followed by desorption of component 1 by lowering the adsorber column pressure and back purging the adsorbent with a part of the product gas.[1, 2]

A low value of S_{12} increases the co-adsorption of component 2 which causes loss of component 2 during the desorption steps resulting in a lower recovery of that component in the product gas. Co-adsorption of component 2 also reduces the potential adsorption capacity of component 1 by the adsorbent, resulting in a larger adsorber size for the separation. A large S_{12}, on the other hand, increases the quantity of the product gas required for desorption of component 1 by back purge, thereby lowering the recovery of component 2.[3] Similarly, a basic thermal swing adsorption (TSA) process for removal of a trace or dilute impurity (component 1) from a bulk gas (component 2) calls for a very high selectivity of adsorption for the impurity ($S12>>1$) in order to minimize the co-adsorption of the bulk gas , and thus reduce the adsorber size, the column pressure drop, and heat requirement for adsorbent regeneration, which are desirable process design goals.

The effects of higher selectivity on RPSA process performance cannot be reliably studied by model simulations of the process because of the myriads of uncertainty in accurate estimation of the complex mass, heat and momentum transfer resistances inside an adiabatic adsorber which influence the process performance.[2] Model simulations can be particularly very difficult if the adsorbent is energetically heterogeneous. Experimental process performance data are generally needed for reliable design as well as for empirically readjusting the afore-mentioned transfer resistances for increasing the reliability of the process model.[2, 4] Experimental process performance data are essential to demonstrate the practical viability of a RPSA process design. Unfortunately, such data for MOC - RPSA processes are few in the published literature and they are mostly confined in the patent literature.[5] Thus, the present work fills a major gap and provides valuable insights into the subject.[4]

The purpose of this chapter is to report actual experimental data on process performance of our MOC design using another commercial LiX zeolite (Material B) produced by Arkema Corporation of the U.S.A which exhibits a much higher selectivity of adsorption for N_2 over O_2 than that by Material A. It may be apparent that higher thermodynamic selectivity of N_2 over O_2 on a zeolite adsorbent will facilitate the efficiency of air separation by a pressure swing adsorption (PSA) process but the actual effects of higher selectivity on BSF and R_O of a RPSA process can be complex and non-intuitive. The adsorption literature does not cover this topic.[5] This chapter also included a literature search for a period from 1995 to 2015 on experimental data for

binary and ternary gas adsorption selectivity and their predictions from the corresponding pure gas adsorption isotherms by IAST.

5.1 Physical properties of LiLSX zeolite samples

The key physical properties of the samples of LiLSX zeolites were supplied by the manufacturers. They are reported in Table 5-1. It may be seen from Table 5-1 that sample A had larger average particle size than sample B. Their bulk densities and helium void fractions in a packed column were, however, very close. Chemically, the binder materials in the two samples were different as well as the degrees of Li exchanges (~ 70-90% for A and > 90% for B).

Table 5-1. Physical properties of LiLSX zeolites A and B.

	A (Zeochem)	B (Arkema)
Shape	bead	bead
Particle size (μm)	500~600	300~400
Bulk density (g/cm^3)	0.615	0.606
Helium void volume (cm^3/cm^3)	0.70	0.71
Chemical composition percentage (by wt)	Lithium sodium (potassium)aluminasilicate 70-90 % Sodium potassium aluminosilicate <20 % Hydrous aluminum silicate 5-20 %	Zeolite (sodium, calcium, barium, lithium or potassium aluminasilicates) >90% Kaolin 0-10% bentonite clay 0-10% clay, attapulgite 0-10% sepiolite 0-10% Cristobalite <0.2% Tridymite <0.1%

The extent of Li exchange in a LiX zeolite is a critical issue in determining the adsorption characteristics of N_2 and O_2 on the zeolite.[6, 7] Both N_2 adsorption capacity and selectivity of adsorption of N_2 over O_2 increase with increasing degree of lithium exchange in LiLSX zeolite above a threshold value of exchange (~ 70 %). Consequently, Material B is expected to exhibit higher selectivity of adsorption of N_2 over O_2 than Material A.

5.2 Adsorptive properties of the LiLSX zeolites (Material B)

The zeolite sample was regenerated at a temperature of 380 ℃ under a flow of dry N_2 for 6 hours before the measurements. The same isothermal column dynamic apparatus which was used to characterize Material A in Chapter 2 was employed to measure the adsorptive properties of Material B. Column break through (CBT) data were measured under different conditions for pure N_2 and O_2 displacing pure He and binary N_2 + O_2 mixtures displacing pure O_2 through a packed column of the zeolite. The equilibrium adsorption isotherms were estimated using the CBT data. A detailed description of the test apparatus, the experimental procedures, and the protocols used for data analysis can be found in Chapter 2~4.

5.2.1 Pure gas adsorption isotherms of N_2 and O_2

The pure gas adsorption isotherms of N_2 and O_2 on LiLSX zeolite samples A and B are compared in Figure 5-1a and b, respectively. The Gibbs surface excesses (GSE) are plotted against the gas pressure (P) at a constant temperature (T). The data were measured in the pressure range of 0- 6 atm at three different temperatures (0, 30 and

65℃). Material A exhibits higher capacity for both pure N_2 and O_2 in the entire pressure range of the data at all temperatures. However, the relative differences in the capacities of N_2 on Materials A and B at any given pressure are much smaller than the corresponding differences in the capacity of O_2.

5.2.2 Heterogeneous adsorption isotherm model

An analytical pure and mixed gas adsorption isotherm model for energetically heterogeneous adsorbent can be used to describe the isotherm data of Figure 5-1a and b as shown by the dashed lines in the figure. Details of the model can be found elsewhere.[8, 9] The model can well describe the experimental data over all pressure and temperature ranges of the experimental data.

Table 5-2 lists the values of the model parameters for materials A and B. It also gives the Henry's Law selectivities of N_2 over O_2 on the Material B at different temperatures. S_{12}^0 for Material B is much larger than that for Material A at all temperatures in the range of the data. Larger degree of Li exchange in material B is presumably the cause of this behavior. It may be noted that the ψ values for N_2 are larger than those for O_2 indicating that the adsorbent is energetically more heterogeneous for N_2 adsorption than for O_2.[8] Material A also indicated that behavior.[9]

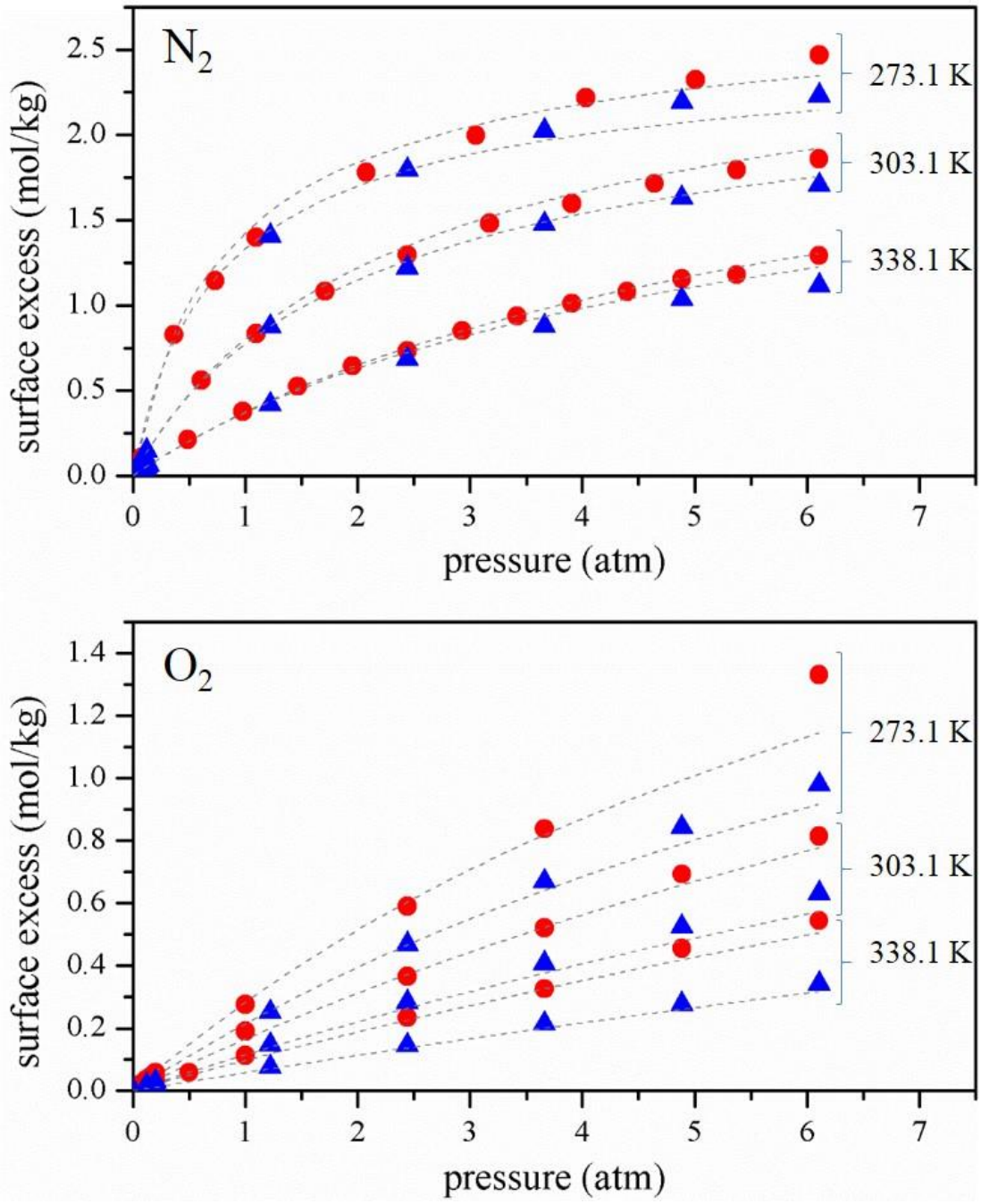

Figure 5-1: Pure gas equilibrium adsorption isotherms on LiLSX zeolite Materials A (circles), B (triangles) and heterogeneous model fitting (dashed line) at different temperatures.

Table 5-2. Parameters of the Heterogeneous Langmuir isotherm model for adsorption of N_2 and O_2 on Materials A and B.

Material	T (K)	Henry's Law Selectivity for N_2 –O_2 Binary	Isotherm model parameters						
			m	N_2			O_2		
				μ_0	q^0	ψ	μ_0	q^0	ψ
A	273.1	12.28	2.87	2.56×10^{-5}	5.87	0.995	2.89×10^{-4}	3.22	0.24
	303.1	7.57				0.884			0.06
	338.1	4.80				0.834			0.0003
B	273.1	13.68	2.57	3.41×10^{-5}	5.75	0.9786	7.41×10^{-5}	3.87	0.0992
	303.1	9.90				0.9463			0.0122
	338.1	7.11				0.9152			0.0095

5.2.3 Pure gas N_2 and O_2 isosteric heats of adsorption

Figure 5-2a plots the isosteric heats (q) of pure N2 and O2 on Materials A and B as functions of GSE (n^m) estimated from the pure gas adsorption isotherms at different temperatures (Figure 5-1) using the thermodynamic relationship $q = -R\left[\frac{\partial lnP}{\partial\left(\frac{1}{T}\right)}\right]_{n^m}$,where R is the gas constant. The Figure shows that q for both gases on both materials decrease with increasing n^m indicating that both materials are energetically heterogeneous for both gases. This behavior on Material A was discussed earlier in Chapter 2.

Figure 5-2b shows the departure of the isosteric heats of the pure gases ($q - q^0$) from their respective Henry's law isosteric heats (q^0) as functions of n^m. The departures for N_2 are larger than those for O_2 on both materials. This indicates that the adsorbents were more heterogeneous for N_2 adsorption than for adsorption of O_2. The data also suggests

that Material A is relatively more heterogeneous than Material B for both gases. The isosteric heats of adsorption in the Henry's law region for both gases are given in Table 5-2. The relative magnitudes of these limiting heats suggest that (a) N_2 is more strongly adsorbed over O_2 on both materials and (b) the relative strengths of adsorption of N_2 on both materials are comparable while (c) O_2 is more strongly adsorbed on Material B than on Material A.

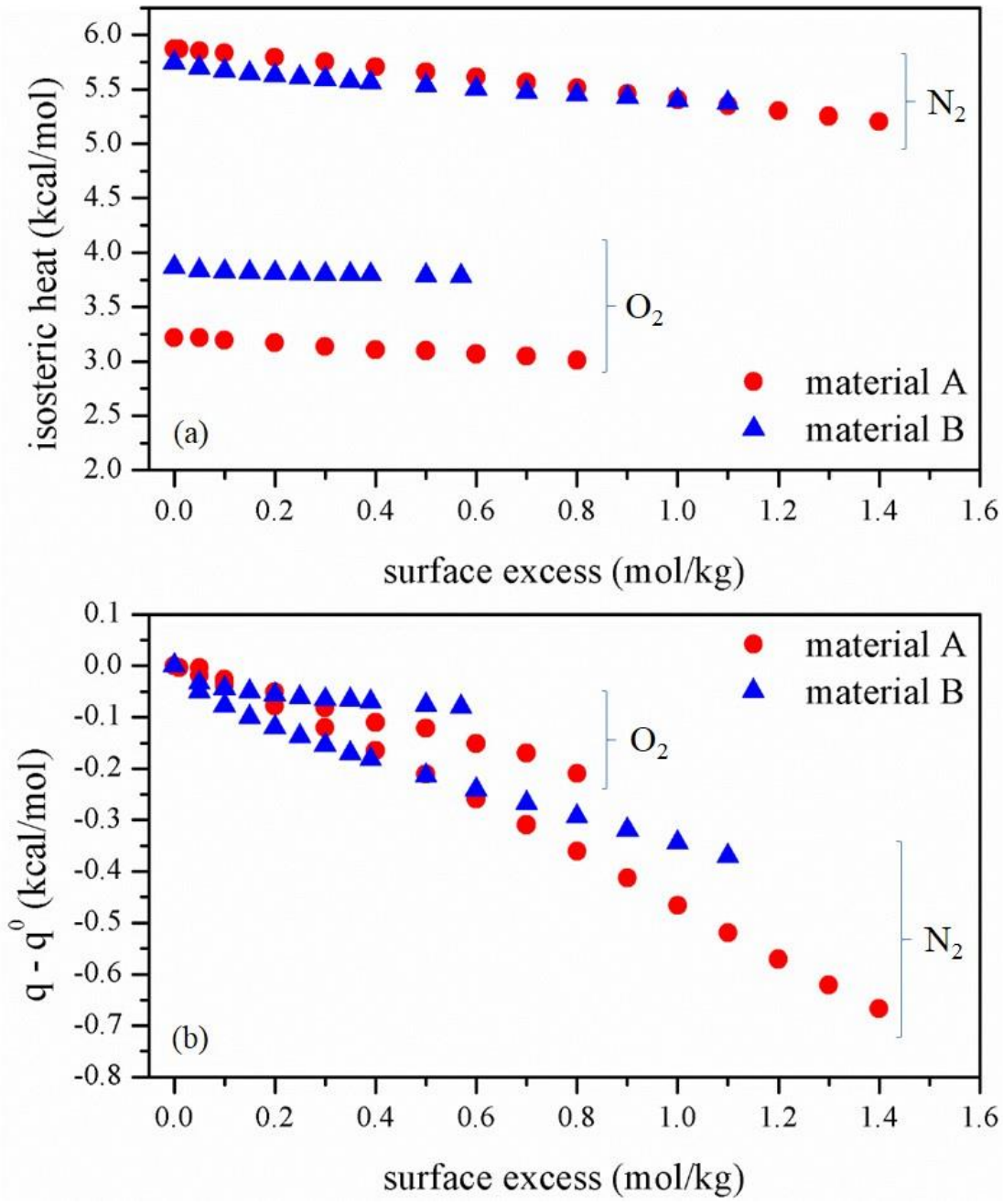

Figure 5-2: (a) Isosteric heats (q) of pure N_2 and O_2 vs GSE (nm); (b) Differences between q of a gas at a given GSE and the isosteric heat of that gas in the Henry's law region (q^0): Material A (circles) and Material B (triangles).

5.2.4 Adsorptive mass transfer coefficients for pure N_2 and O_2

The column breakthrough curves (BTC) for pure N_2 and O_2 displacing pure helium (inert gas) from a zeolite column packed with Material A or B are shown in Figure 5-3, respectively. The abscissa is dimensionless time where t_m is the stoichiometric breakthrough time. The columns were initially saturated with helium at 6 atm and at a temperature of 303.1 K. The feed gas was at the same P and T and the flow rates were approximately the same for all tests.

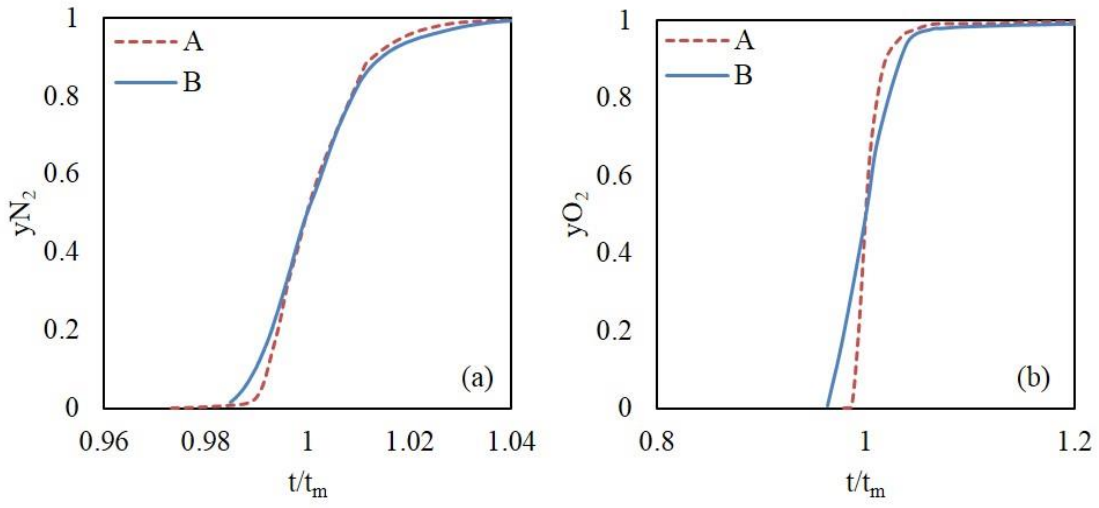

Figure 5-3. Column breakthrough curves at a pressure of 6 atm and 303K for (a) pure nitrogen displacing pure He, and (b) pure oxygen displacing pure He. Material A (dashed lines); Material B (solid lines)

It may be seen from Figure 5-3a that N_2 BTCs on Materials A and B nearly superimpose indicating a very similar pure N_2 mass transfer coefficient for both zeolite samples. The lengths of unused bed (LUB) for both materials were less than ~ 2% of the column length (L). In other words, the mass transfer resistances for adsorption of N_2

in both materials were very small. Figure 5-3b, on the other hand, indicates that the mass transfer coefficient for O_2 adsorption on zeolite A is relatively larger than that on zeolite B. However, the LUB for O_2 on both materials were less than ~ 5% of the column length indicating rather low mass transfer resistances for O_2 too. It should be pointed out that the differences in the particle sizes of the two materials (Table 5-1) did not have significant influence on the column breakthrough characteristics because the effective mass transfer coefficients were large for both particle sizes.

5.2.5 Binary N_2 + O_2 adsorption isotherms and selectivity

. The limiting value of the binary gas selectivity (S_{12}^0) at temperature T in the Henry's law region [$P \rightarrow 0$, $n_i = K_i P y_i$] is given by: [10]

$$S_{12}^0 = \left[\frac{K_1}{K_2}\right];\ K_i = K_i^0 exp[q_i^0/RT] \tag{5-1}$$

where K_i (T) is the Henry's law constant for pure gas i at T; q_i^0 is the isosteric heat of adsorption of pure gas *i* in the Henry's law region; K_i^0 is a constant and R is the gas constant. The thermodynamic selectivity of adsorption (S_{ij}) of component *i* of a gas mixture over another component j is a function of the equilibrium gas phase pressure (P), temperature (T), and mole fraction (y_i) of component i. It is traditionally defined by [11]:

$$S_{ij} = \left[\frac{n_i y_j}{n_j y_i}\right] \tag{5-2}$$

where the variable n_i is the specific equilibrium amount of component *i* adsorbed (moles/kg) from the gas mixture at P, T and y_i . Thus, the selectivity is a derived variable which can be estimated by measuring n_i (P, T, y_i).[1]

The experimentally measured binary adsorption isotherms of N_2 + O_2 at a temperature of 303.1 K and a total gas pressure of 1 atm for both materials are compared in Figure 5-4a. The GSE (n_i^m) of N_2 (component 1) and O_2 (component 2) from their binary mixtures are plotted as function of gas phase mole fraction of N_2 (y_1). The Figure shows that the GSE of N_2 on both zeolites are comparable for any given y_1 , while the corresponding GSE of O_2 for Material B is lower than that for Material A. In other words, the co-adsorption of O_2 from the binary mixture is lower for Material B, which translates to higher selectivity (S_{12} >1) of adsorption of N_2 over O_2 on that material. Figure 5-4b compares the experimentally estimated S_{12} values as function of y_1 for Materials A and B at P = 1.0 atm and T = 303.1K. The variation of S_{12} with changing y_1 is primarily due to adsorbent heterogeneity.[8]

Figure 5-4b shows that the selectivity of adsorption of N_2 over O_2 (S_{12}) exhibited by Material B is much larger than that for Material A for the entire composition range of the data at a total gas pressure of 1.0 atm and a temperature of 303.1K. It indicates that Material B will be a superior adsorbent than Material A for air separation application.

[1] The actual experimental variable to quantify the extent of adsorption of component *i* from a multi-component gas mixture is the Gibbs surface excess of that component, which is loosely called the amount adsorbed in literature. The surface excess can be directly measured as functions of P. T and y_i employing various macroscopic methods [12].

We estimated the ratios of S_{12} values for these two materials using the Heterogeneous Langmuir model and the parameters of Table 5-2 for an air like gas (79 % N2 + 21 % O2) at the same temperature and total gas pressures of 1.0 and 3.2 atm and found practically no effect of pressure on the ratio. Thus Material B is a preferred material for air separation application using a PSA- MOC process.

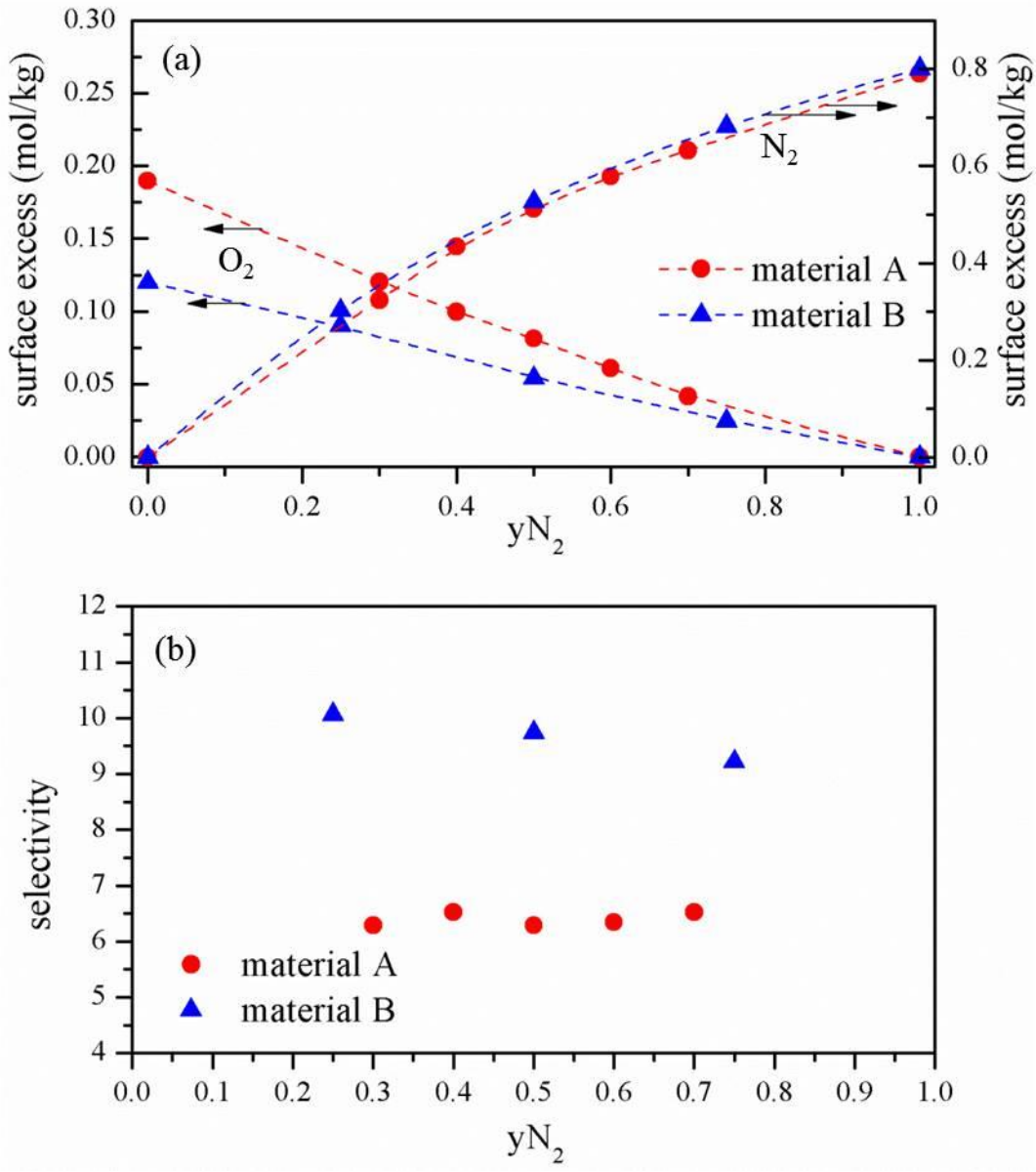

Figure 5-4. (a) Binary gas (N_2 + O_2) adsorption isotherms: circles (Material A); triangles: (Material B); (b) Binary selectivity vs y_1 at 1 atm, 303.1K: Lines are smooth curves through the experimental data points for interpolation purposes.

5.3 MOC- RPSA process performance

The above described comparative evaluation of the characteristics of Materials A and B for adsorption of pure N_2 and O_2 and their binary mixtures indicates that the outstanding difference between these two zeolites for air separation application is the substantially higher value of S_{12} exhibited by Material B over Material A. The differences in other properties like N_2 adsorption capacity, N_2 and O_2 isosteric heats of adsorption, N_2 and O_2 adsorptive mass transfer rates are relatively smaller between the two samples of LiLSX zeolites. Consequently, we measured the actual performance difference exhibited by Materials A and B in a continuous RPSA process designed to produce ~ 90 % O_2 from a dry-CO_2 free compressed air stream (78% N_2 + 21% O_2 + 1% Ar) in order to study the effect of adsorbent selectivity on our MOC process. The description of the experimental RPSA test apparatus, the operational procedure and data collection, and the protocol for data analysis can be found in detail elsewhere.[13, 14]

The RPSA process consisted of four sequential cyclic steps: (a) adsorber pressurization using a part of the product gas, (b) adsorption of N_2 from feed air to produce ~ 90% O_2 enriched product gas at ~ PA, (c) counter-current adsorber depressurization to pressure PD, (d) counter current adsorber purge at ~ PD with a part of the product gas. Effluent gases from steps (c) and (d) were rejected.

Cyclic steady state runs were carried out using different total cycle times (t_c) in the range of 3 - 9 seconds at a feed air pressures of 3.2 atm. The apparatus is kept at ambient temperature (~ 21℃).The performance variables for a RPSA process can be measured

in terms of product purity, product productivity, product recovery, and adsorber bed size factor (BSF).

The key performance variables are product recovery (R_O) and bed size factor (BSF). R_O is a measure of efficiency of separation process, while BSF is an indicator of adsorbent requirement for a specific RPSA process under given operating conditions. The preferred process is to yield desired product purity with lowest BSF and highest product recovery for a given cycle time.

MOC-RPSA process performance tests using material A and B were carried out. Figure 5-5 is a summary of the comparative process performance for the Materials A and B. The solid and dashed lines in Figure 5-5 are smooth lines through the experimental data points. The BSF for both materials decrease with decreasing cycle time (larger frequency of cycling) at higher cycle times as expected. However, the BSF cannot be decreased indefinitely due to detrimental effects of various transport resistances at lower cycle times.[2, 5, 13] The R_O increases with increasing cycle time and levels off at higher cycle times.

Figure 5-5 shows that the BSF vs t_c profiles are qualitatively similar for both materials exhibiting a minimum BSF. However, the BSF yielded by Material B is consistently lower than that for Material A at all cycle times. The minimum in BSF occurs approximately at the same cycle time for both materials. The curvature of the BSF- t_c plot is, however, much flatter for Material B than that for Material A. The values of R_O are significantly higher for Material B than that for Material A at all values of t_c.

Consequently, Material B, which has a higher selectivity of adsorption than Material A, is a superior adsorbent for the MOC process.

The complexity and nuances of the functional dependence of BSF and R_O on RPSA process cycle time for different N_2 selectivities of the adsorbent exhibited by Figure 5-5 are clearly non-intuitive and can only be appreciated by experimental process study.

It may be seen from Figure 5-5 that a practically attractive total cycle time for the MOC process is 6.5 s and not 5.5s where the BSF exhibits its minimum value because a much higher value of R_O can be achieved at the former cycle time while paying a small penalty in the BSF value. Table 5-3 compares the values of BSF and R_O for the two materials at a total cycle time of ~ 6.5 s. According to the data of Table 5-3, the BSF of the MOC process can be reduced by ~ 12.8 % while the R_O is increased by ~42.1 % using the higher selectivity zeolite B.

Higher selectivity reduced the bed size factor and increased the O_2 recovery, which are desirable changes for the process. However, the effects of selectivity on the relative magnitudes of these changes were strong functions of PSA process cycle times which could not be pre-assumed. Variation of selectivity with P, T, and y_i (or n_i and T) under the conditions of operation of a real adsorptive separation process complicates its role in determining the over-all process performance. The effects, in general, are clearly non-intuitive and can only be appreciated by experimental process study.

Table 5-3. RPSA process performance by zeolites A and B

Zeolite	BSF ($lb/TPDO_2$)	Oxygen Recovery (R_O, %)	cycle time (s)
Material A	170.0	21.6	6.5
Material B	148.2	30.7	6.5

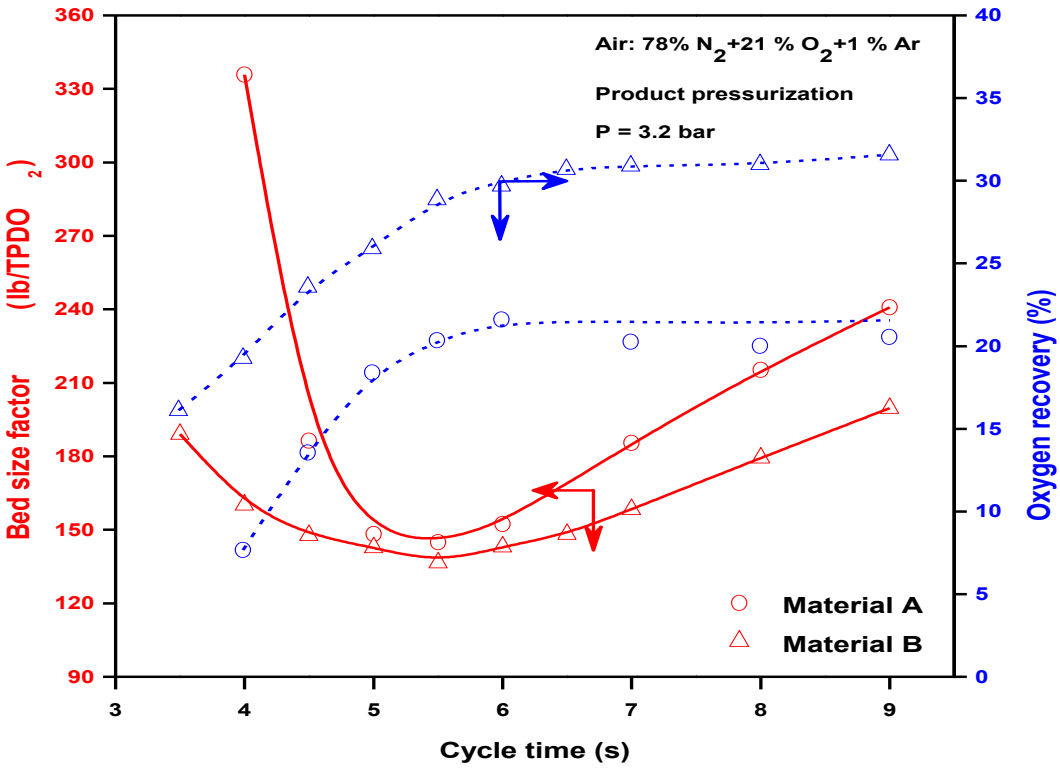

Figure 5-5. Comparative RPSA process performance between Materials A and B. Product pressurization time (tp) = 0.5 s, adsorption time (tad)= 1 to 2s, depressurization time (td) =1 to 5.5s and purge time (tpu)=1s. Lines indicate smoothed B-spline interpolation curves through the experimental data points

5.4 Characteristics of binary gas selectivity

Section 5.3 experimentally demonstrated the key process performance variables (bed size factor and O_2 recovery) were significantly influenced by the selectivity. The selectivity of adsorption of a component of a binary or a ternary gas mixture can be a complex function of equilibrium gas phase pressure, temperature and composition and it must be experimentally measured for reliable design of adsorptive gas separation processes.

Most of the published literature data report selectivity of adsorption from a binary gas mixture. Adsorption selectivity data for three or more component gas mixtures are very few. It is common to measure and describe the binary gas selectivity (S_{12}) as a function of y_1 at constant P and T, or as a function of P at constant y_1 and T. The selectivity is also described as functions of total amount adsorbed ($n = \sum_i n_i$) at constant T and y_i in the literature.[15]

The selectivity is a measure of the competitiveness of adsorption between the components of a gas mixture. Co- adsorption of component j with respect to that for component i is low when S_{ij} is large. A single selectivity (S_{12}) defines the competition for a binary gas mixture comprising of components 1 and 2, while a set of (k-1) binary selectivity (S_{12}, $S_{23,}$ …….) are required to fully define the competitive adsorption between the components in a multi-component system consisting of k components. For example, one needs to define only S_{12} and S_{23} [$S_{13} = S_{12} \times S_{23}$] for a three component system (k =3). It should be pointed out that the selectivity can be very sensitive to errors

in the measurement (or model estimation) of component amounts adsorbed. According to Eq. (5-1), the error in S_{ij} is given by the summation of errors in n_i and n_j.

5.4.1 Temperature dependence of S_{12}:

The temperature coefficients of selectivity of a binary gas (S_{12}) at a given loading (n_1 and n_2) and the Henry's law selectivity (S_{12}^0) are given by the following thermodynamic relationship:

$$\left[\frac{\partial ln S_{12}}{\partial T}\right]_{n_1,n_2} = -\frac{(q_1 - q_2)}{RT^2}; \left[\frac{dln\, S_{12}^0}{dT}\right] = -\frac{(q_1^0 - q_2^0)}{RT^2} \quad (5\text{-}3)$$

Where q_i is the isosteric heat of adsorption of component *i* from the binary mixture at loadings of n_1 and n_2.[16] Thus, S_{12} and S_{12}^0 decrease with increasing T if $q_1 > q_2$ and $q_1^0 > q_2^0$ (or $S_{12} > 1$).

It should be noted that q_i can be a complex function of n_i for an energetically heterogeneous adsorbent.[16-19] Thus, the temperature coefficient of S_{12} can be complex functions of n_1 and n_2, which must be experimentally evaluated. Figure 5-6 is an example of plots of S_{12} as functions of total amount adsorbed at different temperatures.[15] [20]

5.4.2 Pressure and composition dependence of S_{12}:

The functional dependence of S_{12} on P, T and y_1 is governed by the nature of the adsorbates (size, polarity, etc.) and the nature of the adsorbent (energetically homogeneous or heterogeneous, surface polarity, ionic, distributed pore structure, etc.). The dependence can be complex and cannot generally be estimated a priori. A detailed

experimental evaluation of S_{12} at different P and y_1 (constant T) is necessary to reliably establish that functional dependence. Figure 5-7a and b, respectively, show a few experimental examples of variation of S_{12} with y_1 (constant P, T) and with P (constant T and y_1). It may be seen that S_{12} is independent of P and y_1 for some systems while for others S_{12} increases or decreases with increasing P or y_1. The variations in S_{12} with P and y_1 are small to moderate for some systems, and large for others. Figure 5-7c shows two extreme cases of variation of S_{12} with y_1 at constant P and T, where the adsorbent switches selectivity for component 1 ($S_{12}>1$) to component 2 ($S_{12}<1$) at some composition of the gas phase.[13, 22] In other words, an adsorption azeotropy ($S_{12}=1$) is exhibited at that composition where the adsorbed and equilibrium gas phase mole fractions of the components are equal. This behavior can be caused by different degrees of heterogeneity exhibited by an adsorbent for the components of a binary gas mixture or by adsorbate size differences or a combination of the two.[8, 21] Adsorption azeotropy is exhibited by a binary gas system where the pure gas adsorption isotherms are Type I in shape, and where they crisscross each other at some intermediate pressure. Thus, the component of the mixture which is more selective in the Henry's Law region has a smaller saturation capacity than that of the less selective component.

Various simplified analytical binary gas adsorption isotherm models, which explicitly incorporate the effects of unequal adsorbate sizes and adsorbent heterogeneity may provide qualitative information on the dependence of S_{12} on P and y_1 at constant T. Table 5-4 lists some of these models which are thermodynamically consistent (except

empirical Sips model), and which are often used to fit pure and binary gas adsorption isotherms in the literature.

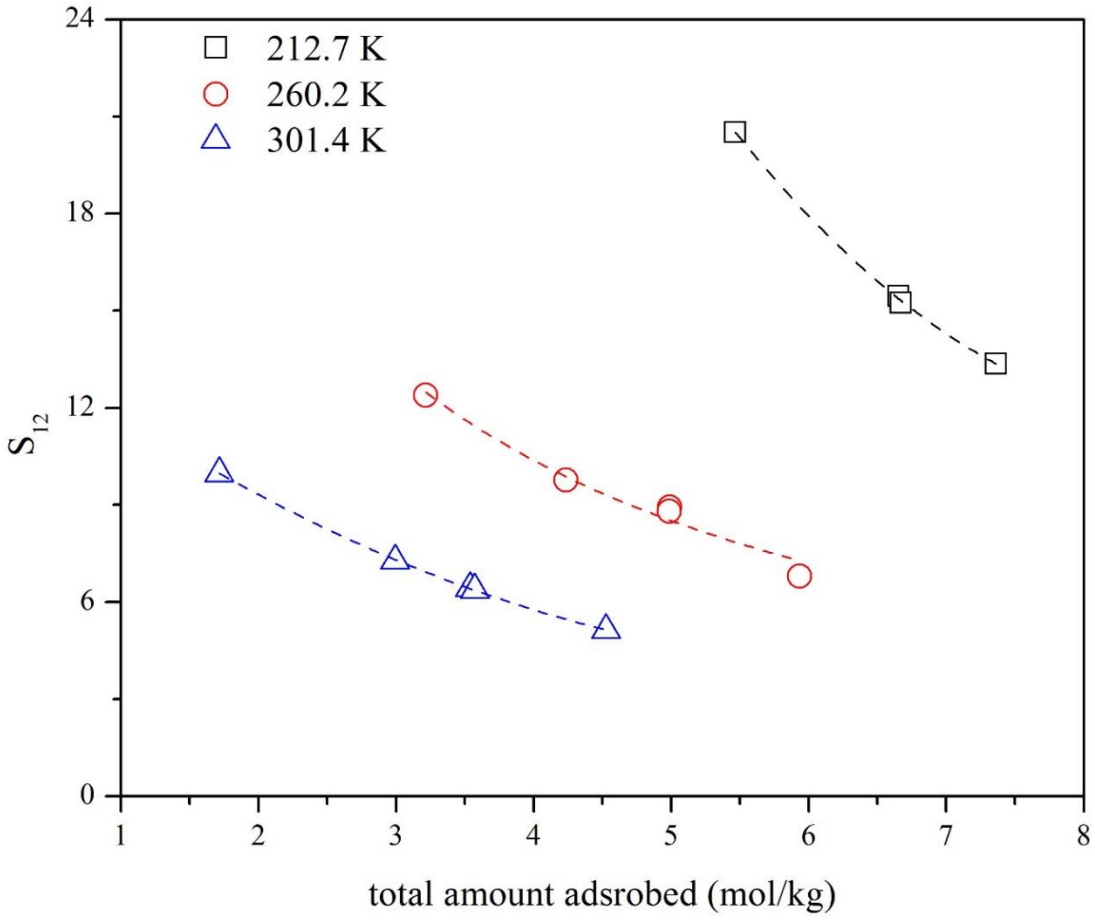

Figure 5-6. Binary selectivity of adsorption of C_2H_4 (1) + CH_4 (2) mixture (y_1 = 0.235) on BPL carbon as functions of total amount adsorbed (n, moles/kg) at different T: □ = 212.7 K, Δ = 260.2 K, ◊ = 301.4 K.[20]

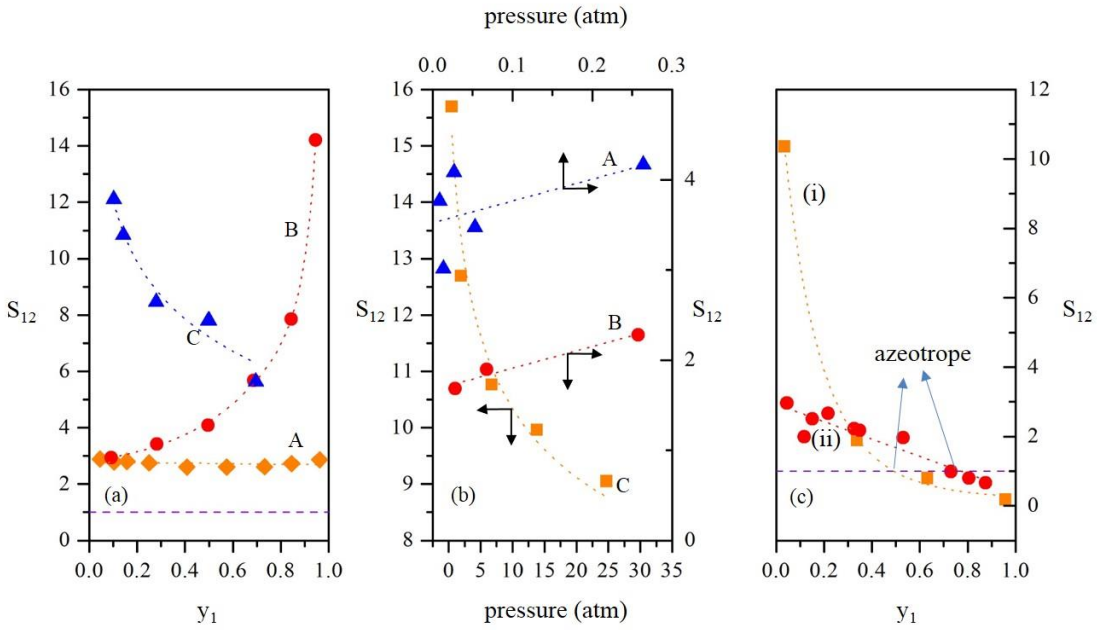

Figure 5-7. (a) Variation of binary gas selectivity (S_{12}) as functions of y1 at constant P and T. A: CF_4(1)+CH_4(2) on silicalite (P=1000kPa, T=298.15K) [22]; B: CO_2(1)+CH_4(2) on Activated carbon (P=530kPa, T=293K[23]; C:C_2H_4(1)+C_2H_6(2) on ETS-10 Zeolite (P=250kPa, T=280K)[24]. (b) Variations of binary gas selectivity with P at constant y_1 and T: A: C_3H_6(1)+C_3H_8(2) on NaX zeolite (y_1=0.5, T=358K)[25]; B: CH_4(1)+N_2(2) on Silicalite (y_1~0.59, T=303K)[26]; C: C_2H_6(1)+CH_4(2) on Activated carbon (y_1=0.511, T=301.4K)[27]. (c) Example of adsorption azeotrope: (i) CO_2(1)+C_3H_8(2) on H-mordenite (P=40.8kPa, T=303.15K) [28]; (ii) i-C_4H_{10} (1) +C_2H_4 (2) on 13X molecular sieve (P=137.8kPa, T=298.15K) [29].

It may be seen from Table 5-4that S_{12} can increase or decrease with increasing P or y_1 under specific conditions due to unequal adsorbate sizes or dissimilar degrees of adsorbent heterogeneity for the adsorbates.

Table 5-4. Pressure and composition dependence of S_{12} by various models; m_i = saturation adsorption capacity of component i for all models; a_i = number of adsorption sites occupied by component i in multi-site Langmuir model; k_i = heterogeneity parameter for component i in Toth model; ψi = Degree of heterogeneity of component i in Heterogeneous Langmuir model.

Mixed Gas Isotherm Model	Adsorbate Size Difference	S_{12} (y_1) at Constant P & T	S_{12} (P) at Constant y_1 & T
Multi -component Langmuir [30] Homogeneous	No $m_1 = m_2$*	$S_{12} \neq S_{12}$ (y_1)	$S_{12} \neq S_{12}$(P)
Multi-site Langmuir Nitta [31] Homogeneous	Yes $m_1 \neq m_2$ $a_1m_1 = a_2m_2$*	S_{12}>1; m_2>m_1: $S_{12} \downarrow$ as $y_1 \uparrow$	m_2>m_1: $S_{12} \downarrow$ as P $\uparrow$
		S_{12}> m_1/m_2; m_1>m_2: $S_{12} \uparrow$ as $y_1 \uparrow$	m_1>m_2: $S_{12} \uparrow$ as P $\uparrow$
		S_{12} < m_1/m_2; m_1>m_2: $S_{12} \downarrow$ as $y_1 \uparrow$	
Toth [32] Heterogeneous	No $m_1 = m_2$ *	$k_1 = k_2$* $S_{12} \neq S_{12}$ (y_1)	$S_{12} \neq S_{12}$(P)
Heterogeneous-Langmuir Sircar [8] Heterogeneous	No $m_1 = m_2$*	$\psi_1 = \psi_2$ $S_{12} \neq S_{12}$ (y_1)	$S_{12} \neq S_{12}$(P)
		$\psi_1 \neq \psi_2$ $S_{12} \downarrow$ as $y_1 \uparrow$	$S_{12} \downarrow$ as P $\uparrow$
Empirical Sips [33] Heterogeneous		Henry's Law region is undefined	

5.5 Prediction of binary gas selectivity:

A practical adsorptive gas separation process generally experiences a very large variation in P, T, n_i and y_i during its cyclic operation. Reliable knowledge of binary gas selectivity of the components of a gas mixture on the adsorbent is required in the entire range of process operating conditions for (a) optimum selection of the adsorbent, (b) optimum design of the process cycle to meet the separation specifications, and (c) numerical model simulation of the process performance.

It may not always be practically possible to experimentally evaluate S_{ij} (P, T, y_i) for the system of interest in the entire range of process conditions. Such experiments can be tedious and time consuming. Hence, a common practice is to use an analytical multi-component gas adsorption isotherm model, which can adequately describe the experimental isotherm data for the system of interest, for estimation of S_{ij} (P, T, y_i) to be used in process design and simulation employing a numerical adsorptive process model. A detailed experimental verification of the chosen isotherm model is key to ascertain the reliability of this approach. Unfortunately, it is not always followed in practice. Actual pilot plant data for the separation process of interest are always necessary for validation of the assumptions used in a process model.[4]

5.6 Estimation of binary gas S_{12} from pure gas adsorption isotherms:

The thermodynamically consistent Ideal Adsorbed Solution Theory (IAST) is frequently used for estimation of binary gas selectivity using pure gas adsorption isotherms. The IAST is an elegant solution thermodynamic model based on the formation of an ideal adsorbed

phase by mixing of pure components of a gas mixture at constant temperature and surface potential.[34] This approach does not require an analytical model for describing the pure gas adsorption isotherms even though such a model is often used for data interpolation, extrapolation, as well as for estimation of pure gas surface potentials as functions of P and T. The theory, however, does not provide analytical relationships between S_{ij} and P, T and y_i, and thus, may be difficult to use in a numerical adsorptive process simulation. Other predictive models such as the Vacancy Solution Model [35] and the Adsorption Potential Models [36] have been proposed and tested for prediction of binary selectivity from corresponding pure gas adsorption isotherms. They are not included in this work.

Many publications reported the quality of prediction of binary gas selectivity by IAST. An extensive list of pure and binary gas adsorption data and the corresponding IAST prediction was compiled by Valenzuela and Myers in 1984.[37] The study indicated that the IAST predictions of binary gas selectivity were good to fair for some systems while the predictions were poor for other systems. Similar results were reported by other studies.[38-41] None of these studies provide any guideline for prejudging the conditions where IAST will yield reasonable predictions.

A simplified model study of prediction of binary gas adsorption selectivity by IAST for cases, where the adsorbent was homogeneous and the adsorbates had different sizes [31] or where the adsorbent was heterogeneous and the adsorbates had same sizes [8] was carried out.[21] Both models are thermodynamically consistent and provide analytical pure gas adsorption isotherms which were used in IAST to compute binary equilibrium data. The results indicated that IAST predictions were good to fair for systems where the

adsorbent was energetically homogeneous or weakly heterogeneous, and the adsorbates were non-polar and had approximately equal sizes – otherwise, the prediction by IAST could deviate significantly from the binary selectivity of the original input models. The pronounced effect of dissimilar adsorbate sizes on IAST prediction of Henry's law constant of a trace adsorbate from a bulk gas has also been reported.[10]

5.7 Results of new literature search:

The search revealed that a large volume of binary selectivity data covering a large spectrum of adsorbate and adsorbent properties were available. In comparison, the published ternary data were few. The next sections provide an organized summary of the search results.

We selected only those data sets which provide variation of binary or ternary gas selectivity with (a) gas composition (at constant pressure and temperature) or (b) gas pressure (at constant gas composition and temperature), and which provide the selectivity values for at least three different compositions or pressures for cases (a) and (b), respectively. The values of the experimental and IAST estimated values of S_{12} were either tabulated or graphically presented in the original references. For the latter case, the xy coordinates of the data points were read by using the MATLAB function ginput. The complete data Tables can be found in Appendix D. Only a concise gist of the data sets is presented in this chapter for the sake of brevity.

Table 5-5 lists the binary gas adsorption systems and the adsorbents, the properties of the pure adsorbates (kinetic diameter, polarizability, dipole and quadrupole moments), and

the properties of the adsorbents (surface polarity and heterogeneity). The more selectively adsorbed component of the binary mixture (component 1) is named first. The time periods covered by the table is 1996 –2015.

Table 5-6 lists the corresponding properties for the ternary gas adsorption systems during the entire period of 1996 – 2015. The components of the ternary system are numbered in the descending order of their adsorption selectivity on the adsorbent.

It may be seen from Table 5-5, and Table 5-6 that the published selectivity data cover a large variety of adsorbate and adsorbent properties. The data provide examples of all different types of pressure (constant T and y) and composition (constant T and P) dependence of binary selectivity (S_{12}) discussed earlier. Some of these examples are also plotted in Figure 5-7a and b. On the other hand, the lack of ternary selectivity data is self-evident.

Table 5-5. Properties of adsorbates and adsorbents for binary gas adsorption systems (1995 – 2005)

No.	Mixtures (1) + (2) Adsorbent	Adsorbate properties								Adsorbent properties	Ref.
		Dipole[a]		Quadrupole[b]		Polarizability[c]		Kinetic Dia.[d]			
		(1)	(2)	(1)	(2)	(1)	(2)	(1)	(2)		
1	CO_2 + CH_4 activated carbon	0	0	4.3	0	26.5	26.0	3.3-3.9	3.76	Weakly Polar[a] Heterogeneous[b]	[23]
2	CF_4 + CH_4 Silicalite	0	0	0	0	38.4	26.0	4.7	3.76	Non Polar[a] Homogeneous[b]	[22]
3	CF_4 + CH_4 Silicalite	0	0	0	0	38.4	26.0	4.7	3.76	Non Polar[a] Homogeneous[b]	[42]
4	C_3H_8 + C_2H_6 activated carbon	0.084	0	-	0.65	62.9	44.7	4.3-5.12	4.443	Weakly Polar[a] Heterogeneous[b]	[43]
5	C_2H_6 + CH_4 activated carbon	0	0	0.65	0	44.7	26.0	4.443	3.76	Weakly Polar[a] Heterogeneous[b]	[43]
6	C_3H_8 + CH_4 activated carbon	0.084	0	-	0	62.9	26.0	4.3-5.12	3.76	Weakly Polar[a] Heterogeneous[b]	[43]
7	CO_2 + CH_4 activated carbon	0	0	4.3	0	26.5	26.0	3.3-3.9	3.76	Weakly Polar[a] Heterogeneous[b]	[43]
8	CH_4 + N_2 H-ZSM-5-280[*]	0	0	0	1.52	26.0	17.6	3.76	3.64-3.8	Ionic[a] Heterogeneous[b]	[44]

No.	Mixtures (1) + (2) Adsorbent	Adsorbate properties								Adsorbent properties	Ref.
		Dipole[a]		Quadrupole[b]		Polarizability[c]		Kinetic Dia.[d]			
		(1)	(2)	(1)	(2)	(1)	(2)	(1)	(2)		
9	CO_2 + CH_4 H-ZSM-5-280*	0	0	4.3	0	26.5	26.0	3.3-3.9	3.76	Ionic[a] Heterogeneous[b]	[44]
10	CO_2 + N_2 H-ZSM-5-280*	0	0	4.3	1.52	26.5	17.6	3.3-3.9	3.64-3.8	Ionic[a] Heterogeneous[b]	[44]
11	C_4H_8O + $C_4H_8O_2$ FAU Y*	2.78	0	-	-	-	-	5.2	5.3	Ionic[a] Heterogeneous[b]	[45]
12	C_4H_8O + $C_4H_8O_2$ ZSM-5*	2.78	0	-	-	-	-	5.2	5.3	Ionic[a] Heterogeneous[b]	[45]
13	C_4H_8O + C_7H_8 FAU Y*	2.78	0.375	-	-	-	123	5.2	5.8	Ionic[a] Heterogeneous[b]	[45]
14	$C_4H_8O_2$ + C_7H_8 FAU Y*	0	0.375	-	-	-	123	5.3	5.8	Ionic[a] Heterogeneous[b]	[45]
15	C_2H_6 + CH_4 BPL Carbon	0	0	0.65	0	44.7	26.0	4.44	3.76	Weakly Polar[a] Heterogeneous[b]	[27]
16	C_2H_6 + CH_4 activated carbon	0	0	0.65	0	44.7	26.0	4.443	3.76	Weakly Polar[a] Heterogeneous[b]	[46]

No.	Mixtures (1) + (2) Adsorbent	Adsorbate properties								Adsorbent properties	Ref.
		Dipole[a]		Quadrupole[b]		Polarizability[c]		Kinetic Dia.[d]			
		(1)	(2)	(1)	(2)	(1)	(2)	(1)	(2)		
17	C_3H_8 + CH_4 activated carbon	0.084	0	-	0	62.9	26.0	4.3-5.12	3.76	Weakly Polar[a] Heterogeneous[b]	[46]
18	CO_2 + CH_4 activated carbon	0	0	4.3	0	26.5	26.0	3.3-3.9	3.76	Weakly Polar[a] Heterogeneous[b]	[46]
19	C_2H_6 + CH_4 ETS-10 *	0	0	0.65	0	44.7	26.0	4.443	3.76	Ionic[a] Heterogeneous[b]	[24]
20	C_2H_4 + CH_4 ETS-10 *	0	0	1.5	0	42.6	26.0	4.163	3.76	Ionic[a] Heterogeneous[b]	[24]
21	C_2H_4 + C_2H_6 ETS-10 *	0	0	1.5	0.65	42.6	44.7	4.163	4.443	Ionic[a] Heterogeneous[b]	[24]
22	$C_4H_6O_2$ + C_3H_3N activated carbon	1.77	3.92	-	-	-	-	-	-	Weakly Polar[a] Heterogeneous[b]	[47]
23	CO_2 + CO NaX faujasite*	0	0.112	4.3	2.5	26.5	19.5	3.3-3.9	3.69	Ionic[a] Heterogeneous[b]	[48]
24	C_2H_4 + CH_4 activated carbon	0	-	1.5	0	42.6	26.0	4.163	3.76	Weakly Polar[a] Heterogeneous[b]	[49]

No.	Mixtures (1) + (2) Adsorbent	Adsorbate properties								Adsorbent properties	Ref.
		Dipole[a]		Quadrupole[b]		Polarizability[c]		Kinetic Dia.[d]			
		(1)	(2)	(1)	(2)	(1)	(2)	(1)	(2)		
25	C_2H_6S + n-C_7H_{16} NaX	1.61	0	-	-	-	136.1	-	4.3	Ionic[a] Heterogeneous[b]	[50]
26	C_2H_6S + C_7H_8 NaX	1.61	0.375	-	-	-	123	-	5.8	Ionic[a] Heterogeneous[b]	[50]
27	C_3H_6 + C_3H_8 NaX	0.366	0.084	-	-	62.6	62.9	4.678	4.3-5.12	Ionic[a] Heterogeneous[b]	[25]
28	C_2H_6 + CH_4 templated carbon	0	0	0.65	0	44.7	26.0	4.443	3.76	Weakly Polar[a] Heterogeneous[b]	[51]
29	CO_2 + CH_4 MIL-100(Cr) MOF	0	0	4.3	0	26.5	26.0	3.3-3.9	3.76	Weakly Polar[a] Heterogeneous[b]	[52]
30	CO_2 + CH_4 MIL-53(Al) MOF	0	0	4.3	0	26.5	26.0	3.3-3.9	3.76	Weakly Polar[a] Heterogeneous[b]	[53]
31	CH_4 + N_2 Basolite A100 MOF	0	0	0	1.52	26.0	17.6	3.76	3.64-3.8	Weakly Polar[a] Heterogeneous[b]	[54]
32	CO_2 + N_2 activated carbon	0	0	4.3	1.52	26.5	17.6	3.3-3.9	3.64-3.8	Weakly Polar[a] Heterogeneous[b]	[55]

No.	Mixtures (1) + (2) Adsorbent	Adsorbate properties								Adsorbent properties	Ref.
		Dipole[a]		Quadrupole[b]		Polarizability[c]		Kinetic Dia.[d]			
		(1)	(2)	(1)	(2)	(1)	(2)	(1)	(2)		
33	CO_2 + H_2 activated carbon	0	0	4.3	0.662	26.5	8.0	3.3-3.9	2.89	Weakly Polar[a] Heterogeneous[b]	[55]
34	CO_2 + CH_4 activated carbon	0	0	4.3	0	26.5	26.0	3.3-3.9	3.76	Weakly Polar[a] Heterogeneous[b]	[56]
35	CH_4 + N_2 zeolite 5A*	0	0	0	1.52	26.0	17.6	3.76	3.64-3.8	Ionic[a] Heterogeneous[b]	[57]
36	N_2 + O_2 LiLSX zeolite	0	0	1.52	0.39	17.6	16.0	3.64-3.8	3.467	Ionic[a] Heterogeneous[b]	[58]
37	CO_2 + CH_4 zeolite Na-ZSM-5	0	0	4.3	0	26.5	26.0	3.3-3.9	3.76	Ionic[a] Heterogeneous[b]	[59]
38	CO_2 + CH_4 activated carbon	0	0	4.3	0	26.5	26.0	3.3-3.9	3.76	Weakly Polar[a] Heterogeneous[b]	[60]
39	CH_3OH + C_6H_{14} Basolite C300 MOF	1.7	0	-	0.0	32.3-33.2	119	3.8-4.1	5.949	Weakly Polar[a] Heterogeneous[b]	[61]
40	N_2 + O_2 LiLSX zeolite	0	0	1.52	0.39	17.6	16.0	3.64-3.8	3.467	Ionic[a] Heterogeneous[b]	[62]

No.	Mixtures (1) + (2) Adsorbent	Adsorbate properties								Adsorbent properties	Ref.
		Dipole[a]		Quadrupole[b]		Polarizability[c]		Kinetic Dia.[d]			
		(1)	(2)	(1)	(2)	(1)	(2)	(1)	(2)		
41	$CO_2 + N_2$ zeolite ZSM-5	0	0	4.3	1.52	26.5	17.6	3.3-3.9	3.64-3.8	Ionic[a] Heterogeneous[b]	[63]
42	$CH_4 + N_2$ zeolite 13X*	0	0	0	1.52	26.0	17.6	3.76	3.64-3.8	Ionic[a] Heterogeneous[b]	[64]
43	$CO_2 + N_2$ Cu-BTC MOF	0	0	4.3	1.52	26.5	17.6	3.3-3.9	3.64-3.8	-[a] -[b]	[65]
44	$CO_2 + CH_4$ Cu-BTC MOF	0	0	4.3	0	26.5	26.0	3.3-3.9	3.76	-[a] -[b]	[65]

Unit: a: (x 10^{18} esu-cm), b: (x 10^{26} esu-cm^2), c: (x 10^{-25} cm^2); d: (Å).

a:adsorbent polarity; b: energetic heterogeneity; * with binder

Table 5-6. Properties of adsorbates and adsorbents for ternary gas adsorption systems.

No.	Adsorbent	Adsorbate Properties						Adsorbent Properties	Ref.
		Kinetic Dia. (Å) Polarizability × 10^{-25} (cm^3)			Permanent Poles				
		(1)	(2)	(3)	(1)	(2)	(3)		
45	C_2H_4 + C_2H_6 + CH_4 ETS-10*	K = 4.16 P = 42.6	K = 4.44 P = 44.7	K = 3.76 P = 26.0	D = 0.0 Q = 1.5	D = 0.0 Q = 0.65	D = 0.0 Q = 0.0	Ionic[a] Homogeneous[b]	[24]
46	C_2H_4 + CH_4 + H_2 activated carbon	K = 4.16 P = 42.6	K = 3.76 P = 26.0	K = 2.89 P = 8.0	D = 0.0 Q = 1.5	D = 0.0 Q = 0.0	D = 0.0 Q = 0.66	Weakly polar[a] Heterogeneous[b]	[49]
Adsorbate: D = Permanent dipole moment (x 10^{18} esu-cm); Q = Permanent quadrupole moment (x 10^{26} esu-cm^2); a:adsorbent polarity; b: energetic heterogeneity; * with binder									

Table 5-7, Table 5-8 and Table 5-9 show the pressure and composition ranges of the experimental data for the binary gas systems listed in Table 5-5 and Table 5-6. They also show the average percentage errors for S_{12} estimated by the IAST for the systems. The average represents an arithmetic average of the errors in S_{12} values for different y_1 values (constant P and T) or for different P values (constant y_1 and T). The numbers of independent data points under each P and y_1 ranges, which were reported and used for the averaging process, are given in the parentheses in the Table. The average errors by the IAST for systems listed in Table 5-7 is less than 15%; the errors for the systems listed in Table 5-8 are between 16 – 40 %; and the errors for the systems listed in Table 5-9 are larger than 40%. The Tables also list the analytical pure gas isotherms used by the authors of data sources for carrying out the integral needed for estimation of surface potential in the IAST.

It should be pointed out that a numerical model simulation of sensitivity of a PSA process performance for production of CH_4 from a binary C_2H_4 + CH_4 mixture using an activated carbon indicated that a small error (say ~ 5 %) in the amounts of the components adsorbed (equivalent error in binary selectivity is ~ 10%) could create a large error in the over-all productivity and recovery of the product gas [66]. The tolerance of error may be system specific, but an error of 15 % in estimation of S_{12} may be at the border line for a practically reliable process design.

The compiled data in Table 5-7, Table 5-8 and Table 5-9 indicate that the prediction of binary gas selectivity from the pure gas adsorption isotherms using the IAST may be good to fair to poor depending on the adsorbate-adsorbent system. Thus the prediction of binary

selectivity by IAST may not be reliable for practical process design purpose unless it is experimentally verified under the conditions of interest. An earlier compilation of several binary gas adsorption selectivity data and their comparative estimation by IAST had led to a similar observation [37].

It may be seen from Table 5-5 that the systems listed in Table 5-7, where the agreements between the IAST estimated and experimental selectivity values are good to fair, generally conform with the conditions suggested by model study of limitations of IAST [66]. These conditions include (a) approximate equal adsorbate sizes, (b) non-polar or weakly polar adsorbates, and (c) homogeneous or weakly heterogeneous adsorbents. Otherwise the error in estimation of selectivity by IAST can be large. In particular, it may be seen from Table 5-5, Table 5-8 and Table 5-9 that the errors can be very large when the adsorbates are very polar and the adsorbents are polar, ionic, and heterogeneous.

Table 5-10 shows the errors in estimation of binary pair selectivity from a ternary gas mixture by IAST. The errors were fair to large. No trend could be observed due to limited quantity of available data.

The survey indicates that the estimation of adsorption selectivity between components of a binary or ternary gas mixture by IAST using the corresponding pure gas adsorption isotherms must be experimentally verified under the conditions of interest. The predicted selectivity values can substantially deviate from the real values depending on the properties of the adsorbate and the adsorbent. The quality of IAST prediction may be good to fair when the adsorbates have similar sizes, are non-polar or weakly polar, and the adsorbent is homogeneous or weakly heterogeneous.

Table 5-7. Binary gas systems and data range where the average error for S_{12} estimated by IAST was less than ~ 15%.

No.	Mixtures (Adsorbent)	Data range (number of data points)			Pure gas isotherm model	Average error for S_{12} (%)	Ref. F=figure T=table
		T (K)	P (kPa)	y_1			
2	CF_4+CH_4 (Silicalite)	298.1	100	0.045 ~ 0.96 (9)	Toth	8.4	[22](F7, F8, F9, F12)
			500	0.045 ~ 0.96 (9)		4.8	
			1000	0.045 ~ 0.96 (9)		7.6	
			1700	0.045 ~ 0.96 (9)		11.9	
3	CF_4+CH_4 (Silicalite)	300	1000	0.043 ~ 0.959 (9)	-	13.0	[42](F4, F5)
14	$C_4H_8O_2$+C_7H_8 (FAU Y)	298	0.008	0.063 ~ 0.782 (3)	-	14.8	[45](F4b)
15	C_2H_6+CH_4 (BPL Carbon)	301.4	52	0.035 ~ 0.958 (6)	-	7.6	[27](F6, F7, F8)
			196	0.284 ~ 0.733 (3)		10.4	
			684	0.035 ~ 0.958 (7)		6.4	
			1397	0.035~ 0.958 (5)		3.8	
			2499	0.511 ~ 0.958 (3)		4.7	
19	C_2H_6+CH_4 (ETS-10)	325	150	0.103 ~ 0.642 (10)	Toth	14.8	[24](F1c, T4)

No.	Mixtures (Adsorbent)	Data range (number of data points)			Pure gas isotherm model	Average error for S_{12} (%)	Ref. F=figure T=table
		T (K)	P (kPa)	y_1			
28	C_2H_6+CH_4 (templated carbon)	273	101	0.188 ~0.780 (4)	Sips	9.5	[51](F3)
30	CO_2+CH_4 (MIL-53(Al) MOF)	303.15	100	0.102 ~ 0.902 (5)	Toth	7.8	[53](F3)
			400	0.102 ~ 0.902 (7)		9.7	
34	CO_2+CH_4 (activated carbon)	293	500	0.181 ~ 0.777 (3)	Toth	15.9	[56](F5b)
			1000	0.153 ~ 0.768 (3)		14.3	[56](F6b)
35	CH_4+N_2 (zeolite 5A)	303	300	0.271 ~ 0.892 (4)	Sips	5.9	[57](F5, F6, F8, T10)
			500	0.272 ~ 0.893 (4)		6.9	
			700	0.272 ~ 0.893 (4)		4.9	
		323	103.9 ~ 705.3 (4)	0.884		2.2	[57](F11, T11)
36	N_2+O_2 (LiLSX zeolite)	298.1	25	0.060 ~ 0.891 (7)	Toth	13.5	[58] (F5b)
37	CO_2+CH_4 (zeolite Na-ZSM-5)	393.1	101.3	0.03 ~ 0.65 (7)	Langmuir	14.6	[59] (F6a)
38	CO_2+CH_4 (activated carbon)	303.15	340 ~ 2390 (8)	~ 0.5	Freundlich	12.9	[60](T4, T5)
		323.15	510 ~ 2560 (8)	~ 0.5		8.0	

No.	Mixtures (Adsorbent)	Data range (number of data points)			Pure gas isotherm model	Average error for S_{12} (%)	Ref. F=figure T=table
		T (K)	P (kPa)	y_1			
40	N_2+O_2 (LiLSX zeolite)	303.1	101.3	0.3 ~ 0.7 (5)	-	10.1	[62](T4)
		338.1	101.3	0.3 ~ 0.7 (5)		6.4	
			607.8	0.2 ~ 0.8 (4)		4.6	
41	CO_2+N_2 (zeolite ZSM-5)	298.1	1000	0.202 ~ 0.727 (3)	Sips	5.6	[63](SUP. T2.1, F5)
		318.1	120	0.157 ~ 0.672 (3)		16.0	
42	CH_4+N_2 (zeolite 13)	303	100 ~ 700 (3)	0.4660	Toth	3.9	[64](F7a, F9a, F9b, T9)
			500	0.301 ~ 0.939 (5)		4.0	
		323	100 ~ 700 (4)	0.3010		1.3	
43	CO_2+N_2 (Cu-BTC MOF)	308.1	46.55 ~ 298.96 (9)	~ 0.25	Langmuir	13.0	[65](F2a, TS4)
44	CO_2+CH_4 (Cu-BTC MOF)	308.1	39.49 ~ 299.51 (9)	~ 0.15	Langmuir	12.5	[65](F4a, F4b, TS6, TS7)
			45.77 ~ 299.52 (9)	~ 0.25		12.0	

Table 5-8. Binary gas systems and data range where the average error for S_{12} estimated by IAST was 16 ~ 40%.

No.	Mixtures (Adsorbent)	Data range (number of data points)			Pure gas isotherm model	Average error for S_{12} (%)	Ref. F=figure T=table
		T (K)	P (kPa)	y_1			
1	CO_2+CH_4 (activated carbon)	293	530	0.092 ~ 0.946 (6)	Henry-Dubinin-Astakov	32.3	[23](F6 & F8)
3	CF_4+CH_4 (Silicalite)	300	100	0.043 ~ 0.959 (9)	-	36.9	[42](F4, F5)
4	C_3H_8+C_2H_6 (activated carbon)	303	50	0.2 ~ 0.8 (4)	MPSD	34.9	[43](F4)
		333		0.2 ~ 0.8 (4)		18.5	
		363		0.2 ~ 0.8 (4)		16.1	
7	CO_2+CH_4 (activated carbon)	303	66.7	0.048 ~ 0.869 (6)	MPSD	22.7	[43](F8)
8	CH_4+N_2 (H-ZSM-5-280)	313	101	0.010 ~ 0.950 (9)	Freundlich	23.8	[44](F5)
9	CO_2+CH_4 (H-ZSM-5-280)	313	101	0.020 ~ 0.930 (10)	Freundlich	36.3	[44](F6)
12	C_4H_8O+$C_4H_8O_2$ (ZSM-5)	298	0.01	0.146 ~ 0.769 (3)	Toth	16.4	[45](F3b)

No.	Mixtures (Adsorbent)	Data range (number of data points)			Pure gas isotherm model	Average error for S_{12} (%)	Ref. F=figure T=table
		T (K)	P (kPa)	y_1			
13	C_4H_8O+C_7H_8 (FAU Y)	298	0.005	0.051 ~ 0.761 (3)	-	20.9	[45](F4a)
			0.023	0.113 ~ 0.883 (3)		38.5	
14	$C_4H_8O_2$+C_7H_8 (FAU Y)	298	0.0165	0.109 ~ 0.856 (3)	-	17.3	[45](F4b)
16	C_2H_6+CH_4 (activated carbon)	303	66.7	0.024 ~ 0.807 (5)	MPSD	24.7	[46](F3a)
18	CO_2+CH_4 (activated carbon)	303	66.7	0.049 ~ 0.875 (6)	MPSD	18.6	[46](F4a, F4b)
		273	66.7	0.039 ~ 0.870 (6)		28.4	
19	C_2H_6+CH_4 (ETS-10)	280	150	0.094 ~ 0.659 (10)	Toth	21.4	[24](F1a, T4)
			500	0.055 ~ 0.639 (10)		16.8	[24](F1b, T4)
20	C_2H_4+CH_4 (ETS-10)	280	150	0.077 ~ 0.653 (10)	Virial	19.1	[24](F2a, T4)
			250	0.059 ~ 0.648 (10)		27.7	[24](F2b, T4)
21	C_2H_4+ C_2H_6 (ETS-10)	280	150	0.140 ~ 0.725 (10)	Unilan	29.4	[24](F3a, T4)
23	CO_2+CO (NaX faujasite)	373	100	0.174 ~ 0.804 (3)	Langmuir	28.0	[48](T6)

No.	Mixtures (Adsorbent)	Data range (number of data points)			Pure gas isotherm model	Average error for S_{12} (%)	Ref. F=figure T=table
		T (K)	P (kPa)	y_1			
24	C_2H_4+CH_4 (activated carbon)	303.15	202.65	0.103 ~ 0.720 (4)	Langmuir-Freundlich	35.0	[49](F6)
		313.15	202.65	0.114 ~ 0.630 (4)		27.0	[49](F6)
			1013.25	0.206 ~ 0.496 (3)		17.1	[49](F6)
31	CH_4+N_2 (Basolite A100 MOF)	273	500	0.533 ~ 0.867 (3)	Toth	18.4	[54](F9a)
		298		0.085 ~ 0.867 (4)		27.4	[54](F11b)
		323		0.533 ~ 0.868 (3)		17.0	[54](F9c)
32	CO_2+N_2 (activated carbon)	298.1	2000	0.106 ~ 0.572 (3)	Sips	22.6	[55](SUP. T17)
			3000	0.113 ~ 0.613 (3)		37.6	[55](SUP. T17)
34	CO_2+CH_4 (activated carbon)	293	100	0.297 ~ 0.671 (3)	Toth	32.8	[56](F3b)
			250	0.194 ~ 0.782 (3)		31.1	[56](F4b)
36	N_2+O_2 (LiLSX zeolite)	298.1	100	0.045 ~ 0.815 (11)	Toth	33.1	[58] (F5a)
		348.1	25	0.060 ~ 0.792 (6)		18.2	[58] (F6b)
			100	0.018 ~ 0.965 (10)		32.9	[58] (F6a)
37	CO_2+CH_4 (zeolite Na-ZSM-5)	308.1	101.3	0.03 ~ 0.9 (10)	Langmuir	18.2	[59] (F6a)
		323.1	101.3	0.03 ~ 0.9 (10)		18.4	
		358.1	101.3	0.03 ~ 0.65 (7)		18.4	
38	CO_2+CH_4 (activated carbon)	353.15	600 ~ 2510 (7)	~ 0.5	Freundlich	18.1	[60](T4, T5)

No.	Mixtures (Adsorbent)	Data range (number of data points)			Pure gas isotherm model	Average error for S_{12} (%)	Ref. F=figure T=table
		T (K)	P (kPa)	y_1			
40	N_2+O_2 (LiLSX zeolite)	273.1	101.3	0.3 ~ 0.8 (6)	-	26.1	[62](T4)
		303.1	607.8	0.5 ~ 0.9 (5)		37.3	
41	CO_2+N_2 (zeolite ZSM-5)	298.1	120	0.134 ~ 0.644 (3)	Sips	26.3	[63](SUP. T2.1, F5)
			300	0.162 ~ 0.691 (3)		36.5	
		318.1	300	0.181 ~ 0.701 (3)		19.0	
			1000	0.209 ~ 0.729 (3)		17.0	

Table 5-9. Binary gas systems and data range where the average error for S_{12} estimated by IAST was larger than 40%.

No.	Mixtures (Adsorbent)	Data range (number of data points)			Pure gas isotherm model	Average error for S_{12} (%)	Ref. F=figure T=table
		T (K)	P (kPa)	y_1			
5	C_2H_6+CH_4 (activated carbon)	303	50	0.1 ~ 0.8 (4)	MPSD	76.6	[43](F5)
		333		0.1 ~ 0.8 (4)		75.0	[43](F5)
6	C_3H_8+CH_4 (activated carbon)	303	50	0.1 ~ 0.5 (3)	MPSD	181.7	[43](F6)
		333		0.1 ~ 0.5 (3)		80.5	[43](F6)
		363		0.1 ~ 0.5 (3)		138.1	[43](F6)
7	CO_2+CH_4 (activated carbon)	273	66.7	0.039 ~ 0.866 (6)	MPSD	44.5	[43](F8)
10	CO_2+N_2 (H-ZSM-5-280)	313	101	0.010 ~ 0.950 (12)	Freundlich	59.7	[44](F7)
11	C_4H_8O+$C_4H_8O_2$ (FAU Y)	298	0.285	0.144 ~ 0.893 (3)	Freundlich	71.4	[45](F3a)
17	C_3H_8+CH_4 (activated carbon)	303	66.7	0.026 ~0.759 (4)	MPSD	55.4	[46](F3b)
20	C_2H_4+CH_4 (ETS-10)	325	150	0.079 ~ 0.637 (10)	Virial	51.3	[24](F2c, T4)

No.	Mixtures (Adsorbent)	Data range (number of data points)			Pure gas isotherm model	Average error for S_{12} (%)	Ref. F=figure T=table
		T (K)	P (kPa)	y_1			
21	C_2H_4+ C_2H_6 (ETS-10)	280	250	0.102 ~ 0.696 (6)	Unilan	40.9	[24](F3b, T4)
		325	150	0.139 ~ 0.500 (8)		60.2	[24](F3c, T4)
22	$C_4H_6O_2$+C_3H_3N (activated carbon)	313.1	101	0.282 ~ 0.880 (5)	-	40.8	[47](F3)
23	CO_2+CO (NaX faujasite)	323	100	0.174 ~ 0.804 (3)	Langmuir	49.0	[48](T6)
24	C_2H_4+CH_4 (activated carbon)	293.15	202.65	0.220 ~ 0.578 (4)	Langmuir-Freundlich	68.4	[49](F6)
			1013.25	0.193 ~ 0.480 (3)		99.3	[49](F6)
		303.15	1013.25	0.239 ~ 0.486 (3)		112.0	[49](F6)
25	C_2H_6S+n-C_7H_{16} (NaX)	298	0.001	0.051 ~ 0.661 (5)	-	625.8	[50](F2a, F4a)
			0.02	0.096 ~ 0.898 (5)		79.3	
26	C_2H_6S+C_7H_8 (NaX)	298	0.001	0.170 ~ 0.530 (5)	-	92.5	[50](F2b, F4b)
			0.02	0.106 ~ 0.910 (5)		47.7	
27	C_3H_6+C_3H_8 (NaX)	318	0.86 ~ 53.48 (6)	0.5	-	203.8	[25](F7a, F7c)
		358	0.86 ~ 53.48 (6)	0.5		163.2	
		408	0.86 ~ 53.48 (6)	0.5		127.0	

No.	Mixtures (Adsorbent)	Data range (number of data points)			Pure gas isotherm model	Average error for S_{12} (%)	Ref. F=figure T=table
		T (K)	P (kPa)	y_1			
29	CO_2+CH_4 (MIL-100(Cr) MOF)	303	100	0.25 ~ 0.75 (3)	-	182.9	[52](F3, F7)
			500	0.25 ~ 0.75 (3)		201.2	
			1000	0.25 ~ 0.75 (3)		166.5	
32	CO_2+N_2 (activated carbon)	298.1	6000	0.146 ~ 0.677 (3)	Sips	97.7	[55](SUP. T17)
33	CO_2+H_2 (activated carbon)	298.1	2000	0.072 ~ 0.551 (3)	Sips	246.6	[55](SUP. T18, F8)
			3000	0.081 ~ 0.588 (4)		184.4	
			8000	0.123 ~ 0.683 (3)		331.5	
39	CH_3OH+C_6H_{14} (Basolite C300 MOF)	313	2.7 ~ 11.3 (4)	0.5	-	779	[61](F4a)
40	N_2+O_2 (LiLSX zeolite)	273.1	607.8	0.3 ~ 0.8 (6)	-	70.6	[62](T4)
43	CO_2+N_2 (Cu-BTC MOF)	308.1	41.45 ~ 299.10 (9)	~ 0.15	Langmuir	40.3	[65](F2b, T5)

Table 5-10. Ternary adsorption system data range and errors in S_{12} by IAST

No.	Ternary mixtures (1) + (2) + (3) (Adsorbent)	Data range (number of data points)				Pure gas isotherm model	selectivity	Average error for Sij by IAST (%)	Ref. T=table F=figure
		P (kPa)	T (K)	y_1	y_2				
45	C_2H_4+ C_2H_6+ CH_4 (ETS-10)	200	300	0.054 ~ 0.494 (9)	0.010 ~0.147 (9)	Toth	S_{12}	134.7	[24] (T5)
							S_{23}	50.6	
46	C_2H_4+ CH_4+ H_2 (activated carbon)	1013	303.15	0.029 ~ 0.777 (19)	0.817 ~ 0.142 (19)	Langmuir-Freundlich	S_{12}	60.9	[49] (F7, F8, F9)

5.8 Summary

The effect of larger $N_2 – O_2$ selectivity of Material B on the performance of a MOC-RPSA process, which produced ~ 90% O_2 from a compressed air feed, was experimentally evaluated by testing the material in a continuous test apparatus which was used earlier for testing Material A.[5, 13] An identical RPSA process and test conditions were used for the comparison. It was found that higher selectivity of N_2 over O_2 reduced the BSF and enhanced the oxygen recovery by the process, which were desirable performances.

The selectivity of adsorption between the components of a binary or ternary gas mixture can be complex functions of equilibrium gas phase pressure, composition and temperature, which are determined by the nature of the adsorbate (molecular size, polarity, etc.) and the adsorbent (surface polarity, homogeneity, degree of heterogeneity, etc.) The prediction of binary and ternary gas selectivity from the corresponding pure gas isotherms using the IAST may be good to fair to poor depending on the nature of the adsorbate-adsorbent system. They should be experimentally verified before using them for a practical application like adsorptive process design.

5.9 References

1. Skarstrom, C. W. Method and apparatus for fractionating gaseous mixtures by adsorption. U.S. Patent 2,944,627, 1960.
2. Vemula, R. R.; Kothare, M. V.; Sircar, S. Anatomy of a rapid pressure swing adsorption process performance. *AlChE J.* **2015,** *61*, 2008-2015.
3. Sircar, S.; Kumar, R. Equilibrium Theory for Adiabatic Desorption of Bulk Binary Gas-Mixtures by Purge. *Ind. Eng. Chem. Proc. Des. Dev.* **1985,** *24*, 358-364.
4. Sircar, S. Basic research needs for design of adsorptive gas separation processes. *Ind. Eng. Chem. Res.* **2006,** *45*, 5435-5448.
5. Chai, S. W.; Kothare, M. V.; Sircar, S. Rapid Pressure Swing Adsorption for Reduction of Bed Size Factor of a Medical Oxygen Concentrator. *Ind. Eng. Chem. Res.* **2011,** *50*, 8703-8710.
6. Kirner, J. F. Nitrogen adsorption with highly Li exchanged X-zeolites with low Si/Al ratio. U.S. Patent U.S. Patent 5,268,023, 1993.
7. Jasra, R. V.; Choudary, N. V.; Bhat, S. G. T. Correlation of sorption behavior of nitrogen, oxygen, and argon with cation locations in zeolite X. *Ind. Eng. Chem. Res.* **1996,** *35*, 4221-4229.
8. Sircar, S. Role of Adsorbent Heterogeneity on Mixed Gas-Adsorption. *Ind. Eng. Chem. Res.* **1991,** *30*, 1032-1039.
9. Wu, C. W.; Kothare, M. V.; Sircar, S. Model Analysis of Equilibrium Adsorption Isotherms of Pure N-2, O-2, and Their Binary Mixtures on LiLSX Zeolite. *Ind. Eng. Chem. Res.* **2014,** *53*, 12428-12434.
10. Golden, T. C.; Sircar, S. Equilibrium and Kinetics of Adsorption of Freon-12 at Infinite Dilution. *AlChE J.* **1994,** *40*, 935-943.
11. Young, D. M.; Crowell, A. D., *Physical adsorption of gases*. Butterworths: London, 1962; p xi, 426 p.
12. Sircar, S. Gibbsian surface excess for gas adsorption - Revisited. *Ind. Eng. Chem. Res.* **1999,** *38*, 3670-3682.
13. Vemula, R. R.; Kothare, M. V.; Sircar, S. Performance of a medical oxygen concentrator using rapid pressure swing adsorption process: Effect of feed air pressure. *AlChE J.* **2016,** *62*, 1212-1215.
14. Rao, V. R.; Kothare, M. V.; Sircar, S. Novel design and performance of a medical oxygen concentrator using a rapid pressure swing adsorption concept. *AlChE J.* **2014,** *60*, 3330-3335.
15. S. Sircar; Myers, A. L. Gas adsorption operations: equilibrium, kinetics, column dynamics and design. *Adsorpt. Sci. Technol.* **1985,** *2*.

16. Sircar, S.; Mohr, R.; Ristic, C.; Rao, M. B. Isosteric heat of adsorption: Theory and experiment. *J. Phys. Chem. B* **1999,** *103*, 6539-6546.

17. Sircar, S. Isosteric Heats of Multicomponent Gas-Adsorption on Heterogeneous Adsorbents. *Langmuir* **1991,** *7*, 3065-3069.

18. Sircar, S. Heat of adsorption on heterogeneous adsorbents. *Appl. Surf. Sci.* **2005,** *252*, 647-653.

19. Wu, C. W.; Kothare, M. V.; Sircar, S. Equilibrium Adsorption Isotherms of Pure N2 and O2 and Their Binary Mixtures on LiLSX Zeolite: Experimental Data and Thermodynamic Analysis. *Ind. Eng. Chem. Res.* **2014,** *53*, 7195-7201.

20. Reich, R.; Ziegler, W. T.; Rogers, K. A. Adsorption of Methane, Ethane, and Ethylene Gases and Their Binary and Ternary Mixtures and Carbon-Dioxide on Activated Carbon at 212-301 K and Pressures to 35 Atmospheres. *Ind. Eng. Chem. Proc. Des. Dev.* **1980,** *19*, 336-344.

21. Sircar, S. Influence of Adsorbate Size and Adsorbent Heterogeneity on IAST. *AlChE J.* **1995,** *41*, 1135-1145.

22. Buss, E.; Heuchel, M. Adsorption equilibria of methane and tetrafluoromethane and their binary mixtures on silicalite. *J. Chem. Soc., Faraday Trans.* **1997,** *93*, 1621-1628.

23. Buss, E. GRAVIMETRIC MEASUREMENT OF BINARY GAS-ADSORPTION EQUILIBRIA OF METHANE-CARBON DIOXIDE MIXTURES ON ACTIVATED CARBON. *Gas Sep. Purif.* **1995,** *9*, 189-197.

24. Al-Baghli, N. A.; Loughlin, K. F. Binary and ternary adsorption of methane, ethane, and ethylene on titanosilicate ETS-10 zeolite. *J. Chem. Eng. Data* **2006,** *51*, 248-254.

25. van Miltenburg, A.; Gascon, J.; Zhu, W.; Kapteijn, F.; Moulijn, J. A. Propylene/propane mixture adsorption on faujasite sorbents. *Adsorption* **2008,** *14*, 309-321.

26. Sievers, W.; Mersmann, A., Prediction of High Pressure Multicomponent Adsorption Equilibria. In *Stud Surf Sci Catal*, Motoyuki, S., Ed. Elsevier: 1993; Vol. Volume 80, pp 583-590.

27. He, Y. F.; Yun, J. H.; Seaton, N. A. Adsorption equilibrium of binary methane/ethane mixtures in BPL activated carbon: Isotherms and calorimetric heats of adsorption. *Langmuir* **2004,** *20*, 6668-6678.

28. Talu, O.; Zwiebel, I. Multicomponent Adsorption Equilibria of Nonideal Mixtures. *AlChE J.* **1986,** *32*, 1263-1276.

29. Hyun, S. H.; Danner, R. P. Equilibrium Adsorption of Ethane, Ethylene, Isobutane, Carbon-Dioxide, and Their Binary-Mixtures on 13x Molecular-Sieves. *J. Chem. Eng. Data* **1982,** *27*, 196-200.

30. Markham, E. C.; Benton, A. F. THE ADSORPTION OF GAS MIXTURES BY SILICA. *J. Am. Chem. Soc.* **1931,** *53*, 497-507.

31. Nitta, T.; Shigetomi, T.; Kurooka, M.; Katayama, T. An Adsorption-Isotherm of Multi-Site Occupancy Model for Homogeneous Surface. *J. Chem. Eng. Jpn.* **1984,** *17*, 39-45.

32. Toth, J. Gas-(Dampf-)Adsorption an Festen Oberflächen Inhomogener Aktivität, III. *Acta. Chim. Hung.* **1962,** *32*.

33. Sips, R. On the Structure of a Catalyst Surface. *J. Chem. Phys.* **1948,** *16*, 490-495.

34. Myers, A. L.; Prausnitz, J. M. Thermodynamics of Mixed-Gas Adsorption. *AlChE J.* **1965,** *11*, 121-127.

35. Suwanayuen, S.; Danner, R. P. Vacancy Solution Theory of Adsorption from Gas-Mixtures. *AlChE J.* **1980,** *26*, 76-83.

36. Shapiro, A. A.; Stenby, E. H. Potential theory of multicomponent adsorption. *J. Colloid Interface Sci.* **1998,** *201*, 146-157.

37. Valenzuela, D.; Myers, A. L. Gas-Adsorption Equilibria. *Sep. Purif. Methods* **1984,** *13*, 153-183.

38. Buss, E. *Chem. Tech. (Leipzig)* **1996,** *48*, 189-197.

39. Van Der Vaart, R.; Huiskes, C.; Bosch, H.; Reith, T. Single and mixed gas adsorption equilibria of carbon dioxide/methane on activated carbon. *Adsorption* **2000,** *6*, 311-323.

40. Wang, K.; Qiao, S.; Hu, X. On the performance of HIAST and IAST in the prediction of multicomponent adsorption equilibria. *Sep. Purif. Technol.* **2000,** *20*, 243-249.

41. Bartholdy, S.; Bjorner, M. G.; Solbraa, E.; Shapiro, A.; Kontogeorgis, G. M. Capabilities and Limitations of Predictive Engineering Theories for Multicomponent Adsorption. *Ind. Eng. Chem. Res.* **2013,** *52*, 11552-11563.

42. Heuchel, M.; Snurr, R. Q.; Buss, E. Adsorption of CH4-CF4 mixtures in silicalite: Simulation, experiment, and theory. *Langmuir* **1997,** *13*, 6795-6804.

43. Qiao, S. Z.; Wang, K.; Hu, X. J. Using local IAST with micropore size distribution to predict multicomponent adsorption equilibrium of gases in activated carbon. *Langmuir* **2000,** *16*, 1292-1298.

44. Harlick, P. J. E.; Tezel, F. H. Adsorption of carbon dioxide, methane and nitrogen: pure and binary mixture adsorption for ZSM-5 with SiO2/Al2O3 ratio of 280. *Sep. Purif. Technol.* **2003,** *33*, 199-210.

45. Monneyron, P.; Manero, M. H.; Foussard, J. N. Measurement and modeling of single- and multi-component adsorption equilibria of VOC on high-silica zeolites. *Environ. Sci. Technol.* **2003,** *37*, 2410-2414.

46. Qiao, S. Z.; Hu, X. J. Effect of pore size distribution shape on the prediction of binary adsorption equilibrium and kinetics of gases in activated carbon. *Sep. Purif. Technol.* **2004,** *34*, 177-189.

47. Wang, F.; Li, J.; Wang, J.; Gao, H. Adsorption of acrylonitrile and methyl acrylate on activated carbon in a packed bed column. *Adsorption* **2006,** *12*, 205-212.

48. Belmabkhout, Y.; Pirngruber, G.; Jolimaitre, E.; Methivier, A. A complete experimental approach for synthesis gas separation studies using static gravimetric and column breakthrough experiments. *Adsorption* **2007,** *13*, 341-349.

49. Jeong, B.-M.; Ahn, E.-S.; Yun, J.-H.; Lee, C.-H.; Choi, D.-K. Ternary adsorption equilibrium of H-2/CH4/C2H4 onto activated carbon. *Sep. Purif. Technol.* **2007,** *55*, 335-342.

50. Bellat, J. P.; Benoit, F.; Weber, G.; Paulin, C.; Mougin, P.; Thomas, M. Adsorption equilibria of binary ethylmercaptan/hydrocarbon mixtures on a NaX zeolite. *Adsorption* **2008,** *14*, 501-507.

51. Chen, J.; Loo, L. S.; Wang, K. An Ideal Absorbed Solution Theory (IAST) Study of Adsorption Equilibria of Binary Mixtures of Methane and Ethane on a Templated Carbon. *J. Chem. Eng. Data* **2011,** *56*, 1209-1212.

52. Hamon, L.; Heymans, N.; Llewellyn, P. L.; Guillerm, V.; Ghoufi, A.; Vaesen, S.; Maurin, G.; Serre, C.; De Weireld, G.; Pirngruber, G. D. Separation of CO2-CH4 mixtures in the mesoporous MIL-100(Cr) MOF: experimental and modelling approaches. *J. Chem. Soc., Dalton Trans.* **2012,** *41*, 4052-4059.

53. Heymans, N.; Vaesen, S.; De Weireld, G. A complete procedure for acidic gas separation by adsorption on MIL-53 (Al). *Microporous Mesoporous Mater.* **2012,** *154*, 93-99.

54. Moellmer, J.; Lange, M.; Moeller, A.; Patzschke, C.; Stein, K.; Laessig, D.; Lincke, J.; Glaeser, R.; Krautscheid, H.; Staudt, R. Pure and mixed gas adsorption of CH4 and N-2 on the metal-organic framework Basolite (R) A100 and a novel copper-based 1,2,4-triazolyl isophthalate MOF. *J. Mater. Chem.* **2012,** *22*, 10274-10286.

55. Schell, J.; Casas, N.; Pini, R.; Mazzotti, M. Pure and binary adsorption of CO2, H-2, and N-2 on activated carbon. *Adsorption* **2012,** *18*, 49-65.

56. Rios, R. B.; Stragliotto, F. M.; Peixoto, H. R.; Torres, A. E. B.; Bastos-Neto, M.; Azevedo, D. C. S.; Cavalcante, C. L. Studies on the Adsorption Behavior of Co2-Ch4 Mixtures Using Activated Carbon. *Braz. J. Chem. Eng.* **2013,** *30*, 939-951.

57. Bakhtyari, A.; Mofarahi, M. Pure and Binary Adsorption Equilibria of Methane and Nitrogen on Zeolite 5A. *J. Chem. Eng. Data* **2014,** *59*, 626-639.

58. Mitchell, L. A.; LeVan, M. D. Development of Adsorption Equilibrium Relations for Mixtures from Pure Component Isotherms and Henry's Law Behavior with Components in Excess. *Ind. Eng. Chem. Res.* **2014,** *53*, 15531-15537.

59. Ohlin, L.; Grahn, M. Detailed Investigation of the Binary Adsorption of Carbon Dioxide and Methane in Zeolite Na-ZSM-5 Studied Using in Situ ATR-FTIR Spectroscopy. *J. Phys. Chem. C* **2014,** *118*, 6207-6213.

60. Pino, D.; Plantier, F.; Bessieres, D. Experimental determination of the adsorption isotherms in gas mixtures under extended pressure and temperature range. *J Therm. Anal. Calorim.* **2014,** *117*, 1469-1477.

61. Van Assche, T. R. C.; Duerinck, T.; Van der Perre, S.; Baron, G. V.; Denayer, J. F. M. Prediction of Molecular Separation of Polar-Apolar Mixtures on Heterogeneous Metal-Organic Frameworks: HKUST-1. *Langmuir* **2014,** *30*, 7878-7883.

62. Wu, C.-W.; Kothare, M. V.; Sircar, S. Model Analysis of Equilibrium Adsorption Isotherms of Pure N2, O2, and Their Binary Mixtures on LiLSX Zeolite. *Ind. Eng. Chem. Res.* **2014,** *53*, 12428-12434.

63. Hefti, M.; Marx, D.; Joss, L.; Mazzotti, M. Adsorption equilibrium of binary mixtures of carbon dioxide and nitrogen on zeolites ZSM-5 and 13X. *Microporous Mesoporous Mater.* **2015,** *215*, 215-228.

64. Mofarahi, M.; Bakhtyari, A. Experimental Investigation and Thermodynamic Modeling of CH4/N2 Adsorption on Zeolite 13X. *J. Chem. Eng. Data* **2015,** *60*, 683-696.

65. Yang, Y.; Sitprasert, C.; Rufford, T. E.; Ge, L.; Shukla, P.; Wang, S.; Rudolph, V.; Zhu, Z. An experimental and simulation study of binary adsorption in metal-organic frameworks. *Sep. Purif. Technol.* **2015,** *146*, 136-142.

66. Hartzog, D. G.; Sircar, S. Sensitivity of PSA process performance to input variables. *Adsorption* **1995,** *1*, 133-151.

Chapter 6

Conclusions and Recommendations

The work presented in this dissertation focuses on fundamental knowledge of adsorption characteristics (equilibrium isotherm, isosteric heats, and mass transfer coefficients. This research includes measurement of (a) the pure and binary gas equilibrium adsorption isotherms of N_2, O_2 and Ar, and (b) the effective mass transfer coefficients of the pure gases into the adsorbent particles using the above mentioned LiLSX sample under different conditions of pressure and temperature. Isosteric heats of adsorption of the pure gases are estimated by thermodynamic analysis of the isotherm data. An analysis is also carried out to find an analytical isotherm model which describes the pure gas isotherms adequately and can be used to estimate binary adsorption isotherm from the pure gas isotherms.

The key novelties of this research are:

Equilibrium Adsorption Isotherms of Pure and Binary Mixture

- An **isothermal** column dynamic apparatus was constructed and a protocol for for measurement of pure and binary gas adsorption isotherms at different temperatures, pressures and compositions, pure gas mass adsorptive transfer coefficients, thermodynamic estimation of pure gas isosteric heats as functions of adsorbate loadings was developed.
- Extensive pure and binary gas equilibrium data were measured over a pressure range of 0 – 6 atm and at three different temperatures. The data obey an integral

and a differential thermodynamic consistency test between pure gas and binary adsorption isotherm data, proving their reliability. **Such data are not easily found in literature.**

- Heterogeneous nature of the adsorbent for the gases and different degrees of heterogeneity for the gases on the same adsorbent were recognized which **has never been published before.** This is presumably caused by the subtle differences in the quadrupole-ion interactions between the gas molecules and the cationic adsorption sites in the adsorbent. N_2 exhibits a higher degree of heterogeneity because it has a larger quadrupole moment than O_2 and Ar.

Model Analysis of Equilibrium Adsorption Isotherms of Pure and Binary Mixture

- Three analytical equilibrium isotherm models, i.e. Langmuir (homogeneous), Toth, Heterogeneous Langmuir (heterogeneous), and IAST were tested to describe experimental data. The four models are thermodynamically consistent.
- The superiority of Heterogeneous Langmuir model which accounts for the differences in the heterogeneity of adsorption of the components was demonstrated for the present case.
- The superiority of Heterogeneous Langmuir model over the commonly used IAST was demonstrated for the present case.
- Predictions of multicomponent isotherm data by models **must be extensively tested experimentally**, since their ability to describe pure gas isotherms does not guarantee the quality of multicomponent isotherms predictions.

Column Dynamic Study of Mass Transfer of Pure Gases

- A protocol for measurement of effective mass transfer coefficient for pure gas by analysis of experimental column dynamic data was developed.
- The effective mass transfer coefficients for N_2, O_2 and Ar decreased linearly with increasing pressure and increased with increasing temperature.
- It was demonstrated that the LiLSX zeolite sample exhibits a significant skin resistance for transport of the tested gases, **which is not always recognized**.

Comments on Binary and Ternary Gas Adsorption Selectivity

- The results of a literature search (1996 – 2015) for experimental data on binary and ternary gas adsorption selectivity and their estimation from the corresponding pure gas adsorption isotherms by Ideal Adsorbed Solution Theory (IAST) was summarized.
- The selectivity of adsorption of a binary or a ternary gas mixture can be a complex function of equilibrium gas phase pressure, temperature and composition and it must be experimentally measured for reliable design of adsorptive gas separation processes.
- Adsorption systems having different adsorbate (molecular size, polarity) and adsorbent (energetic heterogeneity, polarity) properties
- Classification of systems where IAST works well.

My recommendations for the future work are:

- There is a need to generate and compile multicomponent adsorption data. The multicomponent equilibrium, multicomponent gas kinetics data and multicomponent isosteric heats data for this system are rare. These data are needed for reliable process design and theoretical model validation.
- The following published correlations for estimation of adsorption equilibria is used in our previous numerical study on a RPSA process performance.[1-3]

  Adsorption equilibria:[4]

  $$n_i^{\infty} = \frac{K_i P y_i}{1+\sum B_j P y_j};\ K_i = K_i^0 exp\left[\frac{Q_{K_i}}{RT_s}\right];\ B_i = KB_i^0 exp\left[\frac{Q_{B_i}}{RT_s}\right] \qquad (6\text{-}1)$$

  Eq. (6-1) is mathematically simple and most widely used for describing gas adsorption on an energetically homogeneous adsorbent. However, in our previous experimentally study, we found that the zeolite exhibites different degrees of energetic heterogeneity for adsorption of pure N_2 and. In order to take into account the degree of heterogeneity, the heterogeneous – Langmuir equilibrium equation will be used in the RPSA process model to numerically study the effects of different equilibria equations on a RPSA performance for air separation.
- The effect of heterogeneity on the RPSA performance will be studied numerically from above future work. The same RPSA performance will be measured experimentally to verify whether a heterogeneous - Langmuir model can improve the quality of a RPSA process simulation.
- Recently, a simplified lumped model which is evaluated by a non-isothermal, adisbatic, four-step Skarstorm-like PSA process for production of pure helium

from a binary nitrogen-helium mixture using 5A zeolite is published.[5] The same PSA performance is measured experimentally measured and the detail can be found in Appendix E. The model will be tested, modified and improved according to the experimental data. In addition, this model will be extend to describe the combined effects of gas-solid mass and heat transfer coefficients as well as the effects of gas phase mass and heat dispersions on the overall performance of a rapid or regular PSA process for air separation.

- Everyone in this lab must follow the lab safety policy when operating the compressed gas cylinders and read the MSDS before using the LiLSX zeolite.

6.1 Reference

1. Chai, S. W.; Kothare, M. V.; Sircar, S. Numerical study of nitrogen desorption by rapid oxygen purge for a medical oxygen concentrator. *Adsorption* **2012,** *18,* 87.
2. Chai, S. W.; Kothare, M. V.; Sircar, S. Efficiency of Nitrogen Desorption from LiX Zeolite by Rapid Oxygen Purge in a Pancake Adsorber. *AlChE J.* **2013,** *59,* 365.
3. Rao, V. R.; Kothare, M. V.; Sircar, S. Numerical simulation of rapid pressurization and depressurization of a zeolite column using nitrogen. *Adsorption* **2014,** *20,* 53.
4. Rege, S. U.; Yang, R. T. Limits for air separation by adsorption with LiX zeolite. *Ind.Eng. Chem. Res.* **1997,** *36,* 5358.
5. Rama Rao, V.; Kothare, M. V.; Sircar, S. Lumped Heat and Mass Transfer Coefficient for Simulation of A Pressure Swing Adsorption Process. *Sep. Sci. Technol.* **2016**, http://dx.doi.org/10.1080/01496395.2016.1242629.

Appendix A : LiLSX zeolite isotherm data

Table A 1. Pure N_2 at 3 different temperature on LiLSX zeolite

	273.1 K		303.1 K		338.1 K	
	P (atm)	n_i^{mo}(mol/kg)	P (atm)	n_i^{mo}(mol/kg)	P (atm)	n_i^{mo}(mol/kg)
N_2	0.366	0.829	0.020	0.025	0.020	0.009
	0.733	1.146	0.030	0.038	0.030	0.014
	1.099	1.400	0.040	0.053	0.040	0.018
	2.076	1.780	0.060	0.079	0.060	0.028
	3.053	1.997	0.080	0.108	0.488	0.213
	4.030	2.218	0.611	0.562	0.977	0.378
	5.007	2.322	1.099	0.835	1.465	0.526
	6.106	2.468	1.710	1.082	1.954	0.646
			2.442	1.295	2.442	0.734
			3.175	1.482	2.931	0.851
			3.908	1.597	3.419	0.937
			4.640	1.714	3.908	1.011
			5.373	1.795	4.396	1.081
			6.106	1.861	4.884	1.155
					5.373	1.180
					6.106	1.293

Table A 2. Pure O_2 at 3 different temperature on LiLSX zeolite

	273.1 K		303.1 K		338.1 K	
	P (atm)	n_i^{mo}(mol/kg)	P (atm)	n_i^{mo}(mol/kg)	P (atm)	n_i^{mo}(mol/kg)
O_2	0.080	0.023	0.080	0.015	0.120	0.014
	0.120	0.036	0.120	0.021	0.160	0.021
	0.160	0.045	0.160	0.028	0.500	0.059
	0.200	0.058	0.200	0.035	1.000	0.113
	1.000	0.277	1.000	0.190	2.442	0.234
	2.442	0.591	2.442	0.366	3.663	0.326
	3.663	0.838	3.663	0.521	4.884	0.455
	6.106	1.331	4.884	0.693	6.106	0.545
			6.106	0.815		

Table A 3. Pure Ar at 3 different temperature on LiLSX zeolite

	273.1 K		303.1 K		338.1 K	
	P (atm)	n_i^{mo}(mol/kg)	P (atm)	n_i^{mo}(mol/kg)	P (atm)	n_i^{mo}(mol/kg)
Ar	0	0	0	0	0	0
	0.08	0.02	0.12	0.019	0.611	0.049
	0.2	0.054	0.16	0.026	1.221	0.1
	0.611	0.127	0.2	0.03	2.442	0.204
	1.221	0.262	0.611	0.08	3.663	0.295
	2.442	0.502	1.221	0.162	4.884	0.388
	3.663	0.719	2.442	0.313	6.106	0.482
	4.884	0.928	3.663	0.448		
	6.106	1.107	4.884	0.583		
			6.106	0.712		

Table A 4. Binary N_2 (1) + O_2 (2) gas adsorption isotherm on LiLSX at constant P and T

Temp. (K)	P=1 atm			P=6 atm		
	y_1	n_1^m (mol/kg)	n_2^m (mol/kg)	y_1	n_1^m (mol/kg)	n_2^m (mol/kg)
273.1	0.00	0.0	0.277	0.00	0.0	1.331
	0.30	0.577	0.162	0.30	1.322	0.529
	0.40	0.766	0.131	0.40	1.671	0.437
	0.50	0.942	0.107	0.50	1.938	0.351
	0.60	1.060	0.087	0.60	2.069	0.269
	0.70	1.141	0.062	0.70	2.208	0.195
	0.80	1.203	0.039	0.80	2.366	0.127
	1.00	1.377	0.00	1.00	2.468	0.0
303.1	0.00	0.0	0.190	0.00	0.0	0.815
	0.30	0.324	0.120	0.50	1.220	0.257
	0.40	0.434	0.100	0.60	1.372	0.200
	0.50	0.512	0.081	0.70	1.538	0.151
	0.60	0.579	0.061	0.80	1.665	0.093
	0.70	0.633	0.042	0.90	1.801	0.047
	1.00	0.790	0.0	1.00	1.861	0.0
338.1	0.00	0.0	0.113	0.00	0.0	0.545
	0.30	0.146	0.080	0.20	0.345	0.328
	0.40	0.193	0.067	0.40	0.653	0.232
	0.50	0.232	0.056	0.60	0.908	0.145
	0.60	0.286	0.039	0.80	1.125	0.072
	0.70	0.321	0.030	1.00	1.293	0.0
	1.00	0.378	0.0			

Appendix B : Additional details of Henry's law constant distributions

In previous study, it was shown that LiLSX zeolite exhibits different degrees of adsorbent heterogeneity for adsorption of pure N_2 and O_2. The Sircar adsorption model can satisfy the requirement of the different degrees of adsorbent heterogeneity and also provide the closest correlation between the estimated and the experimental binary selectivity values for this system under various conditions of P, T and gas composition. In Sircar model, it is assumed $\lambda(b_i)$ is a uniform distribution. b_{iL} and b_{iH} are , respectively, the lowest and highest values of b_i for adsorption of pure gas i on the heterogeneous adsorbent.

Adsorption of pure gas

The heterogeneous Langmuir model is used here. It is assumed that the local adsorption equilibria of the gas on a homogeneous patch is given by Langmuir model and the adsorbent heterogeneity can be described by a uniform distribution (Figure B 1) with different values of Henry's law constants b_i.

However, the real density distribution is not uniform and this assumption may be the source of deviation between model and experimental data. The real density distribution is more like Gaussian distribution (Figure B 2 solid line) which would increase the difficulty and the complex of obtaining an analytical solution. To simplify the calculation, a triangle distribution will be used to mimic the distribution with skewness (Figure B 2 dashed line).

Thus the goal of this work is to (a) derive an analytical heterogeneous Langmuir equilibrium model by using a mimic triangle distribution (Figure B 3), and (b) find out if the different probability density affect the results of model predictions.

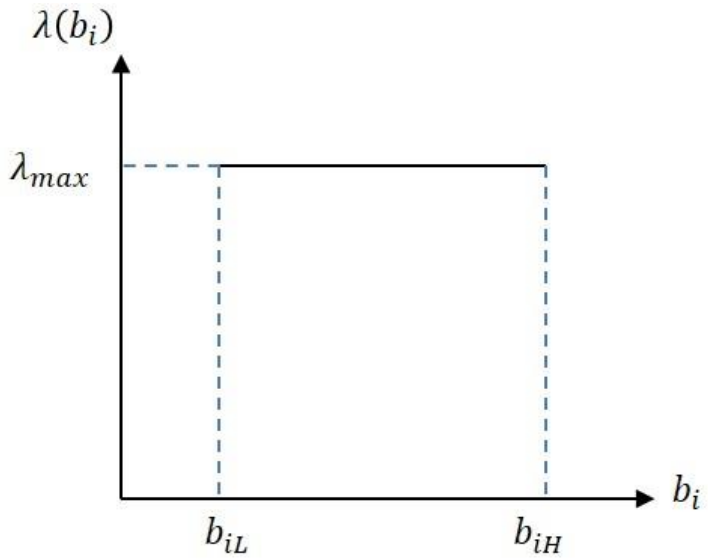

Figure B 1. Uniform distribution

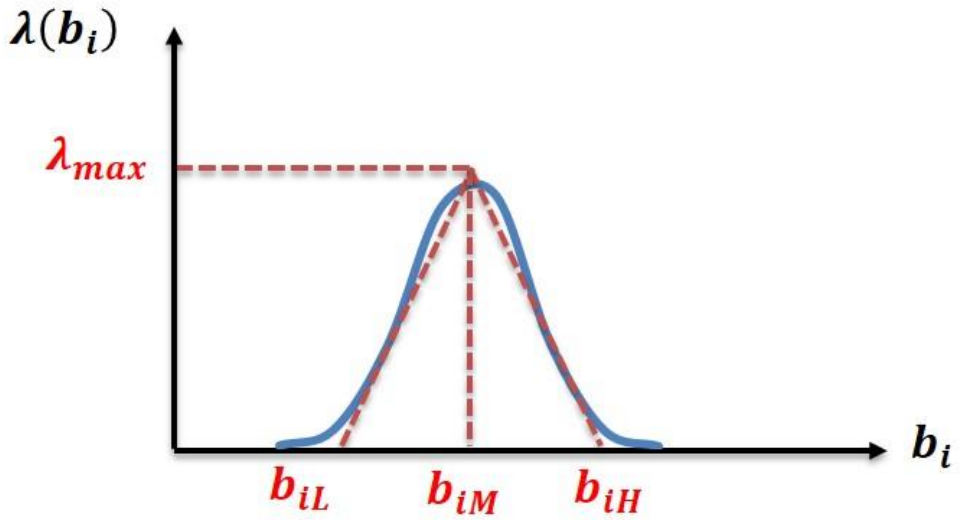

Figure B 2. Gaussian distribution

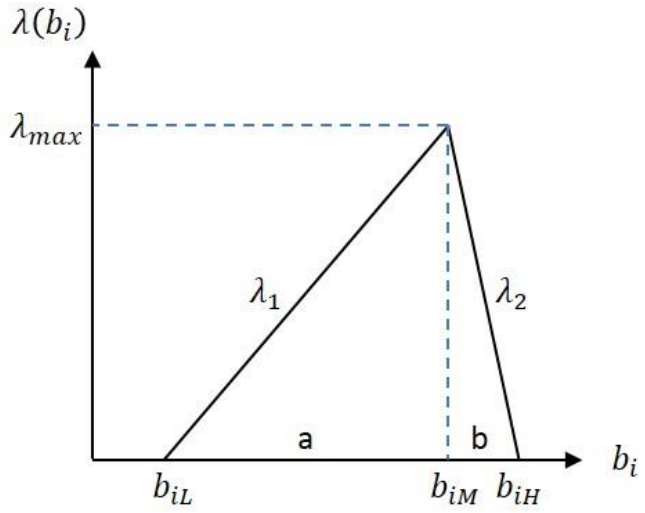

Figure B 3. Triangle distribution

It is assumed that $\lambda(b_i)$ is the normalized probability density of patches with Henry's law constant b_i and comprised of two linear equations $\lambda_1(b_i)$ and $\lambda_2(b_i)$.

$$\lambda(b_i) = \lambda_1(b_i) + \lambda_2(b_i) \tag{B.1}$$

$$\int_{b_{iL}}^{b_{iH}} \lambda(b_i)\, db_i = \int_{b_{iL}}^{b_{iM}} \lambda_1(b_i)\, db_i + \int_{b_{iM}}^{b_{iH}} \lambda_2(b_i)\, db_i = 1 \tag{B.2}$$

b_{iL}, b_{iH} and b_{iM} are, respectively, the lowest and the highest values of b_i for adsorption of pure gas i on the heterogeneous adsorbent and the value which can obtain the maximum probability density λ_{max}.

The mean (μ_i) and the dispersion (σ_i) of the b_i distribution can be given by

$$\mu_i = \int_{b_{iL}}^{b_{iH}} b_i \lambda(b_i)\, db_i = \frac{(2-\delta)b_{iL} + (\delta+1)b_{iH}}{3}; \delta = \frac{a}{a+b} \tag{B.3}$$

$$\sigma_i = \left(\int_{b_{iL}}^{b_{iH}} [b_i - \mu_i]^2 \lambda(b_i)\, db_i \right)^{\frac{1}{2}} = \frac{b_{iH} - b_{iL}}{3\sqrt{2}} (\delta^2 - \delta + 1)^{\frac{1}{2}} \tag{B.4}$$

The degree of heterogeneity is defined by

$$\psi_i = \left[\frac{2}{\delta^2 - \delta + 1} \right]^{\frac{1}{2}} \frac{\sigma_i}{\mu_i} (\delta + 1) \tag{B.5}$$

The boundary values of b_i can be expressed in terms of μ_i and ψ_i as

$$b_{iL} = \mu_i(1 - \psi_i);\ b_{iH} = \mu_i \left(1 + \frac{2 - \delta}{\delta + 1} \psi_i\right);\ b_{iM} = \mu_i \left(1 + \frac{2\delta - 1}{\delta + 1} \psi_i\right) \tag{B.6}$$

The overall fractional adsorption capacity of the pure gas on the heterogeneous adsorbent can be solved by using equations (B.1)-(B.6) as

$$\Theta_i^o(P, T) = \Theta_{iH}^o \left[1 - \frac{(1 - \Theta_{iH}^o)}{\Theta_{iH}^o} f(z_i^o) \right] \tag{B.7}$$

$$z_i^o = \psi_i \Theta_{iH}^o;\ \Theta_{iH}^o = \frac{\mu_i P}{[1 + \mu_i P]} \tag{B.8}$$

$$\left[\frac{\delta \Theta_i^o}{\delta P} \right]_T = \mu_i; P \to 0;\ \frac{d \ln \mu_i}{dT} = -\frac{q_i^o}{RT^2} \tag{B.9}$$

$$f(z_i^o) = \frac{2(\delta + 1)^2}{9 {z_i^o}^2} \ln \left[\frac{(1 - z_i^o)^{\frac{1}{\delta}(1 - z_i^o)} \left(1 + \frac{2 - \delta}{\delta + 1} z_i^o\right)^{\frac{1}{1-\delta}\left(1 + \frac{2-\delta}{\delta+1} z_i^o\right)}}{\left(1 + \frac{2\delta - 1}{\delta + 1} z_i^o\right)^{\frac{1}{\delta}\frac{1}{1-\delta}\left(1 + \frac{2\delta-1}{\delta+1} z_i^o\right)}} \right] - 1 \tag{B.10}$$

Pure gas adsorption isosteric heat can be also derived by using equations (B.7)-(B.10) as:

$$\left[\frac{q_i^o(\theta_i^o) - q_i^*}{q_i^{**} - q_i^*}\right] = \frac{z_i^o \frac{df(z_i^o)}{dz_i^o} \cdot G(\psi_i)}{\Theta_{iH}^o[1 + f(z_i^o)] - (1 - \Theta_{iH}^o)\left\{z_i^o \frac{df(z_i^o)}{dz_i^o}\right\}} \tag{B.11}$$

$$\left[\frac{(q_i^{**} - q_i^*)}{RT^2}\right] = \frac{1}{G(\psi_i)} \frac{d \ln \psi_i}{dT};\ G(\psi_i) = \left(\frac{1 + f(\psi_i)}{\psi_i \frac{df(\psi_i)}{d\psi_i}}\right) \tag{B.12}$$

$$z_i^o \frac{df(z_i^o)}{dz_i^o} = -2\{1 + f(z_i^o)\} + \frac{2(\delta+1)^2}{9z_i^o} \ln\left[\frac{\left(1 + \frac{2-\delta}{\delta+1} z_i^o\right)^{\frac{1}{1-\delta}\left(\frac{2-\delta}{\delta+1}\right)}}{(1 - z_i^o)^{\frac{1}{\delta}} \left(1 + \frac{2\delta-1}{\delta+1} z_i^o\right)^{\frac{1}{\delta}\frac{1}{1-\delta}\left(\frac{2\delta-1}{\delta+1}\right)}}\right] \tag{B.13}$$

Summary

Table B 1 is the comparison of the mean and the dispersion the b_i distribution and the degree of heterogeneity between this work and Sircar model. It can be seen in Table B 2 that different distribution functions cannot influence the quality of model significantly.

Table B 1. Model parameters

model	The mean (μ_i)	The dispersion (σ_i)	The degree of heterogeneity (ψ_i)
This work	$\frac{(2-\delta)b_{iL} + (\delta+1)b_{iH}}{3}$	$\frac{b_{iH} - b_{iL}}{3\sqrt{2}}(\delta^2 - \delta + 1)^{\frac{1}{2}}$	$\left[\frac{2}{\delta^2 - \delta + 1}\right]^{\frac{1}{2}} \frac{\sigma_i}{\mu_i}(\delta+1)$
Sircar	$\frac{b_{iL} + b_{iH}}{2}$	$\frac{b_{iH} - b_{iL}}{2\sqrt{3}}$	$\sqrt{3}\frac{\sigma_i}{\mu_i}$

Table B 2. Average deviation between experimental measurement and model prediction

T (K)	Gas	Average deviation (%)			
		H-Langmuir (Sircar)	Modified H-Langmuir $\delta = 0.02$	Modified H-Langmuir $\delta = 0.05$	Modified H-Langmuir $\delta = 0.1$
273.1	N_2	3.7	3.3	3.4	3.6
	O_2	5.8	5.8	5.9	5.9
	Ar	6.8	6.8	6.9	7.0
303.1	N_2	4.8	3.8	3.8	3.9
	O_2	4.1	4.0	4.1	4.1
	Ar	5.5	5.6	5.5	5.4
338.1	N_2	2.1	1.4	1.6	1.8
	O_2	10.9	8.9	10.6	10.6
	Ar	4.8	9.8	9.7	9.6
T (K)	Gas	Average deviation (%)			
		Modified H-Langmuir $\delta = 0.999$	Modified H-Langmuir $\delta = 0.8$	Modified H-Langmuir $\delta = 0.2$	Modified H-Langmuir $\delta = 0.5$
273.1	N_2	6.7	4.9	3.9	4.6
	O_2	5.9	6.0	5.9	6.0
	Ar	6.5	7.3	7.0	7.3
303.1	N_2	6.8	4.8	4.3	4.3
	O_2	4.1	4.4	4.1	4.4
	Ar	6.5	5.1	5.3	5.1
338.1	N_2	3.3	2.4	2.4	2.3
	O_2	13.5	19.6	16.0	10.1
	Ar	9.7	9.0	9.5	9.1

Appendix C : Experimental breakthrough curves for pure N_2 and O_2 displacing He

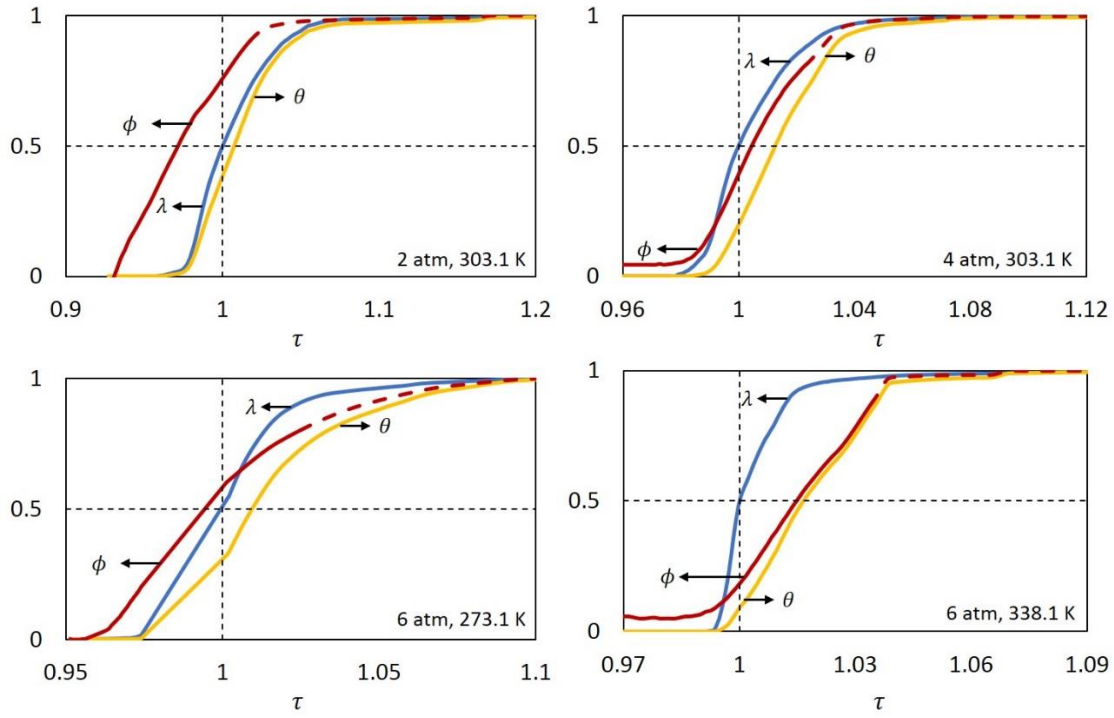

Figure C 1. Experimental breakthrough curves for O_2 displacing He

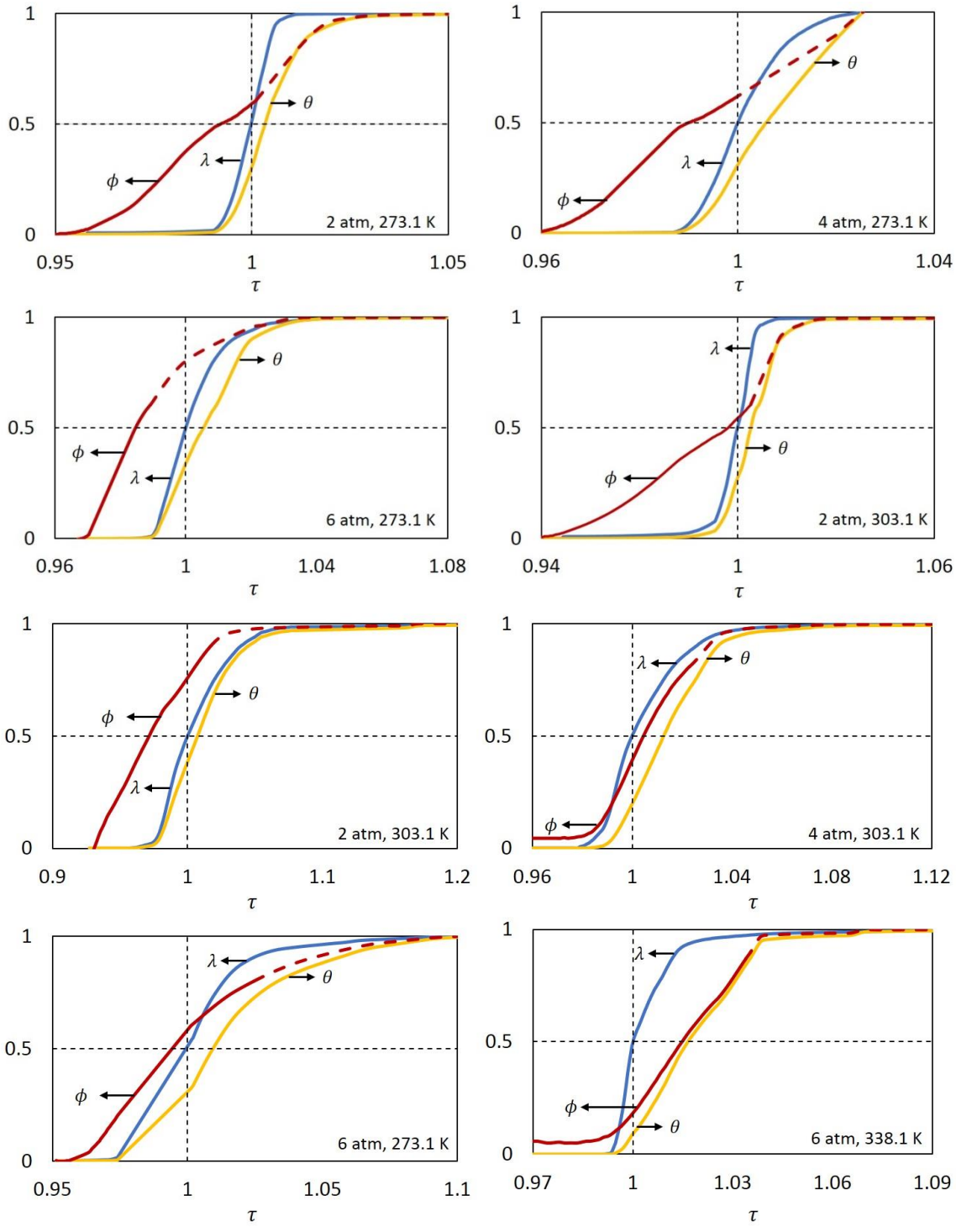

Figure C 2. Experimental breakthrough curves for N_2 displacing He

Appendix D : Gas mixture adsorption selectivity experimental and prediction data

Table D 1. Comparison of binary gas mixtures adsorption selectivity experimental and prediction data

Adsorbate (1) + (2) on adsorbent (measurement; pure gas isotherm modelb)	P (kPa)	T (K)	y_1[a]	selectivity		Error (%)	Ref.
				exp	IAST		
CO_2 + CH_4 Activated Carbon (gravimetric)	530	293	0.092	2.93	3.54	20.88	[1]
			0.282	3.42	3.48	1.95	
			0.496	4.09	3.59	12.12	
			0.688	5.67	3.58	36.96	
			0.844	7.85	3.73	52.54	
			0.946	14.21	4.05	71.48	
	100	293	0.500	3.80	3.41	10.13	
		313	0.500	3.39	3.12	7.89	
		333	0.500	2.90	2.80	3.57	
	530	313	0.500	3.48	3.18	8.70	
		333	0.500	2.99	2.78	6.92	
CF_4 + CH_4 silicalite (high pressure microbalance)	100	298.15	0.045	3.65	3.93	7.67	[2]
			0.104	3.62	3.69	1.89	
			0.158	3.56	3.60	1.07	
			0.250	3.52	3.56	1.03	
			0.408	3.42	3.54	3.45	
			0.574	3.42	3.51	2.71	
			0.732	3.33	3.43	3.02	
			0.845	3.03	3.46	14.06	
			0.962	2.48	3.50	41.09	
			0.045	3.05	3.33	9.40	
			0.104	3.13	3.27	4.65	
	500	298.15	0.158	3.13	3.20	2.06	
			0.250	3.10	3.17	2.37	
			0.408	2.97	3.17	6.98	
			0.574	3.10	3.19	2.80	
			0.732	3.15	3.28	3.96	
			0.845	3.17	3.24	2.18	
			0.962	3.63	3.95	8.86	
	1000	298.15	0.045	2.89	3.14	8.83	
			0.104	2.79	3.02	8.29	

Adsorbate (1) + (2) on adsorbent (measurement; pure gas isotherm modelb)	P (kPa)	T (K)	y_1[a]	selectivity		Error (%)	Ref.
				exp	IAST		
CF_4 + CH_4 silicalite (high pressure microbalance)	1000	298.15	0.158	2.81	2.98	6.11	[2]
			0.250	2.76	2.94	6.63	
			0.408	2.61	2.87	9.91	
			0.574	2.61	2.83	8.42	
			0.732	2.62	2.80	6.81	
			0.845	2.73	2.92	7.23	
			0.962	2.86	3.05	6.60	
	1700	298.15	0.045	2.60	2.81	8.13	
			0.104	2.56	2.77	8.15	
			0.158	2.53	2.74	8.36	
			0.250	2.46	2.69	9.41	
			0.408	2.33	2.63	12.72	
			0.574	2.26	2.57	13.88	
			0.732	2.23	2.53	13.26	
			0.845	2.19	2.50	13.88	
			0.962	2.08	2.47	19.17	
CF_4 + CH_4 slicalite (high pressure microbalance)	100	300	0.043	3.72	4.50	20.79	[3]
			0.103	3.68	4.36	18.62	
			0.158	3.65	4.46	22.34	
			0.250	3.59	4.48	24.85	
			0.405	3.44	4.53	31.83	
			0.571	3.44	4.43	28.79	
			0.728	3.33	4.43	32.93	
			0.842	2.96	4.58	54.82	
			0.959	2.37	4.67	97.03	
	1000	300	0.043	2.94	3.58	21.48	
			0.103	2.90	3.31	14.08	
			0.158	2.88	3.22	11.76	
			0.250	2.79	3.16	13.01	
			0.405	2.63	3.11	18.18	
			0.571	2.61	2.98	13.97	
			0.728	2.60	2.79	7.25	
			0.842	2.48	2.71	9.55	
			0.959	2.18	2.34	7.30	
C_3H_8 + C_2H_6 norit-activated carbon (differential adsorber bed; MPSD)	50	303	0.200	7.59	4.58	39.60	[4]
			0.400	5.30	3.92	26.15	
			0.600	4.88	3.54	27.61	
			0.800	5.97	3.20	46.34	
		333	0.200	6.72	5.02	25.37	

Adsorbate (1) + (2) on adsorbent (measurement; pure gas isotherm modelb)	P (kPa)	T (K)	y_1[a]	selectivity		Error (%)	Ref.
				exp	IAST		
$C_3H_8 + C_2H_6$ norit-activated carbon (differential adsorber bed; MPSD)	50	333	0.400	5.72	4.38	23.39	[4]
			0.600	4.50	4.14	8.16	
			0.800	3.28	3.84	17.00	
		363	0.200	6.69	5.49	17.91	
			0.400	4.84	5.03	4.08	
			0.600	4.33	4.64	6.98	
			0.800	3.15	4.26	35.24	
$C_2H_6 + CH_4$ norit-activated carbon (differential adsorber bed; MPSD)	50	303	0.100	22.71	20.76	8.58	
			0.200	14.56	18.21	25.06	
			0.600	7.92	14.81	86.87	
			0.800	5.17	14.78	185.69	
		333	0.100	14.44	16.64	15.23	
			0.200	11.61	14.31	23.22	
			0.600	6.02	11.37	88.94	
			0.800	3.98	10.86	172.79	
$C_3H_8 + CH_4$ norit-activated carbon (differential adsorber bed; MPSD)	50	303	0.100	42.89	72.38	68.73	
			0.200	29.94	71.43	138.55	
			0.500	14.52	63.60	337.90	
		333	0.100	53.73	69.00	28.43	
			0.200	42.26	61.50	45.52	
			0.500	17.72	47.43	167.62	
		363	0.100	37.22	60.14	61.59	
			0.200	25.65	56.27	119.39	
			0.500	15.15	50.50	233.33	
$C_2H_6 + CH_4$ ajax-activated carbon (volumetric; MPSD)	66.7	303	0.116	14.76	16.50	11.81	
			0.265	13.49	15.98	18.49	
			0.506	10.89	15.21	39.69	
$C_3H_8 + CH_4$ ajax-activated carbon (volumetric; MPSD)	66.7	303	0.107	73.88	77.69	5.16	
			0.374	31.28	51.39	64.28	
			0.754	45.49	46.72	2.69	
$CO_2 + CH_4$ ajax-activated carbon (volumetric; MPSD)	66.7	273	0.039	6.67	3.23	51.66	
			0.190	3.98	3.35	15.93	
			0.389	3.15	3.54	12.41	
			0.614	2.59	3.82	47.46	
			0.796	2.51	4.00	59.18	
			0.866	2.28	4.11	80.37	
	66.7	303	0.048	7.16	3.03	57.61	
			0.222	3.92	3.12	20.51	

Adsorbate (1) + (2) on adsorbent (measurement; pure gas isotherm modelb)	P (kPa)	T (K)	y_1[a]	selectivity		Error (%)	Ref.
				exp	IAST		
CO_2 + CH_4 ajax-activated carbon (volumetric; MPSD)	66.7	303	0.412	3.44	3.22	6.52	[4]
			0.633	2.86	3.34	16.62	
			0.746	3.12	3.37	8.09	
			0.869	2.73	3.46	26.67	
CH_4 + N_2 H-ZEM-5-280 (concentration pulse chromatography; F)	101	313	0.010	2.77	2.42	12.70	[5]
			0.020	2.81	2.23	20.66	
			0.050	3.00	2.25	25.04	
			0.150	2.95	2.21	25.10	
			0.300	2.97	2.16	27.27	
			0.450	2.93	2.11	27.91	
			0.650	2.87	2.04	28.85	
			0.850	2.73	2.02	26.09	
			0.950	2.71	2.14	20.82	
CO_2 + CH_4 H-ZEM-5-280 (concentration pulse chromatography; F)	101	313	0.020	12.17	5.60	53.98	
			0.050	10.10	5.19	48.67	
			0.080	9.08	4.97	45.25	
			0.150	7.93	4.88	38.53	
			0.300	6.77	4.51	33.36	
			0.400	6.47	4.44	31.33	
			0.550	6.06	4.27	29.44	
			0.700	5.65	4.14	26.61	
			0.850	5.36	3.95	26.28	
			0.930	5.71	4.01	29.83	
CO_2 + N_2 H-ZEM-5-280 (concentration pulse chromatography; F)	101	313	0.010	34.57	19.29	44.21	
			0.015	33.57	15.06	55.14	
			0.030	29.92	12.23	59.11	
			0.050	34.01	12.98	61.84	
			0.100	42.05	12.40	70.52	
			0.200	50.13	11.96	76.14	
			0.300	54.74	11.58	78.85	
			0.400	43.84	11.14	74.58	
			0.550	34.38	10.49	69.49	
			0.700	22.03	10.30	53.26	
			0.850	18.60	10.05	45.96	
			0.950	13.42	9.80	26.94	
C_4H_8O + $C_4H_8O_2$ FAU Y (volumetric; F)	0.285	298	0.144	0.83	0.99	19.70	[6]
			0.561	0.56	1.01	80.32	
			0.893	0.47	1.00	114.31	

Adsorbate (1) + (2) on adsorbent (measurement; pure gas isotherm modelb)	P (kPa)	T (K)	y_1[a]	selectivity		Error (%)	Ref.
				exp	IAST		
C_4H_8O + $C_4H_8O_2$ Sil Z (volumetric; L)	0.01	298	0.146	0.87	1.16	32.81	[6]
			0.489	0.84	1.17	39.77	
			0.769	1.38	1.19	13.95	
C_4H_8O + $C_4H_8O_2$ Sil Z (volumetric; T)	0.01	298	0.146	0.87	0.92	5.51	
			0.489	0.84	0.93	11.17	
			0.769	1.38	0.93	32.39	
C_4H_8O + C_7H_8 FAU Y (volumetric)	0.005	298	0.051	3.47	1.72	50.40	
			0.364	1.74	1.70	2.38	
			0.761	1.82	1.64	9.87	
	0.023	298	0.113	1.44	0.57	60.40	
			0.683	0.45	0.69	54.04	
			0.883	0.75	0.74	1.17	
$C_4H_8O_2$ + C_7H_8 FAU Y (volumetric)	0.008	298	0.063	2.73	1.67	38.55	
			0.359	1.55	1.57	1.24	
			0.782	1.45	1.52	4.72	
	0.0165	298	0.109	1.48	1.31	11.60	
			0.514	0.87	1.02	18.00	
			0.856	0.85	1.04	22.38	
C_2H_6 + CH_4 activated carbon (bench-scale high-pressure open-flow ad(de)sorption)	52	301.4	0.035	25.08	26.14	4.23	[7]
			0.094	24.06	23.08	4.07	
			0.284	18.72	19.57	4.58	
			0.511	15.70	17.82	13.51	
			0.733	14.11	16.80	19.09	
			0.958	16.02	16.06	0.25	
	196	301.4	0.284	14.48	15.22	5.15	
			0.511	12.69	14.06	10.77	
			0.733	11.60	13.39	15.40	
	684	301.4	0.035	15.62	15.00	3.92	
			0.094	14.80	13.90	6.06	
			0.284	11.94	12.27	2.73	
			0.511	10.76	11.33	5.31	
			0.733	9.95	10.76	8.20	
			0.898	9.33	10.44	11.80	
			0.958	9.66	10.31	6.76	
	1397	301.4	0.035	14.60	15.38	5.33	
			0.284	10.75	10.50	2.31	
			0.511	9.96	9.83	1.25	
			0.733	8.67	9.04	4.30	

Adsorbate (1) + (2) on adsorbent (measurement; pure gas isotherm modelb)	P (kPa)	T (K)	y_1[a]	selectivity		Error (%)	Ref.
				exp	IAST		
C_2H_6 + CH_4 activated carbon (bench-scale high-pressure open-flow ad(de)sorption)	1397	301.4	0.958	4.97	5.27	6.05	[7]
	2499	301.4	0.511	9.05	8.19	9.47	
			0.733	7.58	7.62	0.54	
			0.958	6.93	7.21	4.12	
C_2H_6 + CH_4 ajax-activated carbon (volumetric; MPSD1)	66.7	303	0.024	19.02	21.41	12.59	[8]
			0.117	14.82	18.91	27.58	
			0.268	13.60	16.53	21.58	
			0.511	11.37	15.37	35.19	
			0.807	21.95	16.10	26.63	
C_2H_6 + CH_4 ajax-activated carbon (volumetric; MPSD2)	66.7	303	0.024	19.02	16.28	14.37	
			0.117	14.82	16.41	10.70	
			0.268	13.60	16.53	21.58	
			0.511	11.37	15.68	37.92	
C_3H_8 + CH_4 ajax-activated carbon (volumetric; MPSD1)	66.7	303	0.026	101.00	175.85	74.12	
			0.107	75.33	99.46	32.03	
			0.377	30.74	61.85	101.22	
			0.759	40.73	34.89	14.33	
C_3H_8 + CH_4 ajax-activated carbon (volumetric; MPSD2)	66.7	303	0.026	101.00	113.49	12.37	
			0.107	75.33	78.92	4.76	
			0.377	30.74	49.27	60.28	
			0.759	40.73	41.87	2.81	
CO_2 + CH_4 ajax-activated carbon (volumetric; MPSD1)	66.7	273	0.039	6.73	3.27	51.46	
			0.190	4.02	3.28	18.42	
			0.391	3.10	3.21	3.39	
			0.619	2.55	3.17	24.07	
			0.801	2.43	3.17	30.25	
			0.870	2.20	3.15	42.95	
		303	0.049	7.14	3.18	55.44	
			0.223	3.87	3.05	21.31	
			0.416	3.41	3.04	11.00	
			0.638	2.83	3.04	7.36	
			0.752	3.05	2.98	2.20	
			0.875	2.63	3.00	14.03	
CO_2 + CH_4 ajax-activated carbon (volumetric; MPSD2)	66.7	273	0.039	6.73	3.34	50.36	
			0.190	4.02	3.38	15.97	
			0.391	3.10	3.52	13.44	
			0.619	2.55	3.70	44.91	

Adsorbate (1) + (2) on adsorbent (measurement; pure gas isotherm modelb)	P (kPa)	T (K)	y_1[a]	selectivity		Error (%)	Ref.
				exp	IAST		
CO_2 + CH_4 ajax-activated carbon (volumetric; MPSD2)	66.7	273	0.801	2.43	3.85	58.34	[8]
			0.870	2.20	3.87	75.68	
		303	0.049	7.14	3.23	54.69	
			0.223	3.87	3.12	19.55	
			0.416	3.41	3.15	7.62	
			0.638	2.83	3.28	16.13	
			0.752	3.05	3.43	12.36	
			0.875	2.63	3.48	32.33	
C_2H_6 + CH_4 Titanosilicate ETS-10 zeolite (volumetric; T)	150	280	0.094	36.70	46.29	26.12	[9]
			0.108	38.40	45.58	18.69	
			0.127	37.19	44.25	18.97	
			0.152	36.37	42.71	17.44	
			0.189	35.08	41.02	16.95	
			0.244	36.12	37.80	4.65	
			0.323	39.82	36.07	9.44	
			0.453	45.24	32.35	28.49	
			0.500	45.23	33.49	25.96	
			0.659	64.16	33.63	47.58	
	500	280	0.055	32.48	38.92	19.85	
			0.066	32.71	37.12	13.50	
			0.081	32.12	35.18	9.51	
			0.105	31.31	33.62	7.38	
			0.140	29.36	31.64	7.76	
			0.196	29.52	29.28	0.81	
			0.283	28.36	26.60	6.21	
			0.419	30.13	23.91	20.65	
			0.500	30.13	24.39	19.05	
			0.639	55.93	20.78	62.84	
	150	325	0.103	27.13	24.85	8.39	
			0.118	26.81	24.61	8.21	
			0.136	26.56	24.14	9.12	
			0.161	26.18	23.45	10.43	
			0.195	27.38	22.78	16.81	
			0.245	26.27	22.34	14.94	
			0.320	26.21	21.25	18.92	
			0.442	27.43	20.24	26.21	
			0.500	27.43	26.06	4.99	
			0.642	27.32	19.07	30.20	

Adsorbate (1) + (2) on adsorbent (measurement; pure gas isotherm modelb)	P (kPa)	T (K)	y_1[a]	selectivity		Error (%)	Ref.
				exp	IAST		
C_2H_4 + CH_4 Titanosilicate ETS-10 zeolite (volumetric; V)	150	280	0.077	227.75	209.31	8.10	[9]
			0.091	202.54	203.54	0.49	
			0.109	181.93	194.46	6.89	
			0.135	171.58	184.73	7.67	
			0.174	143.60	170.53	18.75	
			0.232	129.10	154.15	19.40	
			0.316	118.09	135.53	14.77	
			0.448	174.79	117.05	33.03	
			0.500	27.43	22.38	18.41	
			0.653	265.17	96.22	63.71	
	250	280	280	180.95	198.47	9.68	
			0.072	191.70	191.70	0.00	
			0.090	180.66	180.88	0.12	
			0.116	182.90	161.12	11.90	
			0.153	179.00	148.83	16.85	
			0.210	184.33	130.19	29.37	
			0.298	193.95	112.59	41.95	
			0.431	163.70	96.67	40.95	
			0.500	163.70	95.75	41.51	
			0.648	542.67	83.65	84.58	
	150	325	0.079	122.34	166.43	36.03	
			0.091	126.85	163.75	29.09	
			0.108	122.84	159.80	30.08	
			0.132	119.88	153.12	27.73	
			0.166	109.16	148.91	36.42	
			0.216	100.07	143.51	43.40	
			0.299	87.83	136.48	55.40	
			0.428	72.91	129.09	77.05	
			0.500	72.91	130.99	79.66	
			0.637	62.75	124.56	98.51	
C_2H_4 + C_2H_6 Titanosilicate ETS-10 zeolite (volumetric; U)	150	280	0.140	11.21	9.99	10.85	
			0.161	10.73	10.07	6.06	
			0.187	10.19	10.27	0.79	
			0.220	9.59	10.22	6.61	
			0.266	8.93	10.25	14.73	
			0.328	8.35	10.53	26.09	
			0.416	7.60	10.55	38.92	
			0.500	7.60	10.56	38.95	
			0.541	7.01	10.94	56.12	

Adsorbate (1) + (2) on adsorbent (measurement; pure gas isotherm modelb)	P (kPa)	T (K)	y_1[a]	selectivity		Error (%)	Ref.
				exp	IAST		
C_2H_4 + C_2H_6 Titanosilicate ETS-10 zeolite (volumetric; U)	150	280	0.725	5.84	11.40	95.27	[9]
	250	280	0.102	12.11	10.25	15.37	
			0.142	10.84	10.49	3.21	
			0.280	8.46	10.74	26.87	
			0.497	7.79	11.42	46.56	
			0.500	7.79	11.32	45.31	
			0.696	5.63	11.70	107.85	
	150	325	0.139	7.57	10.93	44.36	
			0.158	7.45	10.94	46.77	
			0.183	7.25	10.84	49.48	
			0.215	7.09	10.74	51.47	
			0.259	6.84	10.75	57.20	
			0.318	6.47	10.72	65.78	
			0.401	6.05	10.83	78.99	
			0.500	5.65	10.61	87.79	
$C_4H_6O_2$ + C_3H_3N activated carbon (dynamic column)	101	313.1	0.282	2.63	3.56	35.58	[10]
			0.442	3.18	3.80	19.41	
			0.591	3.13	4.04	29.37	
			0.722	2.55	4.10	60.90	
			0.880	2.73	4.34	58.90	
CO_2 + CO NaX faujasite (column breakthrough; L)	100	323	0.174	62.00	28.00	54.84	[11]
			0.484	65.00	33.00	49.23	
			0.804	65.00	37.00	43.08	
		373	0.174	51.00	24.00	52.94	
			0.484	42.00	29.00	30.95	
			0.804	34.00	34.00	0.00	
CO_2 + CO NaX faujasite (column breakthrough; T)	100	323	0.174	62.00	31.00	50.00	
			0.484	65.00	28.00	56.92	
			0.804	65.00	26.00	60.00	
		373	0.174	51.00	24.00	52.94	
			0.484	42.00	30.00	28.57	
			0.804	34.00	43.00	26.47	
C_2H_4 + CH_4 activated carbon (static volumetric; L-F)	202.65	293.15	0.220	10.76	17.07	58.58	[12]
			0.294	10.19	16.01	57.14	
			0.530	7.52	14.19	88.65	
			0.578	8.25	13.94	69.04	
		303.15	0.103	13.03	20.27	55.56	
			0.245	12.78	16.20	26.79	
			0.475	15.01	15.19	1.23	

Adsorbate (1) + (2) on adsorbent (measurement; pure gas isotherm modelb)	P (kPa)	T (K)	y_1[a]	selectivity		Error (%)	Ref.
				exp	IAST		
C_2H_4 + CH_4 activated carbon (static volumetric; L-F)	202.65	303.15	0.720	8.99	14.08	56.54	[12]
		313.15	0.114	14.12	16.19	14.67	
			0.228	11.95	14.74	23.32	
			0.373	10.40	13.64	31.14	
			0.630	8.55	11.86	38.76	
	1013.25	293.15	0.193	6.89	14.04	103.84	
			0.383	6.73	14.16	110.38	
			0.480	7.10	13.04	83.82	
		303.15	0.239	6.33	13.80	117.96	
			0.269	6.33	13.75	117.36	
			0.486	6.85	13.74	100.64	
		313.15	0.206	9.33	11.58	24.13	
			0.351	8.89	11.30	27.11	
			0.496	11.39	11.37	0.18	
CO_2 + CH_4 MIL-100(Cr) MOF (volumetric)	100	303	0.250	7.41	34.00	358.86	[13]
			0.500	7.97	18.80	135.83	
			0.750	8.15	12.56	54.01	
	500	303	0.250	6.81	23.17	240.32	
			0.500	6.33	20.00	216.19	
			0.750	6.75	16.67	147.02	
	1000	303	0.250	6.91	20.07	190.53	
			0.500	6.39	17.69	176.99	
			0.750	7.25	16.81	131.89	
C_2H_6S + n-C_7H_{16} NaX (home made manometric apparatus)	0.001	298	0.051	1.16	5.78	398.17	[14]
			0.122	2.39	7.12	197.65	
			0.211	3.89	9.27	138.37	
			0.452	3.60	42.84	1088.57	
			0.661	4.60	64.69	1306.13	
	0.02	298	0.096	0.84	1.68	99.65	
			0.246	0.98	1.80	83.25	
			0.486	1.13	1.86	64.87	
			0.748	1.11	1.95	75.21	
			0.898	1.24	2.16	73.60	
C_2H_6S + C_7H_8 NaX (home made manometric apparatus)	0.001	298	0.170	0.59	1.98	232.37	
			0.209	1.33	2.01	51.06	
			0.251	2.86	2.06	27.94	
			0.251	9.42	2.08	77.96	
			0.530	8.90	2.40	73.05	
	0.02	298	0.106	0.99	1.41	43.30	

Adsorbate (1) + (2) on adsorbent (measurement; pure gas isotherm modelb)	P (kPa)	T (K)	y_1[a]	selectivity		Error (%)	Ref.
				exp	IAST		
$C_2H_6S + C_7H_8$ NaX (home made manometric apparatus)	0.02	298	0.259	0.97	1.44	47.40	[14]
			0.492	0.99	1.46	46.74	
			0.762	1.00	1.47	48.04	
			0.910	1.01	1.55	53.22	
$C_2H_6 + CH_4$ templated carbon (fixed bed; S)	101	273	0.188	8.41	8.83	4.95	[15]
			0.391	8.75	8.88	1.45	
			0.587	9.49	9.11	3.99	
$CO_2 + CH_4$ MIL-53 (Al)	100	303.15	0.102	7.50	7.85	4.72	[16]
			0.252	6.06	6.67	9.94	
			0.499	5.60	5.94	6.09	
			0.759	4.57	5.35	16.92	
			0.902	4.58	4.51	1.43	
	400	303.15	0.102	6.37	6.69	4.95	
			0.252	6.09	6.36	4.48	
			0.371	5.88	6.32	7.37	
			0.506	5.79	6.31	9.06	
			0.616	5.48	6.53	19.11	
			0.746	6.09	6.69	9.94	
			0.902	5.64	6.39	13.18	
$C_3H_6 + C_3H_8$ NaX (desorption)	0.858	318	0.500	5.15	17.25	234.68	[17]
	1.359		0.500	5.37	17.25	221.40	
	2.696		0.500	5.82	17.44	199.72	
	5.348		0.500	6.12	17.64	188.11	
	26.647		0.500	7.05	18.03	155.67	
	53.482		0.500	5.64	18.23	223.01	
	0.858	358	0.500	4.47	11.56	158.38	
	1.359		0.500	4.47	11.56	158.38	
	2.696		0.500	4.47	11.69	161.27	
	5.348		0.500	4.47	11.82	164.19	
	26.647		0.500	4.47	11.95	167.14	
	53.482		0.500	4.47	12.08	170.13	
	0.858	408	0.500	4.34	8.19	88.66	
	1.359		0.500	4.47	8.19	83.02	
	2.696		0.500	4.61	8.09	75.58	
	5.348		0.500	3.96	8.19	106.65	
	26.647		0.500	3.30	8.28	150.72	
	53.482		0.500	2.34	8.37	257.66	

Adsorbate (1) + (2) on adsorbent (measurement; pure gas isotherm modelb)	P (kPa)	T (K)	y_1[a]	selectivity		Error (%)	Ref.
				exp	IAST		
C_3H_6 + C_3H_8 NaX (breakthrough)	0.858	318	0.500	3.24	17.25	433.12	[17]
	1.359		0.500	3.96	17.25	335.42	
	5.348		0.500	5.21	17.64	238.76	
	26.334		0.500	5.05	18.03	257.06	
	0.858	358	0.500	3.77	11.56	206.89	
	1.359		0.500	3.01	11.56	283.43	
	2.696		0.500	4.08	11.69	186.18	
	5.348		0.500	3.47	11.82	240.25	
	26.647		0.500	4.17	11.95	186.76	
	0.858	408	0.500	2.27	8.19	260.58	
	1.359		0.500	2.27	8.19	260.58	
	2.696		0.500	2.22	8.09	263.88	
	5.348		0.500	1.99	8.19	311.28	
	26.647		0.500	2.46	8.28	236.25	
CH_4 + N_2 novel copper-based 1,2,4-triazolyl isophthalate MOF (gravimetric method and applying the van Ness method; T)	500	273	0.177	4.39	4.81	9.72	[18]
			0.544	5.36	5.05	5.71	
			0.761	4.51	4.93	9.41	
	500	298	0.088	4.54	4.25	6.27	
			0.174	3.59	4.25	18.32	
			0.342	3.90	4.32	10.96	
			0.544	4.73	4.36	7.89	
			0.762	4.70	4.43	5.68	
			0.872	3.61	4.47	23.65	
	500	323	0.174	4.58	3.85	15.95	
			0.341	4.25	3.91	7.95	
			0.543	4.58	3.89	15.01	
			0.760	3.89	3.89	0.00	
			0.871	8.32	3.77	54.67	
CH_4 + N_2 MOF Basolite A100 (gravimetric method and applying the van Ness method; T)	500	273	0.533	3.84	4.69	22.01	
			0.752	4.08	4.57	12.05	
			0.867	4.90	3.86	21.18	
	500	298	0.085	3.20	4.07	27.37	
			0.535	3.66	4.11	12.20	
			0.755	3.18	4.11	29.21	
			0.867	2.93	4.13	40.85	
	500	323	0.533	3.12	3.57	14.57	
			0.753	4.20	3.37	19.82	
			0.868	3.62	3.02	16.65	

Adsorbate (1) + (2) on adsorbent (measurement; pure gas isotherm modelb)	P (kPa)	T (K)	y_1[a]	selectivity		Error (%)	Ref.
				exp	IAST		
$CO_2 + N_2$ activated carbon (gravimetric; S)	2000	298.1	0.106	10.46	13.27	26.93	[19]
			0.287	11.01	14.28	29.65	
			0.572	14.35	15.94	11.10	
	3000	298.1	0.113	11.19	13.69	22.36	
			0.311	12.38	15.90	28.49	
			0.613	11.85	19.20	62.05	
	6000	298.1	0.146	10.85	16.55	52.51	
			0.373	12.18	22.11	81.54	
			0.677	11.65	30.16	158.95	
$CO_2 + H_2$ activated carbon (gravimetric; S)	2000	298.1	0.072	26.36	97.44	269.69	
			0.243	27.60	88.56	220.85	
			0.551	26.80	93.55	249.12	
	3000	298.1	0.081	33.63	89.73	166.85	
			0.084	26.79	90.54	237.91	
			0.289	26.41	91.03	244.68	
			0.588	52.47	98.80	88.28	
	8000	298.1	0.123	23.34	92.17	294.84	
			0.370	17.66	115.36	553.34	
			0.683	60.47	148.99	146.38	
$CO_2 + CH_4$ activated carbon (volumetric; T)	100	293	0.297	4.96	3.98	19.87	[20]
			0.475	8.68	5.28	39.19	
			0.671	6.51	9.09	39.48	
	250	293	0.194	4.54	3.52	22.37	
			0.485	4.33	3.92	9.41	
			0.782	4.53	7.32	61.61	
	500	293	0.181	4.28	3.61	15.58	
			0.352	4.10	3.75	8.49	
			0.777	4.93	3.77	23.50	
	1000	293	0.153	4.24	3.69	13.06	
			0.355	5.23	4.05	22.53	
			0.768	4.82	4.46	7.38	
$CH_4 + N_2$ zeolite 5A (static volumetric; S)	300	303	0.271	1.55	1.83	17.54	[21]
			0.484	1.89	1.87	0.75	
			0.712	1.82	1.83	0.50	
			0.892	1.81	1.90	4.98	
	500	303	0.272	1.65	1.88	13.62	
			0.486	1.94	1.90	2.45	
			0.714	1.82	1.87	2.34	
			0.893	1.83	2.00	9.22	

Adsorbate (1) + (2) on adsorbent (measurement; pure gas isotherm modelb)	P (kPa)	T (K)	y_1[a]	selectivity		Error (%)	Ref.
				exp	IAST		
$CH_4 + N_2$ zeolite 5A (static volumetric; S)	700	303	0.272	1.67	1.93	15.91	[21]
			0.487	1.95	1.96	0.26	
			0.714	1.97	1.96	0.49	
			0.893	1.92	1.97	2.78	
	103.9	323	0.884	1.61	1.61	0.42	
	301.8		0.884	1.67	1.72	2.97	
	498.1		0.884	1.70	1.76	3.47	
	705.3		0.884	1.76	1.79	2.06	
$N_2 + O_2$ LiLSX zeolite (volumetric; T)	25	298.1	0.060	5.84	6.38	9.40	[22]
			0.134	7.73	9.30	20.31	
			0.307	11.92	12.06	1.21	
			0.461	14.36	13.80	3.88	
			0.627	20.20	20.82	3.06	
			0.803	22.89	17.49	23.59	
			0.891	21.93	14.71	32.91	
	100	298.1	0.045	4.49	8.59	91.29	
			0.106	6.10	9.59	57.17	
			0.161	6.67	9.72	45.63	
			0.228	7.87	10.12	28.67	
			0.287	9.49	10.30	8.59	
			0.337	10.13	10.16	0.32	
			0.396	10.55	10.10	4.24	
			0.513	11.99	10.00	16.56	
			0.643	14.08	10.03	28.78	
			0.721	14.90	10.01	32.83	
			0.815	20.63	10.41	49.51	
	25	348.1	0.060	6.38	7.75	21.38	
			0.105	6.86	8.45	23.09	
			0.149	7.20	8.60	19.43	
			0.399	13.48	16.66	23.56	
			0.633	29.53	34.43	16.60	
			0.792	39.76	41.87	5.31	
	100	348.1	0.018	3.62	6.06	67.42	
			0.172	4.33	6.11	41.01	
			0.298	4.95	6.70	35.28	
			0.420	5.44	6.45	18.44	
			0.515	6.07	5.68	6.43	
			0.613	6.49	5.00	23.07	
			0.728	7.10	4.42	37.70	

Adsorbate (1) + (2) on adsorbent (measurement; pure gas isotherm modelb)	P (kPa)	T (K)	y_1[a]	selectivity		Error (%)	Ref.
				exp	IAST		
N_2 + O_2 LiLSX zeolite (volumetric; T)	100	348.1	0.795	7.98	4.27	46.55	[22]
			0.918	9.66	6.89	28.73	
			0.965	24.61	18.64	24.26	
CO_2 + CH_4 zeolite Na-ZSM-5 (in Situ ATR-FTIR spectroscopy; L)	101.3	308.1	0.030	20.30	19.60	3.46	[23]
			0.100	16.17	18.47	14.24	
			0.150	15.26	18.17	19.02	
			0.200	14.66	17.94	22.36	
			0.350	14.51	17.79	22.59	
			0.500	15.41	17.94	16.39	
			0.650	16.92	18.17	7.38	
			0.800	21.95	18.39	16.23	
			0.850	23.23	18.47	20.51	
			0.900	31.05	18.54	40.29	
	101.3	323.1	0.030	18.50	18.39	0.56	
			0.100	14.59	17.41	19.37	
			0.150	14.44	17.04	18.00	
			0.200	13.53	16.73	23.64	
			0.350	13.53	16.36	20.86	
			0.500	13.38	16.06	19.96	
			0.650	13.68	16.06	17.33	
			0.800	17.37	16.06	7.56	
			0.850	20.83	16.06	22.91	
			0.900	24.44	16.13	33.99	
	101.3	358.1	0.030	15.04	17.64	17.29	
			0.100	12.71	15.68	23.39	
			0.150	12.26	14.70	19.93	
			0.200	11.95	13.94	16.64	
			0.350	12.71	12.59	0.94	
			0.500	13.46	11.91	11.51	
			0.650	18.72	11.46	38.80	
	101.3	393.1	0.030	8.20	6.71	18.14	
			0.100	7.29	6.71	8.02	
			0.150	6.77	6.71	0.86	
			0.200	6.99	6.63	5.14	
			0.350	7.67	6.63	13.51	
			0.500	8.20	6.63	19.06	
			0.650	10.55	6.63	37.14	

Adsorbate (1) + (2) on adsorbent (measurement; pure gas isotherm modelb)	P (kPa)	T (K)	y_1[a]	selectivity		Error (%)	Ref.
				exp	IAST		
CO_2 + CH_4 activated carbon (manometric device combined with a gas chromatograph; F)	340	303.15	0.398	2.30	2.88	25.40	[24]
	680		0.430	2.55	2.96	16.17	
	980		0.451	2.66	2.98	12.07	
	1290		0.465	2.69	3.01	12.08	
	1620		0.475	2.66	2.92	9.82	
	1910		0.481	2.66	2.89	8.74	
	2130		0.485	2.67	2.90	8.53	
	2390		0.488	2.67	2.94	10.11	
	510	323.15	0.422	1.88	2.41	27.92	
	800		0.451	2.05	2.30	12.06	
	1270		0.468	2.07	2.21	7.23	
	1630		0.478	2.07	2.17	4.59	
	1860		0.485	2.09	2.14	2.56	
	2060		0.489	2.14	2.13	0.36	
	2220		0.490	2.20	2.11	3.86	
	2560		0.490	2.22	2.09	5.64	
	600	353.15	0.440	1.62	2.31	42.20	
	930		0.467	1.72	2.23	29.74	
	1250		0.478	1.81	2.18	20.83	
	1470		0.486	1.84	2.14	16.28	
	1880		0.488	1.89	2.10	10.91	
	2230		0.488	2.04	2.08	2.27	
	2510		0.490	2.16	2.06	4.80	
CH_3OH + C_6H_{14} MOF Basolite C300	2.7	313	0.500	3.96	9.40	137.69	[25]
	4.2		0.500	3.09	16.34	428.93	
	7.3		0.500	3.72	35.21	846.65	
	11.3		0.500	4.08	73.56	1702.69	
N_2 + O_2 LiLSX (column dynamic)	101.3	273.1	0.300	8.30	10.91	31.45	[26]
			0.400	8.80	10.69	21.48	
			0.500	8.84	10.49	18.67	
			0.600	8.12	10.30	26.85	
			0.700	7.94	10.12	27.46	
			0.800	7.63	9.96	30.54	
		303.1	0.300	6.29	7.15	13.67	
			0.400	6.52	7.09	8.74	
			0.500	6.29	7.04	11.92	
			0.600	6.34	6.98	10.09	
			0.700	6.52	6.93	6.29	
		338.1	0.300	4.27	4.64	8.67	

Adsorbate (1) + (2) on adsorbent (measurement; pure gas isotherm modelb)	P (kPa)	T (K)	y_1[a]	selectivity		Error (%)	Ref.
				exp	IAST		
$N_2 + O_2$ LiLSX (column dynamic)	101.3	338.1	0.400	4.32	4.62	6.94	[26]
			0.500	4.16	4.61	10.82	
			0.600	4.86	4.59	5.56	
			0.700	4.58	4.58	0.00	
	607.8	273.1	0.300	5.83	9.19	57.63	
			0.400	5.74	9.05	57.67	
			0.500	5.52	8.96	62.32	
			0.600	5.13	8.90	73.49	
			0.700	4.85	8.86	82.68	
			0.800	4.66	8.85	89.91	
		303.1	0.500	4.74	6.26	32.07	
			0.600	4.58	6.20	35.37	
			0.700	4.37	6.15	40.73	
			0.800	4.50	6.10	35.56	
			0.900	4.24	6.06	42.92	
		338.1	0.200	4.20	4.40	4.76	
			0.400	4.22	4.33	2.61	
			0.600	4.17	4.28	2.64	
			0.800	3.91	4.24	8.44	
$CO_2 + N_2$ zeolite ZSM-5 (gravimetric; S)	120	298.1	0.134	23.34	29.26	25.38	[27]
			0.360	16.57	25.24	52.33	
			0.644	26.29	25.97	1.22	
	300	298.1	0.162	21.79	26.78	22.90	
			0.409	16.00	25.57	59.82	
			0.691	24.75	31.37	26.73	
	1000	298.1	0.202	26.17	25.42	2.87	
			0.458	27.20	27.89	2.51	
			0.727	30.81	34.34	11.46	
	120	318.1	0.157	21.79	22.71	4.21	
			0.391	16.33	22.45	37.51	
			0.672	18.23	17.08	6.33	
	300	318.1	0.181	18.27	20.17	10.40	
			0.426	15.28	21.55	41.09	
			0.701	20.21	19.10	5.50	
	1000	318.1	0.209	21.55	20.45	5.07	
			0.463	15.35	20.30	32.26	
			0.729	27.82	23.98	13.80	

Adsorbate (1) + (2) on adsorbent (measurement; pure gas isotherm modelb)	P (kPa)	T (K)	y_1[a]	selectivity		Error (%)	Ref.
				exp	IAST		
CH_4 + N_2 zeolite 13X (volumetric; T)	100	303	0.466	1.86	1.95	4.58	[28]
	300		0.466	2.03	2.12	4.32	
	700		0.466	2.22	2.28	2.72	
	500	303	0.301	2.04	2.19	7.59	
			0.465	2.19	2.16	1.03	
			0.832	2.15	2.17	0.60	
			0.886	2.17	2.18	0.77	
			0.939	2.17	2.39	10.13	
	100	323	0.301	1.95	1.93	1.12	
	300		0.301	2.08	2.04	1.78	
	500		0.301	2.10	2.12	1.16	
	700		0.301	2.20	2.18	1.03	
CO_2 + N_2 MOF Cu-BTC (gravimetric and volumetric; L)	41.451	308.1	0.101	96.54	32.64	66.19	[29]
	72.841		0.084	91.52	39.65	56.67	
	96.43		0.101	85.81	31.61	63.16	
	123.432		0.108	55.28	30.68	44.51	
	148.3		0.115	42.63	28.22	33.80	
	173.474		0.120	39.19	26.79	31.65	
	200.842		0.142	30.29	22.01	27.34	
	248.934		0.138	30.26	23.19	23.37	
	299.099		0.144	26.41	22.08	16.40	
	46.545	308.1	0.165	51.31	33.09	35.52	
	62.871		0.366	15.98	11.62	27.31	
	97.168		0.202	24.85	27.02	8.74	
	122.937		0.225	26.96	22.60	16.14	
	147.5		0.203	26.54	26.32	0.83	
	175.537		0.233	18.94	23.70	25.13	
	200.648		0.235	23.02	23.29	1.17	
	248.25		0.232	23.61	23.86	1.04	
	298.96		0.236	23.02	23.18	0.71	
CO_2 + CH_4 MOF Cu-BTC (gravimetric and volumetric; L)	39.494	308.1	0.138	18.80	7.43	60.49	
	71.898		0.108	13.07	10.04	23.19	
	96.125		0.122	9.04	8.64	4.50	
	120.229		0.122	9.07	8.73	3.70	
	144.307		0.125	8.34	8.43	1.16	
	172.775		0.123	7.99	8.58	7.34	
	199.963		0.143	7.02	7.22	2.87	
	248.912		0.142	7.45	7.31	1.96	
	299.508		0.146	6.66	7.13	6.92	

Adsorbate (1) + (2) on adsorbent (measurement; pure gas isotherm modelb)	P (kPa)	T (K)	y_1[a]	selectivity		Error (%)	Ref.
				exp	IAST		
CO_2 + CH_4 MOF Cu-BTC (gravimetric and volumetric; L)	45.772	308.1	0.206	12.13	8.92	26.48	[29]
	66.619		0.203	9.48	8.98	5.27	
	96.305		0.230	9.49	7.57	20.28	
	122.881		0.249	6.99	6.84	2.25	
	146.958		0.242	7.83	7.20	8.11	
	172.558		0.252	6.54	6.87	4.98	
	196.757		0.250	6.25	6.96	11.45	
	249.177		0.239	6.58	7.43	12.99	
	299.524		0.241	6.38	7.41	16.18	
a: gas phase mole fraction b: MPSD: micro-pore-size distribution; F: Freundlich; L: Langmuir; T: Toth; V: Virial; U: Unilan; L-F: Langmuir-Freundlich; S: Sips							

Table D 2. Comparison of ternary gas mixtures adsorption selectivity experimental and prediction data

Adsorbate (1) + (2) + (3) on adsorbent at given conditions (measurement; pure gas isotherm model)	Gas phase molecular fraction		Selectivity			Ref.
			S_{12}			
	y_1	y_2	exp	IAST	Error (%)	
$C_2H_4 + C_2H_6 + CH_4$ ETS-10 P = 200 kPa, T = 300 K (volumetric; Toth)	0.494	0.147	5.48	13.99	155.05	[9]
	0.331	0.094	5.44	13.66	150.95	
	0.231	0.062	5.41	13.34	146.38	
	0.166	0.042	5.43	13.15	142.15	
	0.123	0.030	5.57	12.98	133.09	
	0.096	0.022	5.62	12.88	128.98	
	0.076	0.017	5.91	12.81	116.89	
	0.063	0.013	5.94	12.74	114.48	
	0.054	0.010	5.67	12.70	124.05	
			S_{23}			
	y_2	y_3	exp	IAST	Error (%)	
	0.147	0.359	13.84	8.15	41.08	
	0.094	0.575	24.98	9.24	62.99	
	0.062	0.707	20.17	10.28	49.02	
	0.042	0.792	23.85	11.31	52.56	
	0.030	0.847	24.03	12.31	48.77	
	0.022	0.882	26.97	13.15	51.23	
	0.017	0.907	26.68	13.94	47.73	
	0.013	0.924	28.62	14.65	48.80	
	0.010	0.936	32.70	15.22	53.47	
			S_{12}			
	y_1	y_2	exp	IAST	Error (%)	
$C_2H_4 + CH_4 + H_2$ activated carbon P = 1013 kPa, T = 303.15 K (static volumetric; Langmuir-Freundlich)	0.029	0.817	10.92	16.13	47.70	[12]
	0.039	0.610	20.88	16.91	19.02	
	0.043	0.134	6.65	17.47	162.78	
	0.055	0.654	10.17	15.32	50.69	
	0.063	0.603	10.49	15.34	46.20	
	0.086	0.272	8.54	15.44	80.76	
	0.087	0.580	19.81	15.34	22.57	
	0.088	0.447	10.23	14.99	46.60	
	0.114	0.286	10.02	14.77	47.41	

Adsorbate (1) + (2) + (3) on adsorbent at given conditions (measurement; pure gas isotherm model)	Gas phase molecular fraction		Selectivity			Ref.
	y_1	y_2	S_{12}		Error (%)	
			exp	IAST		
$C_2H_4 + CH_4 + H_2$ activated carbon P = 1013 kPa, T = 303.15 K (static volumetric; Langmuir-Freundlich)	0.129	0.407	8.47	14.45	70.46	[12]
	0.133	0.161	11.65	14.42	23.78	
	0.139	0.128	16.33	15.55	4.76	
	0.163	0.514	7.82	14.23	82.04	
	0.210	0.660	7.12	13.92	95.61	
	0.210	0.502	15.35	13.99	8.87	
	0.272	0.462	13.04	13.85	6.16	
	0.468	0.338	11.04	13.79	24.91	
	0.693	0.195	6.42	13.29	107.24	
	0.777	0.142	4.56	14.12	209.60	

Reference :

1. Buss, E. Gravimetric measurement of binary gas-adsorption equilibria of methane-carbon dioxide mixtures on activated carbon. *Gas Sep. Purif.* **1995,** *9*, 189-197.
2. Buss, E.; Heuchel, M. Adsorption equilibria of methane and tetrafluoromethane and their binary mixtures on silicalite. *J. Chem. Soc., Faraday Trans.* **1997,** *93*, 1621-1628.
3. Heuchel, M.; Snurr, R. Q.; Buss, E. Adsorption of CH4-CF4 mixtures in silicalite: Simulation, experiment, and theory. *Langmuir* **1997,** *13*, 6795-6804.
4. Qiao, S. Z.; Wang, K.; Hu, X. J. Using local IAST with micropore size distribution to predict multicomponent adsorption equilibrium of gases in activated carbon. *Langmuir* **2000,** *16*, 1292-1298.
5. Harlick, P. J. E.; Tezel, F. H. Adsorption of carbon dioxide, methane and nitrogen: pure and binary mixture adsorption for ZSM-5 with SiO2/Al2O3 ratio of 280. *Sep. Purif. Technol.* **2003,** *33*, 199-210.
6. Monneyron, P.; Manero, M. H.; Foussard, J. N. Measurement and modeling of single- and multi-component adsorption equilibria of VOC on high-silica zeolites. *Environ. Sci. Technol.* **2003,** *37*, 2410-2414.
7. He, Y. F.; Yun, J. H.; Seaton, N. A. Adsorption equilibrium of binary methane/ethane mixtures in BPL activated carbon: Isotherms and calorimetric heats of adsorption. *Langmuir* **2004,** *20*, 6668-6678.
8. Qiao, S. Z.; Hu, X. J. Effect of pore size distribution shape on the prediction of binary adsorption equilibrium and kinetics of gases in activated carbon. *Sep. Purif. Technol.* **2004,** *34*, 177-189.
9. Al-Baghli, N. A.; Loughlin, K. F. Binary and ternary adsorption of methane, ethane, and ethylene on titanosilicate ETS-10 zeolite. *J. Chem. Eng. Data* **2006,** *51*, 248-254.
10. Wang, F.; Li, J.; Wang, J.; Gao, H. Adsorption of acrylonitrile and methyl acrylate on activated carbon in a packed bed column. *Adsorption* **2006,** *12*, 205-212.
11. Belmabkhout, Y.; Pirngruber, G.; Jolimaitre, E.; Methivier, A. A complete experimental approach for synthesis gas separation studies using static gravimetric and column breakthrough experiments. *Adsorption* **2007,** *13*, 341-349.
12. Jeong, B.-M.; Ahn, E.-S.; Yun, J.-H.; Lee, C.-H.; Choi, D.-K. Ternary adsorption equilibrium of H-2/CH4/C2H4 onto activated carbon. *Sep. Purif. Technol.* **2007,** *55*, 335-342.
13. Hamon, L.; Heymans, N.; Llewellyn, P. L.; Guillerm, V.; Ghoufi, A.; Vaesen, S.; Maurin, G.; Serre, C.; De Weireld, G.; Pirngruber, G. D. Separation of CO2-

CH4 mixtures in the mesoporous MIL-100(Cr) MOF: experimental and modelling approaches. *J. Chem. Soc., Dalton Trans.* **2012,** *41*, 4052-4059.

14. Bellat, J. P.; Benoit, F.; Weber, G.; Paulin, C.; Mougin, P.; Thomas, M. Adsorption equilibria of binary ethylmercaptan/hydrocarbon mixtures on a NaX zeolite. *Adsorption* **2008,** *14*, 501-507.
15. Chen, J.; Loo, L. S.; Wang, K. An Ideal Absorbed Solution Theory (IAST) Study of Adsorption Equilibria of Binary Mixtures of Methane and Ethane on a Templated Carbon. *J. Chem. Eng. Data* **2011,** *56*, 1209-1212.
16. Heymans, N.; Vaesen, S.; De Weireld, G. A complete procedure for acidic gas separation by adsorption on MIL-53 (Al). *Microporous Mesoporous Mater*. **2012,** *154*, 93-99.
17. van Miltenburg, A.; Gascon, J.; Zhu, W.; Kapteijn, F.; Moulijn, J. A. Propylene/propane mixture adsorption on faujasite sorbents. *Adsorption* **2008,** *14*, 309-321.
18. Moellmer, J.; Lange, M.; Moeller, A.; Patzschke, C.; Stein, K.; Laessig, D.; Lincke, J.; Glaeser, R.; Krautscheid, H.; Staudt, R. Pure and mixed gas adsorption of CH4 and N-2 on the metal-organic framework Basolite (R) A100 and a novel copper-based 1,2,4-triazolyl isophthalate MOF. *J. Mater. Chem.* **2012,** *22*, 10274-10286.
19. Schell, J.; Casas, N.; Pini, R.; Mazzotti, M. Pure and binary adsorption of CO2, H-2, and N-2 on activated carbon. *Adsorption***2012,** *18*, 49-65.
20. Rios, R. B.; Stragliotto, F. M.; Peixoto, H. R.; Torres, A. E. B.; Bastos-Neto, M.; Azevedo, D. C. S.; Cavalcante, C. L. Studies on the Adsorption Behavior of Co2-Ch4 Mixtures Using Activated Carbon. *Braz. J. Chem. Eng.* **2013,** *30*, 939-951.
21. Bakhtyari, A.; Mofarahi, M. Pure and Binary Adsorption Equilibria of Methane and Nitrogen on Zeolite 5A. *J.Chem.Eng. Data* **2014,** *59*, 626-639.
22. Mitchell, L. A.; LeVan, M. D. Development of Adsorption Equilibrium Relations for Mixtures from Pure Component Isotherms and Henry's Law Behavior with Components in Excess. *Ind. Eng. Chem. Res.* **2014,** *53*, 15531-15537.
23. Ohlin, L.; Grahn, M. Detailed Investigation of the Binary Adsorption of Carbon Dioxide and Methane in Zeolite Na-ZSM-5 Studied Using in Situ ATR-FTIR Spectroscopy. *J. Phys. Chem. C* **2014,** *118*, 6207-6213.
24. Pino, D.; Plantier, F.; Bessieres, D. Experimental determination of the adsorption isotherms in gas mixtures under extended pressure and temperature range. *J. Therm. Anal. Calorim.* **2014,** *117*, 1469-1477.
25. Van Assche, T. R. C.; Duerinck, T.; Van der Perre, S.; Baron, G. V.; Denayer, J. F. M. Prediction of Molecular Separation of Polar-Apolar Mixtures on

Heterogeneous Metal-Organic Frameworks: HKUST-1. *Langmuir* **2014,** *30*, 7878-7883.

26. Wu, C.-W.; Kothare, M. V.; Sircar, S. Model Analysis of Equilibrium Adsorption Isotherms of Pure N2, O2, and Their Binary Mixtures on LiLSX Zeolite. *Ind. Eng. Chem. Res.* **2014,** *53*, 12428-12434.
27. Hefti, M.; Marx, D.; Joss, L.; Mazzotti, M. Adsorption equilibrium of binary mixtures of carbon dioxide and nitrogen on zeolites ZSM-5 and 13X. *Microporous Mesoporous Mater.* **2015,** *215*, 215-228.
28. Mofarahi, M.; Bakhtyari, A. Experimental Investigation and Thermodynamic Modeling of CH4/N2 Adsorption on Zeolite 13X. *J. Chem. Eng. Data* **2015,** *60*, 683-696.
29. Yang, Y.; Sitprasert, C.; Rufford, T. E.; Ge, L.; Shukla, P.; Wang, S.; Rudolph, V.; Zhu, Z. An experimental and simulation study of binary adsorption in metal-organic frameworks. *Sep. Purif. Technol.* **2015,** *146*, 136-142.

Appendix E : Experimental apparatus, measurement protocol and data processing for a RPSA process for bulk N_2 – He separation

The experimental PSA process performance data is generated by using a novel RPSA unit built at Lehigh University. The PSA process consists of (a) adsorber pressurization using feed gas to adsorption pressure (P_A), (b) adsorption of N_2 from feed air to produce ~ 99.5% He enriched product gas at ~ P_A, a part of whiche is withdrawn as the product gas, (c) counter-current adsorber depressurization (blowdown) to lowest desorption pressure P_D, (d) counter current adsorber purge at ~ P_D with a part of the product gas from step (b). Effluent gases from steps (c) and (d) were wasted.

Figure E 1 is a schematic drawing of the experimental set-up.[1] This unit consists of a single adsorbent column (I.D = 0.0498 m, Length = 0.127 m) surrounded by a coaxial gas storage space (volume = 1.54 sl) that is used to store the He enriched effluent gas from step (b). A part of storage gas is withdrawn continuously as the product gas through a separate port. The column is packed with a screened sample of commercial, pelletized LiLSX zeolite (particle diameter = 200 – 400 μm, bulk density = 0.61 g/cm^3, weight = 145.82 g, obtained from Arkema Inc) after thermal regeneration at 350 ℃ under dry N_2 flow. The helium void fraction in the column was 0.71 cm^3/ cm^3.

The figures also show the locations of different valves [four two-way 1/2 in. solenoid (C_V = 4), and one check], mass flow meters and controllers, pressure sensors, controller,

and gauges. The transient adsorbent temperature was measured using a 1/16 in. exposed-tip thermocouple located at the center point inside the adsorber.

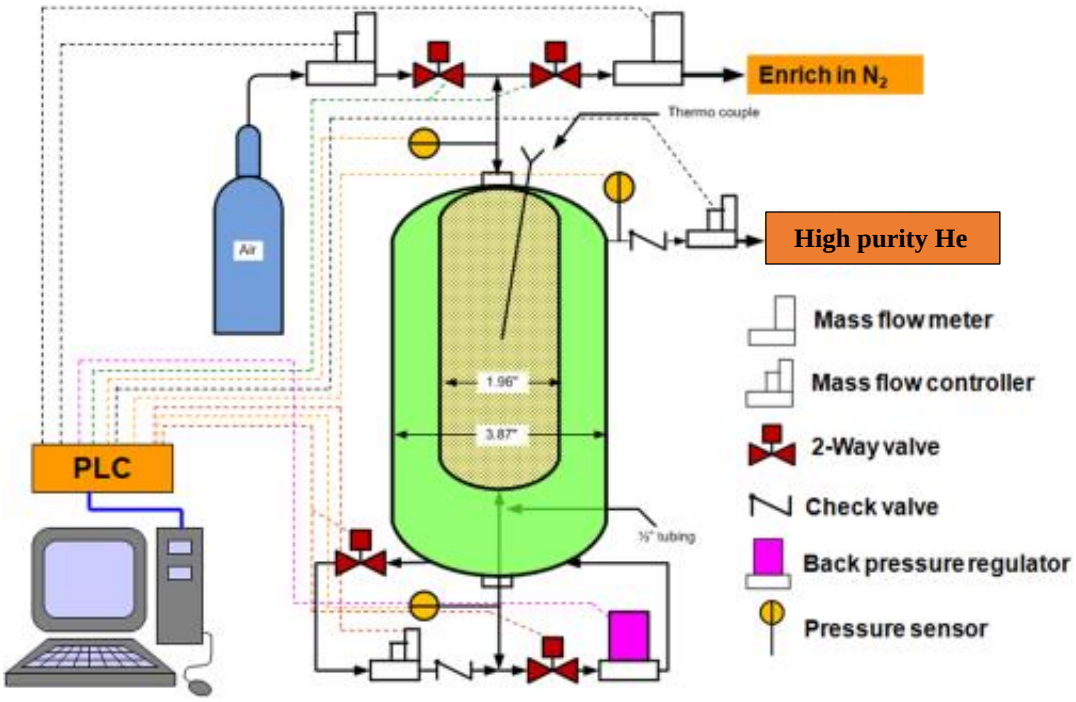

Figure E 1. Schematic drawing of the experimental set-up.[1]

The effluent gas composition was continuously monitored using a thermal conductivity analyzer (manufactured by Gowmac Corporation). A PLC (Eaton Corp) was used for cycle times setting and process control. A data acquisition system (OMB-DAQ-3000 Series, manufactured by OMAGA) was used for continuously for data measurement, collection, and storage in an integrated computer. The pressure of the gas storage tank cyclically increased and decreased during RPSA cycle but always maintaining a super-ambient pressure level in the tank.

Cyclic steady state runs were carried out using different total cycle times (t_c) in the range of 6 ~ 24 seconds at a feed mixture (50% N_2 + 50% He) pressures of 4 atm. The apparatus

is kept at ambient temperature (~ 21℃). The RPSA cycle was operated between P_A~4 atm and P_D ~ 1 atm. A continuous product stream was withdrawn at given rate. The molar flow rate per cycle of feed mixture is fixed at different total cycle times. Different purge flow rate and product flow rate are tested to obtain 99.5% helium in product gas. A cyclic steady state operation was achieved within 150 cycles.

Figure E 2 is a block diagram depicting the overall performance of a generic PSA gas separation system producing 99.5% He-enriched product gas. The total amount of zeolite adsorbent in the system is w (kg) and the total cycle time of the PSA process is t_c (seconds). The variables F, P and W are, respectively, the amounts (moles) of mixture feed, He-enriched product gas, and N_2-rich waste gas from the system per cycle of operation.

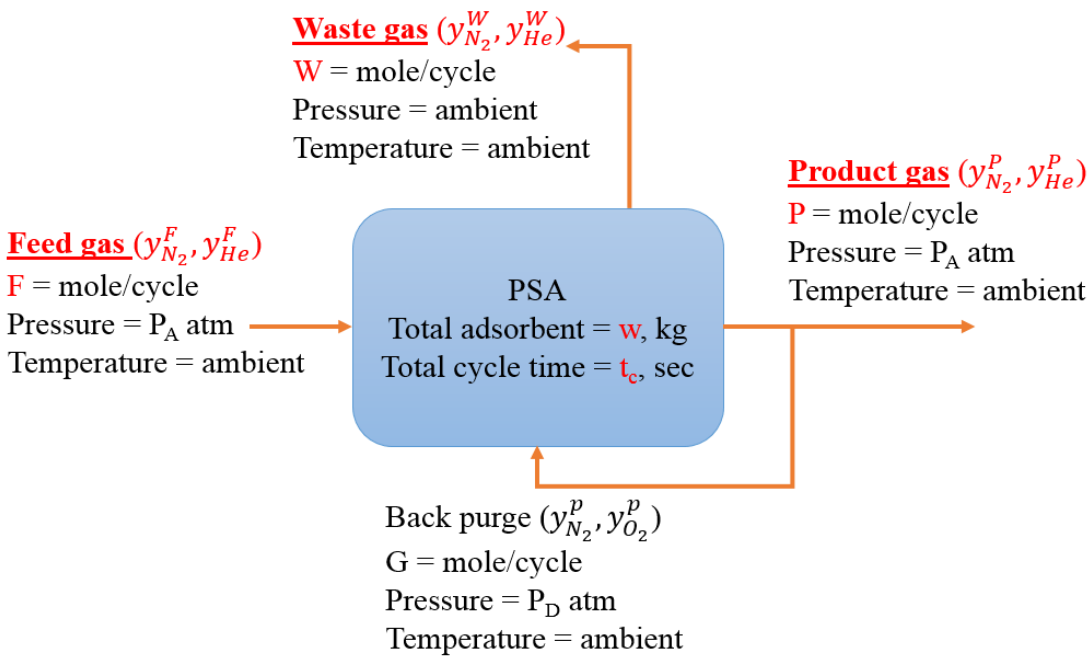

Figure E 2. Block diagram of a generic PSA gas separation system

According to Figure E 2, the overall mass balance, N_2 mass balance, BSF, and recovery of helium can be written as:

$$overall\ mass\ balance: F = P + W \tag{6-2}$$

$$N_2\ mass\ balance: Fy_{N_2}^{F} = Py_{N_2}^{P} + Wy_{N_2}^{W} \tag{6-3}$$

$$bed\ size\ factor\ (BSF, \frac{kg\ of\ adsorbent}{kg\ \text{of}\ helium/_{hr}}) = (6.94 \times 10^{-5}) \times \frac{wt_c}{Py_{He}^{P}} \tag{6-4}$$

$$Helium\ recovery\ from\ mixture\ feed\ (R_{He}) = \frac{Py_{He}^{P}}{Fy_{He}^{F}} \tag{6-5}$$

The results of experimental performances at various total cycle time are shown in Table E 1.

Table E 1. Results of experimental performances. Individual step times: t_p = pressurization, t_{ad} = adsorption, t_{bd} = blow down, t_{pu} = back purge, P/F = molar ratio of back purge to feed gas quantities per cycle.

Adsorbent weight: 145.82g, P_A=4bar, P_D=1bar									
Cycle times				Mass balance deviation	Molar P/F ratio	Total feed (moles/cycle)	BSF	RHe	Purity
tp	tad	tbd	tpu						
0.5	2	2.5	1	2.69	0.34	0.123	2.55	38.86	99.59
1	4	5	2	4.89	0.27	0.145	4.26	39.42	99.57
2	8	10	4	6.67	0.24	0.149	8.81	36.97	99.62
Units: cycle times (sec); mass balance deviation, RHe and purity (%); total feed (moles/cycle); BSF (kg/kg/hr)									

Reference:

1. Rao, V. R.; Kothare, M. V.; Sircar, S. Novel design and performance of a medical oxygen concentrator using a rapid pressure swing adsorption concept. *AlChE J.* **2014,** *60*, 3330.

Biography

Chin-Wen Wu received her Ph. D. degree in Chemical and Biomolecular Engineering from Lehigh University (Jan 2017) under the mentorship of Prof. Mayuresh V. Kothare and Prof. Shivaji Sircar. Her doctoral thesis focused on study of thermodynamic and dynamic properties of heterogeneous LiLSX zeolite for use in a medical oxygen concentrator. Prior to enrolling at Lehigh, she worked for 4 years as research assistant in National Synchrotron Radiation Research Center on the area of X-ray crystallography and biochemistry. She holds a master's degree in college of life science and a B. A. in chemical engineering from National Tsing Hua University in Taiwan.

The main publication during her doctoral pursuit are (1) Equilibrium Adsorption Isotherms of Pure N2 and O2 and Their Binary Mixtures on LiLSX Zeolite: Experimental Data and Thermodynamic Analysis. Ind. Eng. Chem. Res. 2014, (2) Model Analysis of Equilibrium Adsorption Isotherms of Pure N-2, O-2, and Their Binary Mixtures on LiLSX Zeolite. Ind. Eng. Chem. Res. 2014, (3) Column Dynamic Study of Mass Transfer of Pure N2 and O2 into Small Particles of Pelletized LiLSX Zeolite. Ind. Eng. Chem. Res. 2014, (4) Equilibrium Isotherm and Mass Transfer Coefficient for Adsorption of Pure Argon on Small Particles of Pelletized Lithium-Exchanged Low Silica X Zeolite. Ind. Eng. Chem. Res. 2015, (5) Experimental Study of a Novel Rapid Pressure Swing Adsorption (RPSA) based Medical Oxygen Concentrator (MOC): Effect of Adsorbent Selectivity of N_2 over O_2. Ind. Eng. Chem. Res. 2016, (6) Comments on Binary and Ternary Gas Adsorption Selectivity. Sep. Purif. Technol. 2016.